



# A FIBRE OPTIC BASED RANGING SENSOR

Thesis submitted for  
the Degree of Master of Science

by

Wen Xin Huang, B. Sc.

Department of Applied Physics  
Faculty of Science  
Victoria University of Technology  
August 1993

FTS THESIS  
681.2 HUA  
30001002329557  
Huang, Wen Xin  
A fibre optic based ranging  
sensor

*This thesis is dedicated to my family*

## Abstract

The remote determination of distance is an important requirement in a wide variety of technical and industrial applications. Ranging techniques have evolved from geometrical to bulk optical or radar methods. There is however a demand for low-cost short to medium range sensors, for operation in potentially hazardous environments, which may be satisfied by optical fibre based sensors. In this thesis the development of an optical ranging sensor, based on fibre optic technology, is described for range measurements over a few metres. Its operation requires an intensity modulated frequency-swept signal which is split and transmitted along two unequal paths before being recombined to form a beat signal. The frequency of this beat signal varies proportionally with the path difference. Incoherent light, from a 780 nm modulated laser diode, was launched into a fibre optic Michelson interferometer which was realised using a 3 dB coupler, with the ranging performed in a free-air path which, formed part of one arm. A variety of optical launching schemes were investigated, and processing electronics were developed progressively to improve the determination of the beat frequency. The sensor was calibrated over a free air path of several metres, and a conservative resolution of 1% was achieved.

## Acknowledgments

I wish to express my thanks to Professor David Booth for the opportunity to undertake postgraduate research in the Department of Applied Physics and his much appreciated encouragement.

I must thank my supervisors, Dr. Stephen Collins and Dr. Michael Murphy, for their counsel and support throughout this project. Many thanks also to Alex Shelamoff for his assistance and guidance with the electronics.

I wish to acknowledge the technical staff (Umit Erturk, Tibor Kovacs, Hayrettin Arisoy and Mark Kivinen) for their engineering/electronic support. Special thanks to Dr. Jakub Szajman, Neil Caranto and Charles Kaddu for their help in the vacuum laboratory. Also the help from the staff and post-graduate students in the Department of Applied Physics was appreciated.

Finally many thanks to my parents, my brother's family and my uncle for their love, and to Ian Johnson and his parents for their care and kindness.

# Contents

Contents	page
<b>Chapter 1</b>	<b><i>Introduction</i></b>
1.1	Fibre optic sensors 1.1
1.2	Project aim 1.1
1.3	Summary of thesis contents 1.2
<b>Chapter 2</b>	<b><i>Fibre optic sensing systems</i></b>
2.1	Introduction 2.1
2.2	System components 2.2
2.2.1	Light sources 2.2
2.2.2	Optical fibres 2.4
2.2.3	Photodetectors 2.5
2.3	System coupling efficiency 2.6
<b>Chapter 3</b>	<b><i>Review of ranging techniques</i></b>
3.1	Introduction 3.1
3.2	Distance measurements by visual means 3.1
3.3	Non-optical distance measurements 3.2
3.4	Range measurements based on laser and optical fibre techniques 3.4
3.4.1	Time of flight 3.5
3.4.2	Phase shift measurement 3.5
3.4.3	Coherent FMCW 3.7
3.4.4	Incoherent FMCW 3.12
3.5	Summary 3.16

**Chapter 4 Theoretical analysis**

4.1	Introduction	4.1
4.2	Fourier analysis of FMCW ranging	4.1
4.2.1	The beat waveform expression	4.1
4.2.2	Production of the beat note	4.3
4.2.3	Frequency analysis of the beat signal	4.4
4.2.4	Examination of the spectrum	4.6
4.2.5	Determination of the beat frequency	4.11
4.3	Noise in electrical circuits	4.12
4.3.1	Thermal noise	4.12
4.3.2	Shot noise	4.12
4.3.3	Signal-to-noise ratio (SNR)	4.13
4.3.4	Summary	4.15

**Chapter 5 Experimental details**

5.1	Introduction	5.1
5.2	Laser diode source	5.2
5.2.1	Laser diode source and modulation circuit	5.2
5.2.2	Modulation optimisation for the laser diode circuit	5.4
5.3	Photodetector circuit	5.6
5.4	Frequency response of the combined source and detector system	5.8
5.5	Voltage-controlled oscillators (VCOs)	5.9
5.5.1	Attenuators for the VCO output	5.11
5.6	Optical fibres and directional coupler	5.13
5.6.1	Optical fibres	5.13
5.6.2	Directional coupler	5.14
5.7	Other optical components	5.15

5.7.1	Collimators	5.15
5.7.2	Reflectors	5.15
5.8	Electrical processing of detector output	5.16
5.8.1	Bandpass filters	5.16
5.8.2	Pre-amplifier	5.18
5.8.3	Electrical signal processor	5.19
5.9	Tektronix oscilloscope	5.27
<b>Chapter 6</b>	<b><i>Experimental results</i></b>	
6.1	Introduction	6.1
6.2	Electrical simulation	6.1
6.3	Optimisation of the optical coupling efficiency of the experimental system	6.5
6.4	Range determination from the modulation envelope	6.9
6.5	Range determination from the beat frequency	6.15
6.5.1	Range measurements using a Type 9036 VCO	6.16
6.5.2	Range measurements using a VTO-9032 VCO	6.19
6.6	Range measurements when an anti-reflection (AR) coating is present on the fibre tip in the target path	6.24
6.6.1	Effect of the signal returned from the fibre tip of the target path	6.24
6.6.2	Range measurements	6.28
6.7	Conclusion	6.31
<b>Chapter 7</b>	<b><i>Final conclusion and future work</i></b>	
7.1	Final conclusion	7.1
7.2	Future work	7.1
<b>References</b>		<b>R1</b>
<b>Publication</b>		<b>P1</b>

# Chapter 1 Introduction

## 1.1 Fibre optic sensors

Fibre optic sensors are relatively new devices that are finding applications in a number of areas and, have become possible due to the advances in fibre optic technology (Dakin and Culshaw, 1988). In operation, the light guided within an optical fibre is modified in response to an external physical, chemical, or electromagnetic influence, which may change the intensity, phase, frequency, or polarisation of the light. Compared to other sensing systems, fibre optic sensors have well-recognised advantages such as:

- \* Immunity from electromagnetic interference
- \* Electrical isolation
- \* Chemical passivity
- \* Small size and low weight
- \* High sensitivity and the ability to interface with a wide range of measurands
- \* More information-carrying capacity (ie. greater bandwidth)

## 1.2 Project aim

The aim of this project was to construct and evaluate a fibre optic sensor for the non-contact measurement of range through the air. The sensor developed, employed techniques which were first used with radar ranging systems (section 3.3). It is comprised of compact, low-cost fibre optic components and does not require coherent light for its operation. To assist in the interpretation of the sensor's signals, an electronic processing scheme was developed, and a range

resolution of several cm was achieved. Possible applications of this sensor include the ullage of inflammable fluids in storage vessels, vehicle ranging for automatic braking schemes, robotics, machine vision and structure monitoring. For these applications, a straightforward and inexpensive device which is potentially mass-produced, would be desirable.

### **1.3 Summary of thesis contents**

The basic components required in fibre optic sensors and the factors affecting optical coupling efficiency in such systems are discussed in Chapter 2. There follows in Chapter 3 a review of existing ranging techniques, where different methods are described and their advantages and disadvantages are discussed.

The operating principles of the sensor under investigation, including a Fourier analysis of the sensor signal and its signal to noise ratio (SNR), are given in detail in Chapter 4. Chapter 5 introduces all the optical and electrical components which were designed and used, including their performance characteristics.

Chapter 6 details the experimental results which includes those from an electrical simulation, optimisation of the free-space optical arrangement (launching, collimation and reception), the various measurement approaches and the resultant ranging measurements. Finally a conclusion and some proposals for future work are presented in Chapter 7.

## Chapter 2 Fibre optic sensing systems

### 2.1 Introduction

Fibre optic sensors were introduced earlier (section 1.1) and may be classified simply in terms of where optical modulation occurs in the sensing loop. That is, if light propagates along a fibre to an external modulator before being recaptured by a second (or the same) fibre, it is called an extrinsic sensor. Alternatively if the light responds to the measurand whilst still being guided, it is known as an intrinsic sensor (Fig 2.1).

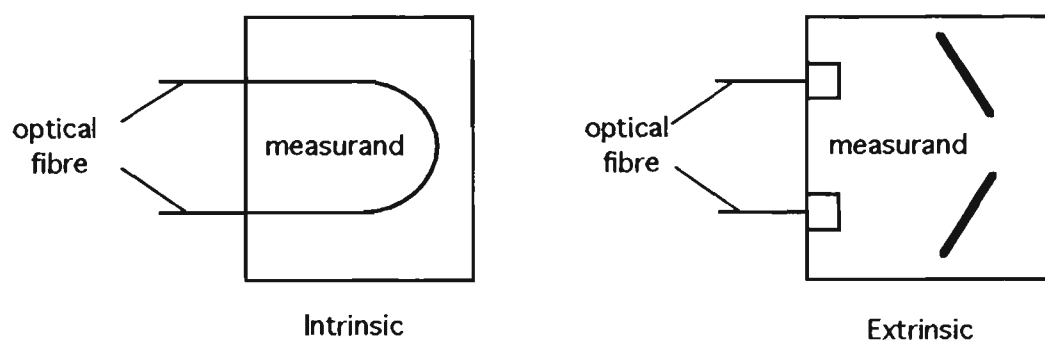


**Fig 2.1** Intrinsic and extrinsic fibre optic sensing system

In general, optical fibre based ranging schemes are extrinsic unless properties of optical fibres are to be investigated (Dakin and Culshaw, 1988). In the work presented in this thesis, an air path is involved and so the sensor developed was extrinsic (section 5.1).

Fibre optic components, of relevance to the ranging sensor developed, are briefly discussed in this chapter.

## 2.2 System components

### 2.2.1 Light sources

Semiconductor light sources (laser diodes (LD) and light-emitting diodes (LED)) are the most important sources for fibre optic communication and sensing systems (Palais, 1984). Their small size and adequate radiance are compatible with the diameter of fibres, and their compact solid structure and low-power requirements are suitable for modern solid-state electronics. Furthermore, their amplitude or frequency may be modulated easily by an appropriate change in bias current. The choice of light sources depends upon the intended application. For example, LEDs involve spontaneous emission, and have a very short coherence length (typically less than 30  $\mu\text{m}$ ). Their rise times range from a few ns to 250 ns, so the highest possible modulation frequency is  $\sim 100$  MHz. Therefore they are normally selected for simple incoherent sensors using multimode fibres and requiring low modulation frequencies. In contrast, LDs employ stimulated emission and have a much narrower linewidth and therefore have much greater coherence lengths ( $\sim 1$  mm for compact disc (CD) lasers). They are widely used in optical communication, optical recording and optical measuring systems because of their efficiency and capability for frequency modulation (Imai and Kawakita, 1990 and Manhart and Barthel, 1984). Furthermore their rise time may be between 0.1 and 1 ns and so they can be modulated at frequencies as high as several gigahertz. Laser diodes may be single-moded or multimoded (Palais, 1984). Single-mode laser diodes have narrower linewidths and therefore longer coherence lengths. The typical spectral width for a multimode laser diode is 1 to 5 nm, whilst for a single-mode laser diode, it is less than 0.2 nm. For coherent interferometric sensors which use unbalanced optical paths, single-mode laser diodes are essential

(Dakin and Culshaw, 1988). Single frequency laser diodes such as a distributed feedback (DFB) laser diode have longer coherence lengths (typically  $\sim 1$  m) but are very expensive. Bragg gratings are used to select the operational wavelength which is determined by the grating spacing. The spectra for single-mode and multimode laser diodes are compared in Fig 2.2.

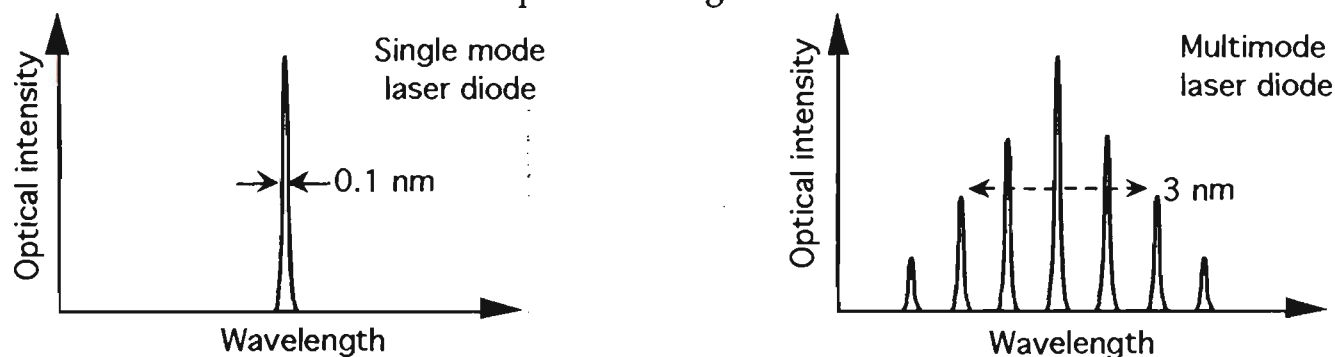


Fig 2.2 Spectra of typical single-mode and multimode laser diodes

The relationship between the optical output power and drive current of the laser diode used in this project (section 5.2.1) is given in Fig 2.3. However, laser diodes are very sensitive to temperature, which affects the threshold current (Fig 2.3) and shifts the operational wavelength (Fig 3.3). Since unwanted temperature changes may distort modulated signals, a feedback element such as a thermoelectrical cooler may be necessary.

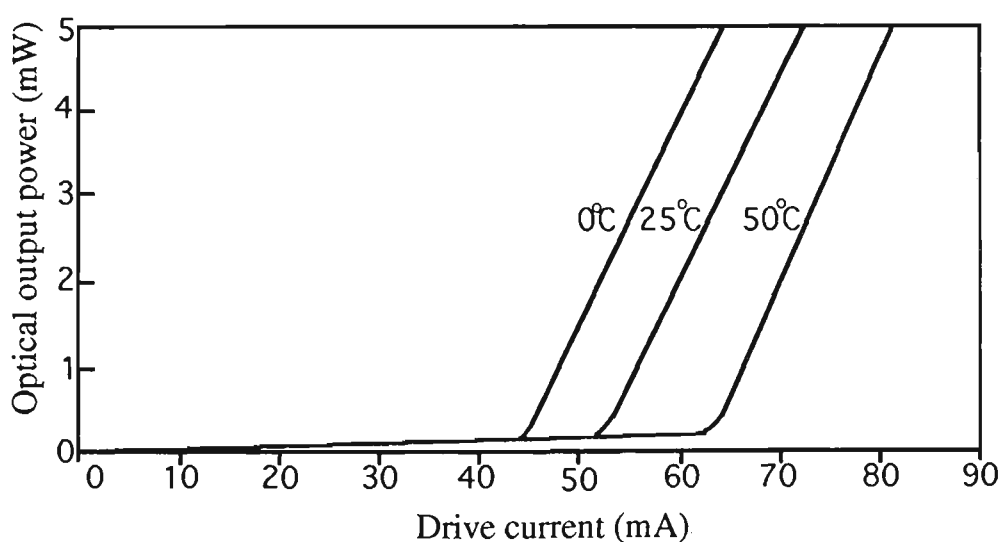
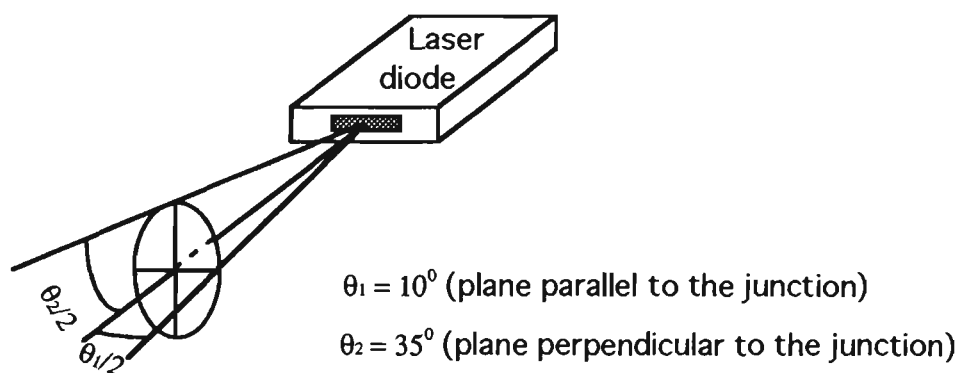


Fig 2.3 Optical output power versus drive current

LDs are edge emitting, and a typical radiation pattern is shown in Fig 2.4. Compared to an LED, the light from an LD is confined within a much smaller angular spread, and so can be coupled more efficiently into an optical fibre. In this work, an inexpensive (less than A\$10), single mode CD player LD was used (section 5.2.1).



**Fig 2.4** Typical radiation pattern of a laser diode

### 2.2.2 Optical fibres

There are essentially three types of optical fibres; single-mode, multimode step index and multimode graded index (Palais, 1984). Single-mode fibres do not suffer from modal dispersion but their power transmittance is limited. In multimode fibres the modulation bandwidth for a specific length is limited by modal dispersion, but greater power transfer is possible than in the single-mode case.

To ensure maximised power coupling into an optical fibre, the fibre numerical aperture (NA) should be large. Numerical aperture is defined by  $NA = n_0 \sin \theta$ , where  $n_0$  is the refractive index of the external medium (Hewlett Packard, 1988). The light rays within a cone of half-angle  $\theta$  are captured by the fibre. The NA of a step index fibre is greater than that of a graded index fibre. The source

coupling efficiencies of single-mode fibres are much lower than for multimode fibres since their core diameter is reduced (8  $\mu\text{m}$  compared to 50  $\mu\text{m}$ ). In this work, 50/125  $\mu\text{m}$  graded-index multimode silica fibre ( $\sim$  \$1/metre) was selected (section 5.6.1), because the optical power transmission had to be maximised.

### 2.2.3 Photodetectors

Important photodetector characteristics are their responsivity, spectral response and rise time (Palais, 1984). There are five types in common use, namely vacuum photodiodes, photomultipliers and semiconductor pn, PIN and avalanche photodiodes (APD). Vacuum photodiodes are not suitable for fibre sensing, and although photomultipliers (PMT) are fast and have high gain, their cost, size, weight and high bias voltage make them inappropriate for fibre sensing systems.

The pn, PIN and APD detectors are small, low in weight, require a low bias voltage and have the potential for fast response. Typical pn diodes have rise times of the order of microseconds, and so are useful for the detection of low frequencies only. Although the bandwidths of PIN diodes and APDs are both about 1 GHz, PIN diodes are preferred because they are lower in cost, less sensitive to temperature and require a smaller bias voltage. Silicon, germanium and InGaAs PIN photodiodes are widely used and have their own operational wavelength range. Silicon diodes are ideal for shorter wavelengths ( $\sim$ 0.8  $\mu\text{m}$ ) whilst the others are suitable for longer wavelengths ( $>$ 1  $\mu\text{m}$ ). Germanium and InGaAs diodes introduce more noise than silicon devices. APDs have internal gains, which gives them increased responsivity compared with pn or PIN diodes, and are appropriate for the detection of weak signals. In

this work the carrier wavelength being detected was 780 nm, and so a PIN silicon photodiode was selected (section 5.3).

### 2.3 System coupling efficiency

Often, in a fibre sensing system, light must be coupled from a light source to a fibre, or from a fibre to a detector and so losses are inevitable. The losses in coupling light into a fibre are due to the Fresnel end-reflection, and core and numerical aperture (NA) mismatches. Coupling efficiency depends on the radiation pattern (Fig 2.4) of the source and the NA of the fibre (section 2.2.2) (Palais, 1984). Lenses or fibre pigtailed sources can be used to improve the coupling.

Losses also occur in mechanical fibre to fibre connections and are caused by lateral, longitudinal and angular misalignment and poorly cleaved ends. Fusion splicing overcomes these inadequacies since less than 0.1 dB loss is possible, whilst less than 0.5 dB loss is reasonable with a mechanical splice. In this work, two GTE Fastomeric mechanical splices (Fibre Optic Products) and some fusion splices were used (section 5.6.1).

When light is coupled from a fibre to a photodetector, the selection of a large area device ensures efficient coupling, although this generally implies a large electrical capacitance and hence a slow response (Dakin and Culshaw, 1988). However reflection losses are inevitable, even when the fibre end is simply butted to the cap of the photodetector, which is the case in the sensing system demonstrated in this work.

Note that the use of multilayer anti-reflection coatings can reduce Fresnel reflection effects significantly. Such a coating process was implemented at the launch end of the fibre sensing system (section 6.6.1).

## Chapter 3 Review of ranging techniques

### 3.1 Introduction

The remote measurement of distance (ie. ranging) is a requirement in various scientific and industrial applications. Ranging involves the launching of a wave into air and its subsequent detection after reflection by a distant object (commonly referred to as the target). A wide variety of techniques are currently available, each of which is particularly suited to some combination of measurement range and resolution.

The best known technique is radar, invented in the 1930's, in which distant objects are located by reflected radio waves (Lynn, 1987). In more recent times the development of devices such as the laser and laser diode have resulted in a variety of ranging sensors which employ visible or infrared light.

This chapter will review the ranging techniques currently in use, and discuss the fibre optic based ranging sensors which have been developed in recent years.

### 3.2 Distance measurements by visual means

All visual methods for determining distance are geometric in nature and are based on the formation of an acute-angled triangle which can be solved by various combinations of base and angle measurements (Hodges and Greenwood, 1971).

An example of a fixed base rangefinder is shown in Fig 3.1. A person views the object through the rangefinder with both eyes. For a fixed base AB (of length  $b$  being the distance between the eyes) and fixed angle at A, the angle at B ( $=\alpha$ ) is

varied until the images of Y as seen through A and B with both eyes are coincident in the field of view of the instrument. Distance AY is a direct function of the variable  $\alpha$  and the constant  $b$ . If the object moves to  $Y'$ , the angle  $\alpha$  changes to  $\alpha'$ . Normally, angle A is arranged as a right angle.

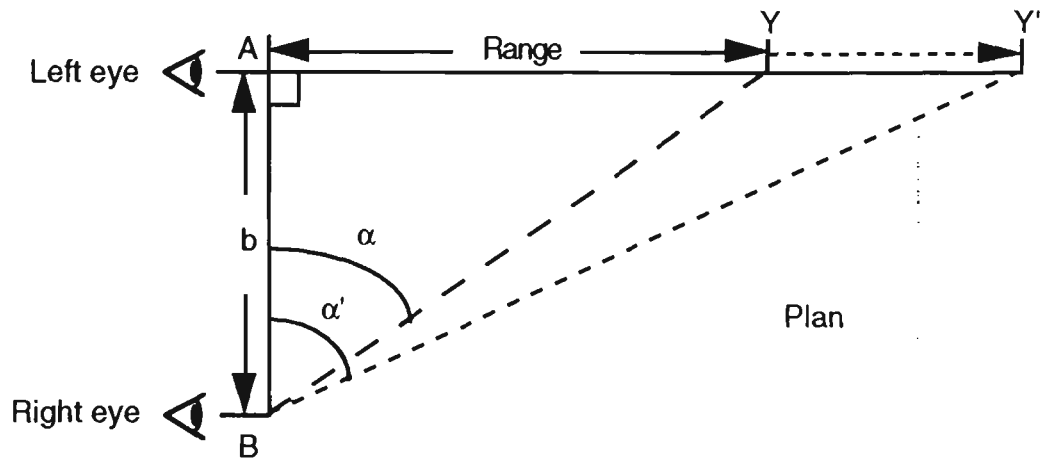


Fig 3.1 Principle of fixed base rangefinders

Visual methods for remote distance measurement are straightforward in principle and easy to operate. However, their resolution and dynamic range are limited by the optical components used and their reliance on the human eye.

### 3.3 Non-optical distance measurements

Radar is the best-known example of non-optical distance measurement. The invention of radio ranging techniques earlier this century was possible because of developments in electrical engineering. Simply, a transmitter launches a radio wave at a target which reflects the wave so that it is received some time later by a radio receiver, where the signals are processed to yield distance information (Rueger, 1990).

Two types of radar are commonly used. In the pulse radar technique, the transmitter emits a train of short pulses, and the target range is found by

measuring the pulse travel time. The resolution depends on the temporal response of the signal processor.

The second approach is the frequency-modulated continuous-wave (FMCW) method. The output frequency from the transmitter is modulated by a sawtooth waveform (period =  $T_s$ ), ie. the output carrier frequency varies linearly in time (chirping). The frequency of an echo will be different to the instantaneous transmitter frequency because of the time delay (Fig 3.2). The transmitter emits a frequency modulated signal into the air, whilst simultaneously directing this signal to the receiver. The signal travelling through the air will be reflected by a target back to the receiver. The frequency difference between the two signals at the receiver depends upon the target distance, so by measuring the difference frequency (beat frequency), its range may be found (Lynn, 1987 and Gnanalingam, 1954). Details of FMCW ranging are discussed in section 4.2.

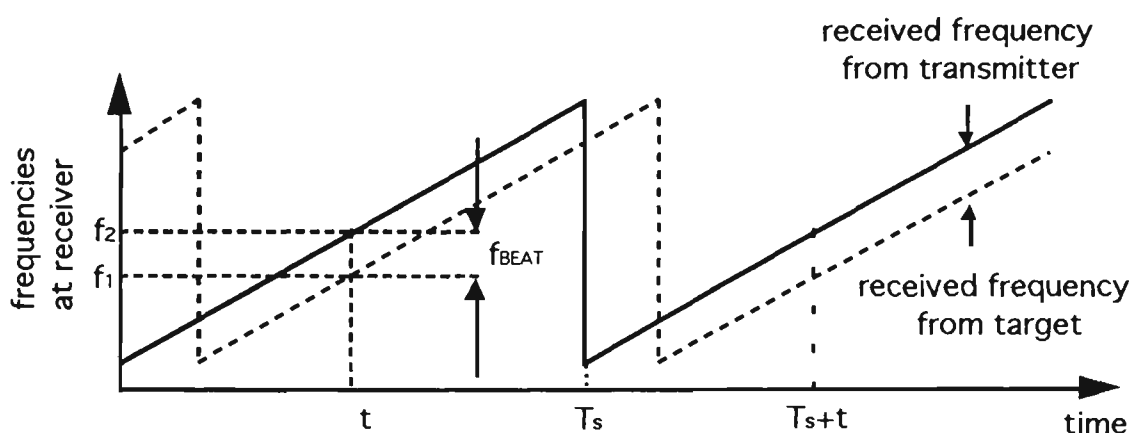


Fig 3.2 Instantaneous frequencies at the receiver

This technique has also been applied to an ultrasonic carrier in order to assist the poorly sighted (Kay, 1985). In this case, the beat frequency is within the audio range. Upon hearing the beat note, a trained person can tell the distance

to the reflecting object and its reflection characteristics. The ability to discriminate between small objects (100 mm) of different shape within a distance of 1 m has been demonstrated.

### **3.4 Range measurements based on laser and optical fibre techniques**

Non-contact range measurement methods make use of radio, gamma rays, ultrasonic or acoustic waves, microwaves and laser beams. Radio, microwave and ultrasonic systems generally show poor collimation of radiation. For example, an accurate determination of target distance using radar requires a narrow radio beam. This is only possible if the antenna aperture is much greater than the radio wavelength. However large antennae are expensive, difficult to steer and suffer from heavy wind loading (Lynn, 1987 and Schwarte, 1984). Alternatively, light from lasers or laser diodes can be focused or collimated simply using lenses or mirrors, which is a great advantage because a well-collimated beam enables accurate definition and restriction of the measurement point (Jelalian, 1992). The light signal can also be transmitted by optical fibres from an electronic unit to a remote sensing head, which is of great importance in some situations due to environmental hazards (Koskinen et al, 1988). Applications of lasers or laser diodes include laser radar, robotics, liquid level measurement, automated manufacturing, surface quality control and aircraft control (Dakin and Culshaw, 1988). The methods used include laser pulse time of flight (section 3.4.1), CW laser intensity modulation (by measuring a phase shift of the modulated signal intensity) (section 3.4.2) and FMCW (sections 3.4.3 and 3.4.4) (de la Chapelle et al, 1989 and Grattan et al, 1990).

### 3.4.1 Time of flight

Conceptually the simplest method is the measurement of the transit time for a short pulse of light reflected back from a remote target. This is the same principle as the pulse radar (section 3.3) and is suitable for the measurement of long distances (~20 m). In terms of resolution, however, this method is limited by the need to measure the time taken between sending and receiving a pulse, and the pulse width. Light (in air) travels at a speed of  $3 \times 10^8$  m/s and so a temporal resolution of 1 ns yields a spatial resolution of 30 cm. Thus to obtain good resolution, high bandwidth and sophisticated signal processing are needed.

Määttä et al (1988) investigated a time of flight rangefinder system, which was intended for measuring the thickness profile of the fire-brick sheathing of a converter (ie. a harsh industrial environment). A high power (15 W) laser diode was used to send out a very short pulse (pulse width = 10 ns). The accuracy of the system was reported to be better than 1 cm for a measurement range of 6 - 17 metres with a signal processing time of less than 1 second per measurement. A similar microprocessor based laser range finder was also reported by Rao and Tam (1990). A GaAlAs laser diode with 22 W peak radiant flux and 20  $\mu$ s pulse time was used, and a range resolution of 1.5 m was achieved.

### 3.4.2 Phase shift measurement

Another approach for range measurement is to direct intensity modulated continuous light at the target, so that the phase of the reflected light will be

different to that of the source oscillator (Grattan et al, 1990). This measured phase difference is related to the range by

$$\begin{aligned} \text{phase difference} &= 2\pi f \left( \frac{2 \times \text{range}}{c} \right) = \frac{2\pi (2 \times \text{range})}{c/f} \\ &= \frac{2\pi (2 \times \text{range})}{\text{modulation wavelength}} \end{aligned} \quad (3.1)$$

where  $f$  = modulation frequency

and  $c$  = speed of light in air.

Thus, by measuring the phase difference with a fixed modulation wavelength, target range may be determined.

A disadvantage with this technique is a possible range ambiguity. That is, since phase can only be determined to within  $2\pi$  (ie. it can not distinguish  $\theta$  and  $2\pi + \theta$ ), the unambiguous spatial range is equal to one half the modulation wavelength (Eqn. 3.1) (Eichen et al, 1987). The resolution depends upon the modulation frequency and is limited in commercial instruments by their phase sensitivity of 1 milliradian. For example, a modulation frequency of a few GHz gives a resolution of  $< 10 \mu\text{m}$  with an unambiguous range of about 1 m. The ambiguous range problem may be solved by introducing a further modulation wavelength, wherein the resolution depends on the shortest modulation wavelength and the true range is obtained using the longest modulation wavelength. Use of multiple discrete frequencies, transmitted either simultaneously or sequentially, permits wider applications of this method, but with increased complexity of device hardware and possibly reduced data rates (McClure, 1990).

The Hewlett Packard 3850A Industrial Distance Meter (Smith, 1980 and Smith and Brown, 1980) measures the range of either a stationary or moving target using this method. An intensity modulated infrared beam is modulated at three frequencies (15 MHz, 375 kHz and 3.75 kHz), corresponding to wavelengths of 20 m, 800 m and 80 km respectively. To obtain an absolute distance measurement, the 3850A measures the phase at each modulation frequency and merges the three readings into one which guarantees a wide measurement range (40 km) and good resolution (3 mm). The output of the phase detector is fed into a microprocessor which performs all necessary computation, control and input/output functions.

A high precision non-contact optical level gauge employing this method for the measurement of the liquid height in a remote storage tank was described by Taylor et al (1986). The signals from the target and the reference paths were detected separately by two photodiodes, and the relative phase between these two electronic signals were measured by a lock-in phase detector. A measurement range greater than 5 m with a resolution of 1 mm was reported.

A similar method has been demonstrated by Rogowski et al (1986) for distance and displacement measurements. A  $10^{-6}$  fractional resolution for displacement was reported.

### 3.4.3 Coherent FMCW

Both the time of flight method and the phase shift measurement require sophisticated electronic circuits for high resolution, and so the frequency-modulated continuous-wave (FMCW) method may be a worthwhile alternative. It was originally developed for ranging measurement using radar

(section 3.3), and more recently it has been used with laser diodes, since they are easily frequency chirped over a wide range. The coherent FMCW method requires the optical carrier frequency to be varied in a sawtooth manner. This signal is split into two components which travel unequal paths before recombination. Thus the signal at the photodetector consists of two components, which have the same form but differ in instantaneous frequency by a constant amount over most of the ramp (Fig 3.2). The delay time is assumed to be small compared with the chirp period, and so a beat waveform results. If the delay time is  $\tau$ , the chirp period is  $T_s$  and the frequency sweep range is  $\Delta f$ , then the beat frequency ( $f_{\text{BEAT}}$ ) will be:

$$f_{\text{BEAT}} = \frac{\Delta f \times \tau}{T_s} \quad (3.2)$$

Let  $R$  be the optical path length difference (in air) between the target path and a reference path. Now  $\tau = \frac{2R}{c}$ , where  $c$  is the speed of light, and so

$$f_{\text{BEAT}} = \frac{\Delta f \times 2R}{T_s c} \quad (3.3)$$

Thus for a known  $\Delta f$  and  $T_s$ , a measurement of the beat frequency enables the range  $R$  to be calculated.

The major factors that affect the optical frequency of a laser diode are its drive current and environmental temperature (Fig 3.3) (section 2.2.1). Frequency modulation is achieved, therefore, by changing the diode's drive current, or by changing the laser diode's temperature by supplying an appropriate signal as the reference to a temperature control circuit. Temperature-controlled frequency modulation is limited by the need for fine thermal control over the entire experimental set-up and a slow response time (Fuhr et al, 1988).

Furthermore, to prevent discontinuities in the frequency caused by mode hopping, the laser diode should be confined to one mode by restricting the temperature variation (Fig 3.3).

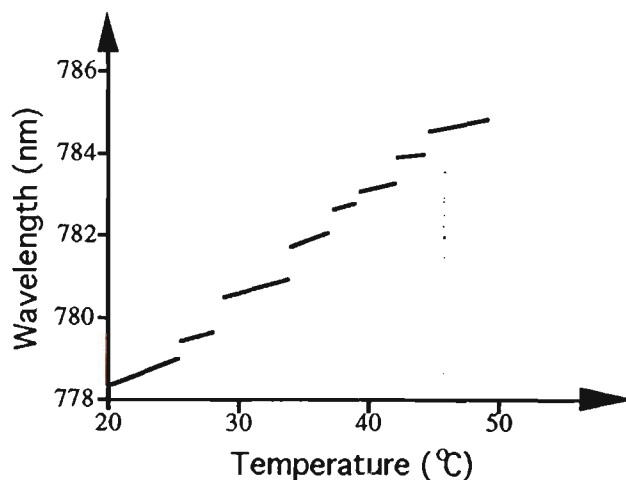


**Fig 3.3** Typical relationship between the output wavelength and the temperature of a laser diode (Sharp LTO22PS)

The resolution of a FMCW ranging device is an important parameter, and from Equation (3.3), it can be seen that a small change in the beat frequency ( $f_{\text{BEAT}}$ ) implies a resolution in range of:

$$\delta R = \frac{T_s c}{2\Delta f} \times \delta f_{\text{BEAT}} \quad (3.4)$$

Thus for fixed resolution of  $f_{\text{BEAT}}$ , the wider the sweep frequency  $\Delta f$ , the better the resolution in  $R$ . The resolution in  $f_{\text{BEAT}}$  is proportional to the ramp frequency ( $f_{\text{ramp}} = \frac{1}{T_s}$ ) (eg. on an oscilloscope or a spectrum analyser), and therefore  $\delta R$  is not affected by a change in  $T_s$ .

In this thesis, this method is referred to as "coherent FMCW" since, to obtain a beat signal, the two signals at the receiver must be coherent. Thus the dynamic range using this method will be limited by the coherence length of the light

source. For a dynamic range of metres an expensive laser diode is required (section 2.2.1).

An optical-fibre ranging sensor based on FMCW was demonstrated by Giles et al (1983) where the signal from a frequency modulated laser diode was coupled into a Mach-Zehnder interferometer, and the beat frequency was monitored with a spectrum analyser. Direct current modulation of a laser diode gives the possibility of nearly 100 GHz of sweep range, allowing resolutions of 0.1 to 1  $\mu\text{m}$ .

Kubota et al (1987) also demonstrated an interferometer for measuring displacement and distance using FMCW. A frequency modulated laser diode was used and the light was collimated by a lens and separated by a beam splitter. Distance was determined by a fringe counter placed after the photodiode. The direction of the fringe change told the sense of a displacement. For a typical detectable fringe fraction of 1/20, a displacement resolution of 0.02  $\mu\text{m}$  and a distance resolution of 100  $\mu\text{m}$  were achieved, whilst the dynamic range was a few metres.

Ohba et al (1990) reported a similar interferometric method for the determination of a static optical path difference using a frequency swept laser diode. The frequency of the laser diode was modulated by a temperature control circuit through a ramped time signal. The difference with the interferometer above is that here a reference etalon was used to compensate for the unknown optical frequency sweep range. The number of intensity changes of the interference fringe was counted simultaneously during the frequency sweep for both the reference etalon and the measurement path. The unknown path difference was given by the product of the length of the reference etalon and

the ratio of the number of fringe changes. For this method, neither the precise value of the frequency sweep range nor very strict frequency stability was required for the light source. The minimum range was 1.5 mm, with a resolution of 3.2  $\mu\text{m}$ .

Kobayashi and Jiang (1988) reported a similar technique using a frequency modulated heterodyne interferometer to measure the range and displacement of specular and diffuse targets. An additional Michelson interferometer with a known optical path difference was introduced as the reference. For range measurement, a resolution of better than 7  $\mu\text{m}$  was achieved for a diffuse target, whilst for a specular target the resolution was about 1 nm, with the range limited to about 2 m .

Coherent FMCW has also been demonstrated using a temperature-tuned long coherence length Nd:YAG ring laser (Sorin et al, 1990), in an all optical fibre arrangement. Laser sources have better collimation and longer coherence lengths than laser diodes, but unfortunately are bulky and expensive. A 50 km dynamic range and better than 10 cm spatial resolution was reported.

The performance of a system employing the coherent FMCW technique, with its associated heterodyne detection scheme, may be substantially degraded by the high sensitivity of a laser diode's operating frequency to environmental temperature fluctuations (approximately 25 GHz/ $^{\circ}\text{C}$ ). Thus instabilities in the source may produce fluctuations in the output from the interferometer which cannot be removed using a signal processor. Therefore, the interferometric implementation of coherent FMCW tends to rely on sophisticated source control systems for optimum system performance (Fuhr et al, 1988).

Furthermore, as already noted, coherent FMCW sensors require long coherence length sources for an appreciable dynamic range.

#### 3.4.4 Incoherent FMCW

For coherent FMCW the maximum range which can be measured is limited by the coherence length, and to compensate for environmental fluctuations additional components are required (Jackson et al, 1982). Alternatively, an incoherent approach based on intensity modulated FMCW would be an attractive possibility since coherent light is not required. In this approach a subcarrier is modulated instead of the optical carrier. Incoherent FMCW may alleviate some of the noise sources encountered in the coherent FMCW system while significantly reducing the overall system complexity. By modulating a laser diode's drive current, the intensity of the emitted light is varied (section 5.2). Hence, to achieve an FMCW output, the modulation frequency of the drive current is chirped (Collins, 1991). The required modulation behaviour is shown in Fig 3.4.

Since only intensity variations are of interest, a multimode laser diode can be used, giving the added advantage of greater power, which is desirable for long air paths. More importantly, there are no coherence length restrictions on the ranges to be measured.

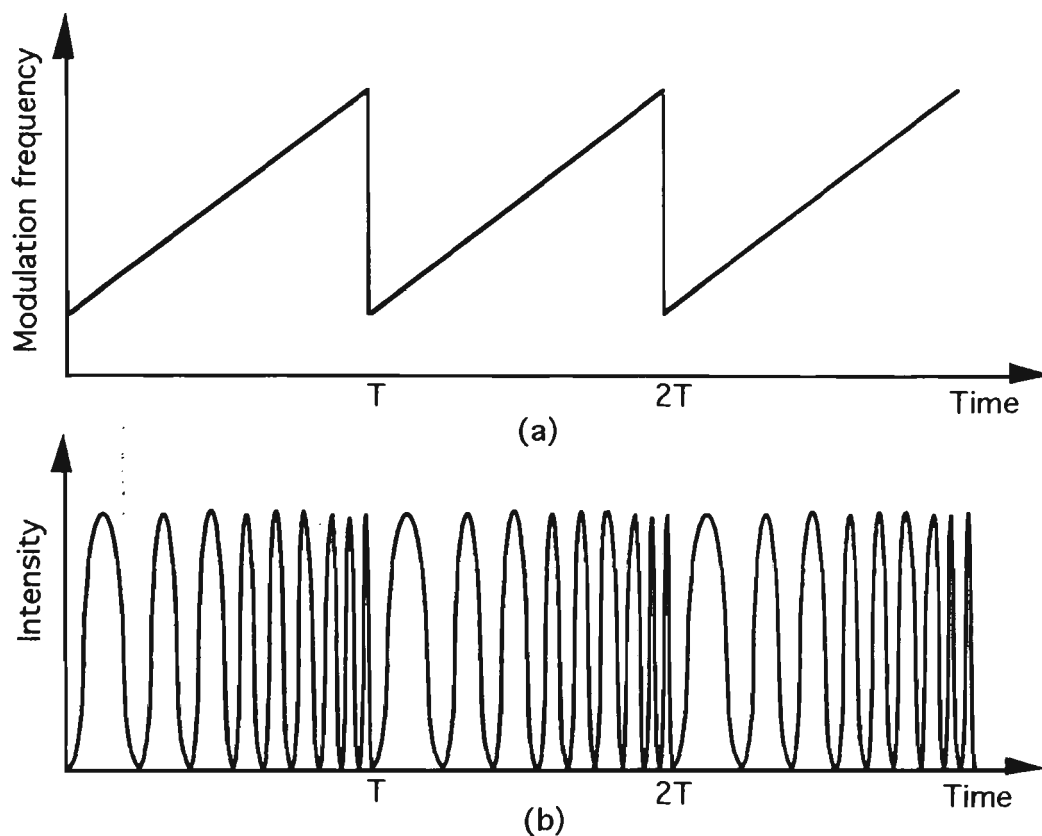


**Fig 3.4** Modulation behaviour: (a) modulation frequency and (b) intensity

The modulation frequencies used in incoherent FMCW are normally within the RF range to ensure that the resolution is reasonable. If these are extended into the microwave region, specialised electronics are required. In either case the sweep frequency is at least 2 orders of magnitude smaller than those obtained in coherent FMCW. According to Eqn. 3.4, the wider the sweep frequency range, the better the range resolution. Thus the possible resolution for incoherent FMCW will be less than for the coherent case. However, since incoherent FMCW can measure a wider range, the fractional resolution should be similar in both instances.

The incoherent FMCW method was first demonstrated by MacDonald (1981), as a method for the detection of faults in optical fibres. This frequency domain reflectometer employed a CW optical carrier modulated by a constant-

amplitude RF signal with a periodic linear sweep frequency. The detected optical reflections were delayed by propagation through the fibre to produce a difference in the modulation frequency. This was mixed with the local source drive signal to produce a beat waveform, which was observed on a spectrum analyser. The frequency axis of the spectrum was proportional to distance along the fibre, and very weak reflections in optical fibres were measured. With this experimental system it was possible to detect end reflections from a 2.2 km length of fibre whose far end was immersed in index-matching fluid to eliminate the Fresnel reflection.

Recently the Boeing Aircraft Corporation (Abbas et al, 1990, de la Chapelle et al, 1991 and Vertatschitsch et al, 1991) investigated a high-precision laser radar based on this incoherent FMCW technique for possible use in aircraft monitoring and control systems. The basic arrangement of this chirped intensity modulated laser radar is depicted in Fig 3.5.

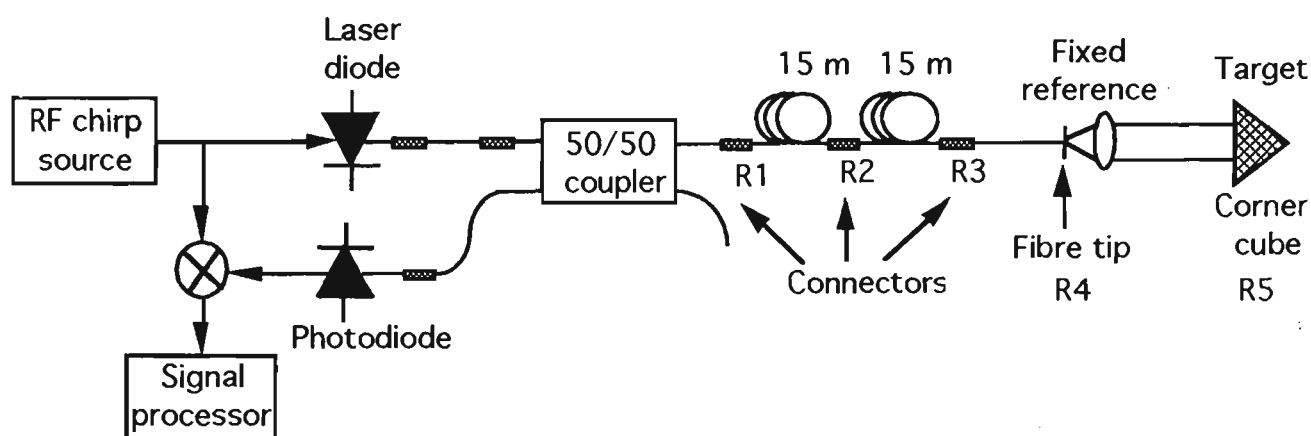


**Fig 3.5** Basic principle of the chirped-intensity modulated laser radar (after Abbas et al, 1990)

The signals from the movable target (corner cube) and the reference end (fibre tip) were reflected back into the fibre where they combined with the other returned signals from the connectors and were directed into the photodiode.

The reflections from the target and the fibre tip were both 4%. The output from the photodiode was mixed with the signal from the RF chirped source to produce several beat frequencies. Fourier processing was used to estimate the beat frequencies of the target and the reference end whilst minimising the effects of the extraneous signals produced by the unwanted connector reflections. By use of the reference reflection, environmentally induced variations in the fibre propagation length were subtracted from the target range. A typical beat spectrum is shown in Figure 3.6.

The chirp frequency used was in the microwave region (2 GHz to 8 GHz), with a target range of up to 120 mm and 0.1 mm resolution. However, the electronics required were complex and therefore expensive.

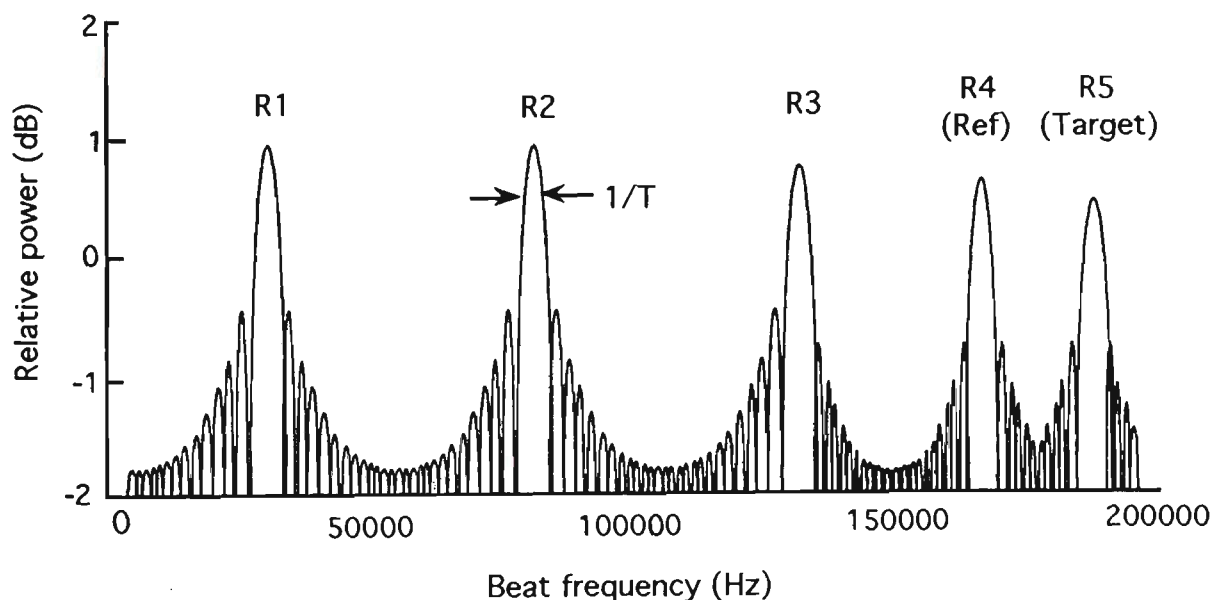


Fig 3.6 Beat frequency spectrum (after de la Chapelle et al, 1991)

Several sensor heads were optically multiplexed by a single laser transmitter using a reflective or transmissive network. However, with an increased number of multiplexed sensors, both the SNR and resolution decreased.

### 3.5 Summary

As discussed in this chapter, range measurements based on laser diodes (or lasers) and optical fibres have several advantages over other measurement methods (sections 3.2, 3.3), including high collimation, high resolution and low weight. Amongst the methods using laser diodes, the time of flight method is straightforward in principle but needs complex electronic processing for high resolution (section 3.4.1). The phase shift measurement needs more than one intensity modulation frequency to overcome possible ambiguous range problems (section 3.4.2). The coherent FMCW method has excellent resolution but the measurement range is limited by the coherence length of the source (section 3.4.3). Expensive single-mode laser diodes are required when large ranges are to be determined (section 2.2.1), and additional stabilising components are necessary.

The incoherent FMCW approach offers a much more practical system, since it has no special demands on sources, optical fibres or detectors. Furthermore it has a greater dynamic range since there is no requirement for coherent light. However, the frequency sweep range is much smaller than that of the coherent FMCW method and therefore, the range resolution will be reduced (section 3.4.4). Also the modulation frequency will be detected whereas for coherent FMCW the detector does not respond to the modulated optical carrier. Thus additional circuitry is required for incoherent FMCW to enable the beat frequency to be demodulated from the carrier.

## Chapter 4 Theoretical analysis

### 4.1 Introduction

Applications of FMCW techniques were discussed in Chapter 3 and its principle was described briefly. A detailed examination of FMCW is presented in this chapter including Fourier analysis, from which the beat frequency may be inferred (section 4.2). This is based on the treatment given by Hymans and Lait (1960). The signal to noise ratio (SNR) of the whole system is also calculated and compared with that measured (section 4.3).

### 4.2 Fourier analysis of FMCW ranging

#### 4.2.1 The beat waveform expression

In an FMCW system, the modulated source produces a signal whose frequency is varied in a sawtooth fashion (Fig 4.1(a)). The solid line is the instantaneous frequency from the reference path, while the dotted line is the instantaneous frequency due to the reflection from the target (Fig 4.1(a)). The returned signal from the target has a time delay  $\tau$  compared with the reference path. The ramp period is  $T_S$  and the angular frequency sweep is  $\Delta\omega$ . For convenience, the sweep rate is taken as  $2\alpha$  ( $2\alpha = \frac{\Delta\omega}{T_S}$ ,  $\Delta\omega = 2\pi\Delta f$  where  $\Delta f$  is the frequency sweep as introduced in section 3.4.3) and the origin of time is set at the centre of one sweep cycle. The instantaneous frequency difference between the signals returned from the reference path and the target path is shown in Fig 4.1(b). This frequency difference is equal to  $f_{\text{BEAT}}$  (Eqn. 3.2) for most of the ramp period, provided the time delay is small compared to that period. A higher frequency difference occurs when the signals at the receiver are obtained from adjacent chirps.

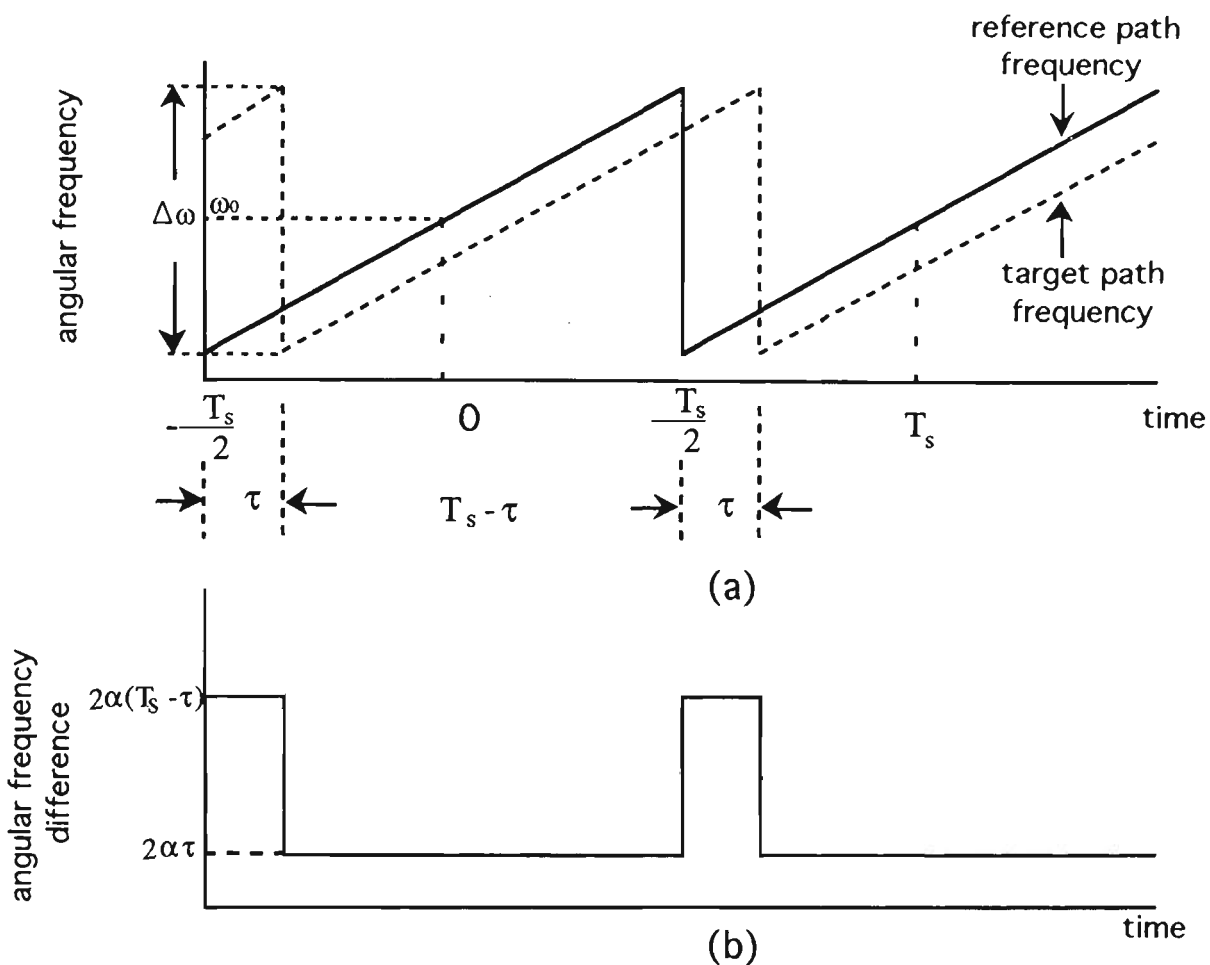


**Fig 4.1** (a) Chirped frequency  
 (b) Instantaneous frequency difference of the two paths

The instantaneous angular frequency  $\omega_i$  is given by the following expressions:

$$\begin{aligned}
 \omega_i &= \omega_0 + 2\alpha t & \text{where } -\frac{1}{2}T_s < t < \frac{1}{2}T_s \\
 &= \omega_0 + 2\alpha(t - T_s) & \text{where } \frac{1}{2}T_s < t < \frac{3}{2}T_s \\
 &\vdots & \vdots \\
 &\vdots & \vdots \\
 &= \omega_0 + 2\alpha(t - nT_s) & \text{where } \frac{1}{2}(2n-1)T_s < t < \frac{1}{2}(2n+1)T_s
 \end{aligned}
 \tag{4.1}$$

where  $T_s$  is the sweep period.

Making the substitution:

$$t_n = t - nT_s \tag{4.2}$$

then

$$\omega_i = \omega_0 + 2\alpha t_n \quad \text{where } -\frac{1}{2}T_s < t_n < \frac{1}{2}T_s \quad (4.3)$$

Now the phase  $\phi_i$  at time  $t$  is obtained by integration of  $\omega_i$ , namely

$$\phi_i = \int_0^t \omega_i dt + \text{constant} \quad (4.4)$$

By substituting Eqn. 4.3 into Eqn. 4.4, the general expression for the phase ( $\phi_i$ ) is found to be

$$\phi_i = \omega_0 t_n + \alpha t_n^2 + n\omega_0 T_s \quad (4.5)$$

#### 4.2.2 Production of the beat note

At the receiver, the reference path produces a signal  $V_g \sin \phi_g$  whilst the target path signal is  $V_e \sin \phi_e$ , where  $\phi_e$  is delayed in time by  $\tau$  compared to  $\phi_g$  and from section 3.4.3,

$$\tau = \frac{\text{measured range}}{\text{velocity of propagation}} = \frac{2R}{c}$$

and  $V_g$ ,  $V_e$  are the amplitudes of the reference signal and the detected signal.

In a non-linear device (section 5.8.3), these two signals will beat together, and the resulting signal will contain a product term  $G V_e V_g \sin \phi_e \sin \phi_g$ , where  $G$  is a constant determined by the non-linear device used (section 5.8.3). Using trigonometrical identities, then

$$V_g V_e \sin \phi_e \sin \phi_g = \frac{1}{2} V_g V_e [\cos(\phi_g - \phi_e) - \cos(\phi_g + \phi_e)]$$

The phase-sum term,  $\frac{1}{2} V_e V_g \cos(\phi_g + \phi_e)$ , is an oscillation at carrier frequencies and can be removed using a low pass filter. The difference term,

$\frac{1}{2}V_eV_g\cos(\phi_g-\phi_e)$  contains all the range information of interest. This term shall now be investigated.

From Fig 4.1(b), it can be seen that two separate cases of the receiver signal arise. These are as follows :

During the time interval  $-\frac{1}{2}T_s < t_n < -\frac{1}{2}T_s + \tau$

$$\phi_e = \omega_0(t_{n-1} - \tau) + \alpha(t_{n-1} - \tau)^2 + (n-1)\omega_0T_s$$

$$\phi_g = \omega_0t_n + \alpha t_n^2 + n\omega_0T_s$$

$$\text{So } \phi_g - \phi_e = \omega_0\tau - \alpha(T_s - \tau)^2 + 2\alpha(\tau - T_s)t_n \quad (4.6)$$

Also during the time interval  $-\frac{1}{2}T_s + \tau < t_n < \frac{1}{2}T_s$

$$\phi_e = \omega_0(t_n - \tau) + \alpha(t_n - \tau)^2 + n\omega_0T_s$$

$$\phi_g = \omega_0t_n + \alpha t_n^2 + n\omega_0T_s$$

$$\text{So } \phi_g - \phi_e = \omega_0\tau - \alpha\tau^2 + 2\alpha\tau t_n \quad (4.7)$$

### 4.2.3 Frequency analysis of the beat signal

Using Fourier transform techniques (Champney, 1985), the beat signal can be resolved into its separate harmonic components. In general, the Fourier transform of the signal  $f(t)$  may be evaluated by

$$F(\omega) = \int_{-\infty}^{\infty} f(t)e^{-j\omega t} dt$$

Thus, for the difference term  $\frac{1}{2}V_eV_g\cos(\phi_g-\phi_e)$ , its Fourier transform is

$$F(\omega) = \int_{-\infty}^{\infty} \frac{1}{2}V_eV_g\cos(\phi_g-\phi_e)e^{-j\omega t}dt$$

By substituting  $t = t_n + nT_s$  (Eqn. 4.2) and using Eqn. 4.6, Eqn. 4.7, then

$$F(\omega) = \frac{1}{2}V_eV_g \left[ \sum_{n=-\infty}^{\infty} e^{-jn\omega T_s} \right] \left[ \int_{-\frac{1}{2}T_s}^{-\frac{1}{2}T_s+\tau} \cos[\omega_0\tau - \alpha(T_s-\tau)^2 + 2\alpha(\tau-T_s)t_n] e^{-j\omega t_n} dt_n \right. \\ \left. + \int_{-\frac{1}{2}T_s+\tau}^{\frac{1}{2}T_s} \cos(\omega_0\tau - \alpha\tau^2 + 2\alpha\tau t_n) e^{-j\omega t_n} dt_n \right]$$

Note that the two integrals in the second bracket are independent of  $n$  and so have been put outside the summation.

The term  $\sum_{n=-\infty}^{\infty} e^{-jn\omega T_s} = \omega_s \delta(\omega - k\omega_s)$ , where  $k = 0, \pm 1, \pm 2 \dots$  and  $\omega_s = 2\pi/T_s$ .

After integration, the Fourier transform of the beat signal (taking the allowed values of  $k$  into account) can be usefully expressed as:

$$F(\omega) = \frac{1}{2}V_eV_g \omega_s \sum_{k=-\infty}^{\infty} [\delta(\omega - k\omega_s)] \times [F_1(k\omega_s) + F_2(k\omega_s) + F_3(k\omega_s) + F_4(k\omega_s)] \quad (4.8)$$

Here

$$F_1(\omega) = (T_s - \tau) \frac{\sin[(\omega - 2\alpha\tau)(\frac{T_s - \tau}{2})]}{2[(\omega - 2\alpha\tau)(\frac{T_s - \tau}{2})]} [e^{j(\omega_0\tau - \frac{1}{2}\alpha\tau^2)}] \quad (4.9)$$

$$F_2(\omega) = (T_s - \tau) \frac{\sin[(\omega + 2\alpha\tau)(\frac{T_s - \tau}{2})]}{2[(\omega + 2\alpha\tau)(\frac{T_s - \tau}{2})]} [e^{j(\omega_0\tau + \frac{1}{2}\alpha\tau^2)}] \quad (4.10)$$

$$F_3(\omega) = \tau \frac{\sin\left\{\left[\omega - 2\alpha(T_s - \tau)\right] \frac{\tau}{2}\right\}}{2\left\{\left[\omega - 2\alpha(T_s - \tau)\right] \frac{\tau}{2}\right\}} \left\{e^{-j[\omega\tau - \frac{1}{2}\alpha(T_s - \tau)]}\right\} \quad (4.11)$$

$$F_4(\omega) = \tau \frac{\sin\left\{\left[\omega + 2\alpha(T_s - \tau)\right] \frac{\tau}{2}\right\}}{2\left\{\left[\omega + 2\alpha(T_s - \tau)\right] \frac{\tau}{2}\right\}} \left\{e^{j[\omega\tau + \frac{1}{2}\alpha(T_s - \tau)]}\right\} \quad (4.12)$$

#### 4.2.4 Examination of the spectrum

The delta function in Eqn. 4.8 ( $\delta(\omega - k\omega_s)$ ) implies that the spectrum has the form of discrete lines lying at integer multiples of the ramp frequency  $\omega_s$ .

From Eqn. 4.9 - 4.12, it can be seen that :

$$\begin{aligned} F_1(\omega) &= F_2^*(-\omega) & F_2(\omega) &= F_1^*(-\omega) \\ F_3(\omega) &= F_4^*(-\omega) & F_4(\omega) &= F_3^*(-\omega) \end{aligned}$$

where the "\*" represents the complex conjugate. Since only  $\omega > 0$  is of interest, Eqn. 4.8 can be rewritten as

$$\begin{aligned} F(\omega) &= \frac{1}{2} V_e V_g \omega_s \sum_{k=0}^{\infty} [\delta(\omega - k\omega_s)] \times [F_1(k\omega_s) + F_2(k\omega_s) + F_3(k\omega_s) + F_4(k\omega_s) \\ &\quad + F_1(-k\omega_s) + F_2(-k\omega_s) + F_3(-k\omega_s) + F_4(-k\omega_s)] \end{aligned}$$

or

$$\begin{aligned} F(\omega) &= \frac{1}{2} V_e V_g \omega_s \sum_{k=0}^{\infty} [\delta(\omega - k\omega_s)] \times [F_1(k\omega_s) + F_2(k\omega_s) + F_3(k\omega_s) + F_4(k\omega_s) \\ &\quad + F_1^*(k\omega_s) + F_2^*(k\omega_s) + F_3^*(k\omega_s) + F_4^*(k\omega_s)] \end{aligned}$$

Now for a complex quantity,  $z + z^* = 2\text{Re}(z)$ , then  $F(\omega)$  can be rewritten as

$$F(\omega) = \frac{1}{2} V_e V_g \omega_s \sum_{k=0}^{\infty} [\delta(\omega - k\omega_s)] \times \left\{ 2\text{Re}[F_1(k\omega_s)] + 2\text{Re}[F_2(k\omega_s)] \right. \\ \left. + 2\text{Re}[F_3(k\omega_s)] + 2\text{Re}[F_4(k\omega_s)] \right\}$$

Thus the full analytical form of the Fourier transform is as follows,

$$F(\omega) = \frac{1}{2} V_e V_g \sum_{k=0}^{\infty} [\delta(\omega - k\omega_s)] \times \left\{ (T_s - \tau) \frac{\sin[(k\omega_s - 2\alpha\tau)(\frac{T_s - \tau}{2})]}{[(k\omega_s - 2\alpha\tau)(\frac{T_s - \tau}{2})]} \cos(\omega_0\tau - \frac{1}{2}k\omega_s\tau) \right. \\ + (T_s - \tau) \frac{\sin[(k\omega_s + 2\alpha\tau)(\frac{T_s - \tau}{2})]}{[(k\omega_s + 2\alpha\tau)(\frac{T_s - \tau}{2})]} \cos(\omega_0\tau + \frac{1}{2}k\omega_s\tau) \\ + \tau \frac{\sin\{[k\omega_s - 2\alpha(T_s - \tau)]\frac{\tau}{2}\}}{\{[k\omega_s - 2\alpha(T_s - \tau)]\frac{\tau}{2}\}} \cos[\omega_0\tau - \frac{1}{2}k\omega_s(T_s - \tau)] \\ \left. + \tau \frac{\sin\{[k\omega_s + 2\alpha(T_s - \tau)]\frac{\tau}{2}\}}{\{[k\omega_s + 2\alpha(T_s - \tau)]\frac{\tau}{2}\}} \cos[\omega_0\tau + \frac{1}{2}k\omega_s(T_s - \tau)] \right\} \quad (4.13)$$

The details of this expression will now be discussed. There are terms of the form  $\frac{\sin(x-x_0)}{x-x_0}$  (ie.  $\text{sinc}(x-x_0)$ ) in Eqn. 4.13 which are shown generally in Fig 4.2.

The maximum for this function occurs when  $x = x_0$ .

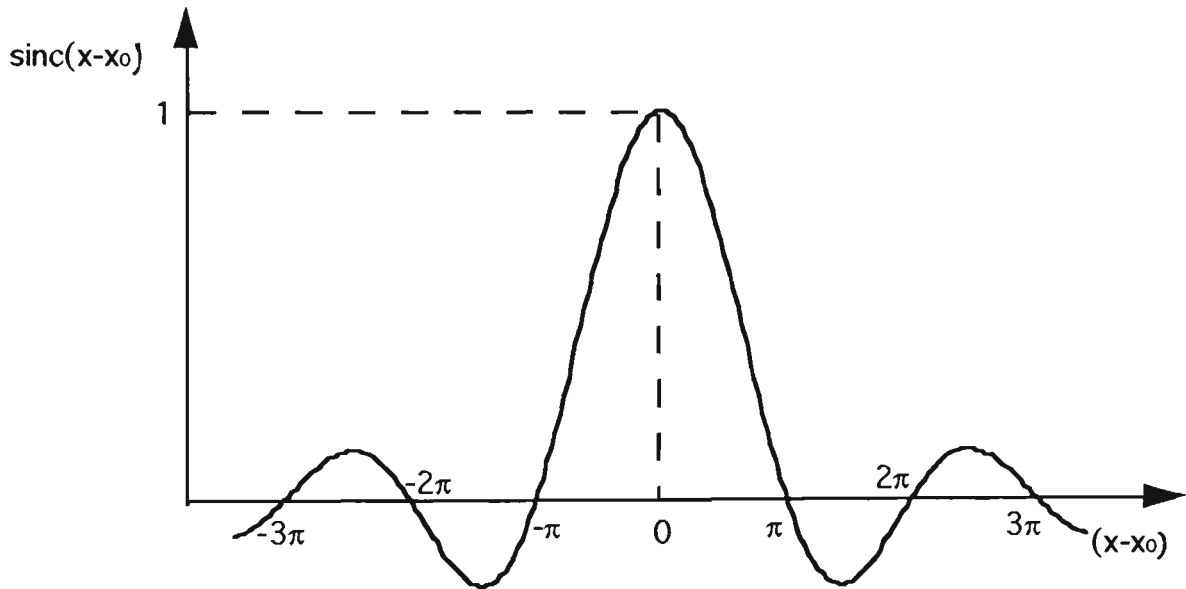


Fig 4.2 General form of  $\text{sinc}(x-x_0)$

Equations 4.9 to 4.12 indicate that only the sinc envelopes for Equations 4.9 and 4.11 have maxima occurring for  $\omega > 0$ . These occur when:

$$\text{for Eqn. 4.9} \quad \omega_{B1} = 2\alpha\tau$$

$$\text{for Eqn. 4.11} \quad \omega_{B2} = 2\alpha(T_S - \tau)$$

Normally  $\tau$  is very small compared to  $T_S$  since the measured range is not particularly large. Thus it is appropriate to call  $\omega_{B1} = 2\alpha\tau$  the "lower" beat note and  $\omega_{B2} = 2\alpha(T_S - \tau)$  is referred to as the "upper" beat note. The time delay  $\tau = \frac{2R}{c}$ , where  $R$  is the range to be measured, so the "lower" beat note ( $\omega_{B1} = 2\alpha\tau$ ) is proportional to  $R$  (in agreement with the simplified analysis given in section 3.4.3). Therefore by measuring  $\omega_{B1}$ ,  $R$  can be determined. In typical FMCW applications where  $\tau \ll T_S$ , the "upper" beat note  $\omega_{B2} = 2\alpha(T_S - \tau) \approx 2\alpha T_S = 2\pi\Delta f$  lies in the RF range and can be readily eliminated by a low pass filter.

Now it remains for the width of the sinc envelope to be considered. From Eqn. 4.9, it has zeros when

$$(\omega - 2\alpha\tau)\left(\frac{T_S - \tau}{2}\right) = \pm m\pi \quad m = 1, 2, \dots, \infty$$

so the "lower" beat spectral width ( $\Delta\omega_{B1}$ ) is given by

$$\Delta\omega_{B1} = \frac{4\pi}{T_S - \tau} \quad (4.14)$$

For Eqn. 4.11, zeros occur when

$$[\omega - 2\alpha(T_S - \tau)]\frac{\tau}{2} = \pm m\pi \quad m = 1, 2, \dots, \infty$$

so in this case, the "upper" beat spectral width ( $\Delta\omega_{B2}$ ) is given by

$$\Delta\omega_{B2} = \frac{4\pi}{\tau}$$

As already stated, the spectrum is composed of a series of discrete lines which are spaced in  $\omega_s$  (the chirp frequency). These discrete lines are modulated by the functions  $\text{sinc}[(\omega-2\alpha\tau)(\frac{T_s-\tau}{2})]$  and  $\text{sinc}\{[\omega-2\alpha(T_s-\tau)]\frac{\tau}{2}\}$ . The actual beat frequency ( $\omega_{B1}$ ) lies at the centre of the sinc envelop ( $\text{sinc}[(\omega-2\alpha\tau)(\frac{T_s-\tau}{2})]$ ) and so is not necessarily equal to a harmonic of  $\omega_s$ . That is, the beat frequency is not normally expected to be one of the discrete lines of the spectrum.

The spectrum of  $F(\omega)$  is given in Fig 4.3, and it should be noted from Eqn. 4.9 and Eqn. 4.11 that

$$\frac{\text{Amplitude of lower beat-note}}{\text{Amplitude of upper beat-note}} = \frac{T_s-\tau}{\tau}$$

From this Fourier analysis, it can be seen that the spectrum of the beat waveform consists of two regions which are composed of discrete lines spaced by  $\omega_s$ . If  $\tau$  is small the spectrum is expected to have the form shown in Fig 4.3(a). On the other hand, if  $\tau > \frac{T_s}{2}$ , the "upper" beat frequency will be smaller than the "lower" beat frequency and the spectrum will appear as shown in Fig 4.3(b). Thus the unambiguous range of the FMCW method is  $\frac{2R}{c} = \frac{T_s}{2}$ , which means that the maximum measurement range is  $R_{\max} = \frac{T_s c}{4}$ . In this work,  $T_s = 0.01$  sec which means  $R_{\max}$  was 750 km.

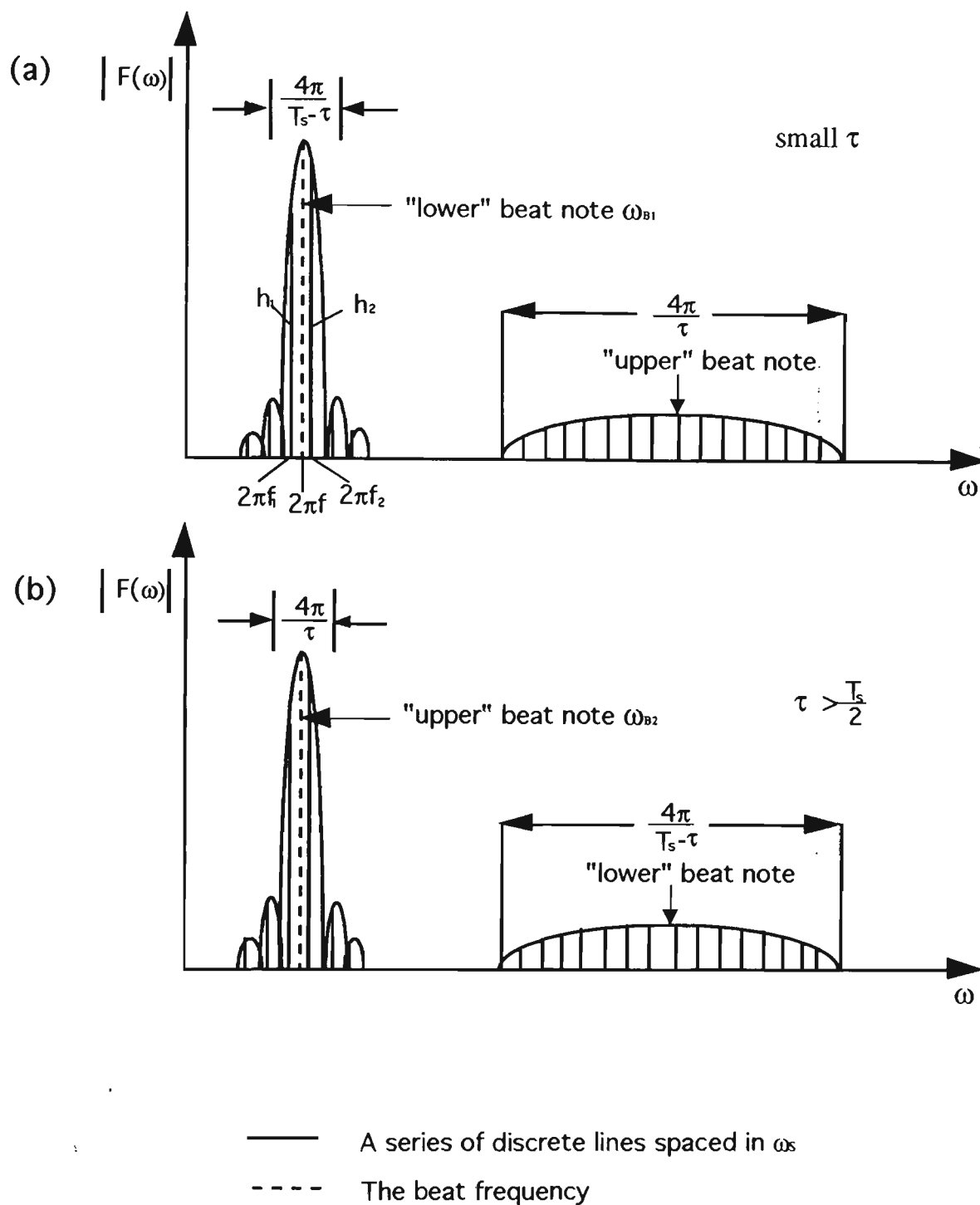


Fig 4.3 Spectrum of beat note of

(a) small  $\tau$  (Spectrum width of "lower" beat =  $\frac{4\pi}{T_s - \tau} < \frac{4\pi}{\tau}$ )  
 (b)  $\tau > \frac{T_s}{2}$  (Spectrum width of "lower" beat =  $\frac{4\pi}{T_s - \tau} > \frac{4\pi}{\tau}$ )

### 4.2.5 Determination of the beat frequency

As described previously (section 4.2.4), the Fourier spectrum of the beat waveform consists of discrete lines spaced by  $\frac{2\pi}{T_s}$ , and the beat frequency is not normally one of the discrete lines. In order to determine the beat frequency, it is necessary to fit these discrete lines into a sinc envelope to locate the position of the central maximum. However, because of noise and VCO non-linearities (section 5.5), this method is impractical. Alternatively, for a short range,  $\tau \ll T_s$ , then for the lower beat note envelope  $\text{sinc}[(\omega - 2\alpha\tau)(\frac{T_s - \tau}{2})] \approx \text{sinc}[(\omega - 2\alpha\tau)(\frac{T_s}{2})]$ . Also from Eqn. 4.14,  $\Delta\omega_{B1} = \frac{4\pi}{T_s - \tau} \approx \frac{4\pi}{T_s} = 2\omega_s$ , which means only two discrete lines lie in the central region of the sinc envelope. If they have the values  $2\pi f_1$  and  $2\pi f_2$  respectively ( $F(2\pi f_1) = h_1$ ,  $F(2\pi f_2) = h_2$ ), and the beat angular frequency is  $2\pi f$  ( $2\pi f = 2\alpha\tau$ ) (Fig 4.3(a)), then as described in section 4.2.4,

$$\frac{\sin[(2\pi f_1 - 2\pi f)(\frac{T_s}{2})]}{(2\pi f_1 - 2\pi f)(\frac{T_s}{2})} = bh_1 \quad (4.15)$$

and

$$\frac{\sin[(2\pi f_2 - 2\pi f)(\frac{T_s}{2})]}{(2\pi f_2 - 2\pi f)(\frac{T_s}{2})} = bh_2 \quad (4.16)$$

where  $b$  is a constant arising from other terms in  $F(\omega)$  (Eqn. 4.13).

Note that  $2\pi f_2 = 2\pi f_1 + \frac{2\pi}{T_s}$  (section 4.2.4), and by dividing Eqn. 4.15 by Eqn. 4.16,

the beat frequency ( $f$ ) can be obtained as

$$f = \frac{h_1 f_1 + h_2 f_2}{h_1 + h_2} \quad (4.17)$$

Thus by measuring the amplitudes ( $h_1$  and  $h_2$ ) of the two observed discrete frequencies ( $f_1$  and  $f_2$ ) in the central region, the beat frequency can be determined.

### 4.3 Noise in electrical circuits

For any detection system, signal-to-noise ratio is an important parameter to consider in terms of signal quality. The major sources of noise are thermal noise (or Johnson noise) and shot noise (Palais, 1984).

#### 4.3.1 Thermal noise

Thermal noise originates in a photodetector's load resistor. Thermal noise power (W) is calculated from

$$P_{TN} = 4 kT \Delta f R_L$$

Where  $P_{TN}$  = thermal noise power

$k$  = Boltzmann's constant

$T$  = temperature (K)

$\Delta f$  = receiver's electrical bandwidth (Hz)

$R_L$  = resistance of load resistor ( $\Omega$ )

Note that the thermal noise spectrum has essentially a uniform frequency distribution (Palais, 1984).

#### 4.3.2 Shot noise

In semiconductor photodetectors, shot noise arises from the random generation and recombination of free electrons and holes. The shot noise power (W) is

$$P_{SN} = 2e(i_s + I_D) \Delta f R_L$$

Where  $e$  = charge of an electron

$i_s$  = the average detector current (A)

$I_D$  = photodetector's dark current (A)

The shot noise spectrum is also generally uniform over all frequencies (Palais, 1984).

From these expressions, it can be seen that both thermal and shot noise power are proportional to the detector's bandwidth. Thus a bandpass filter (which reduces the bandwidth to the range of interest) (section 5.8.1) will usefully decrease the noise level.

### 4.3.3 Signal-to-noise ratio (SNR)

For a photodetector, having an incident optical power  $P(W)$  and responsivity  $\rho$  (A/W), its photocurrent is given by

$$I_s = \rho P$$

Thus the average electrical signal power is

$$P_{ES} = I_s^2 R_L = (\rho P)^2 R_L$$

Therefore the SNR of the detector is

$$SNR = \frac{P_{ES}}{P_{TN} + P_{SN}} = \frac{(\rho P)^2 R_L}{4kT\Delta f R_L + 2e(\rho P + I_D)\Delta f R_L} \quad (4.18)$$

For the PIN photodiode selected (section 5.3), using typical values of  $\rho = 0.4$  A/W,  $R_L = 50 \Omega$ ,  $T = 293$  K,  $I_D = 0.02$  nA (which can be omitted in the calculation since  $I_D \ll i_s$ ),  $\Delta f$  (before bandpass filter) = 400 MHz (which is the selected bandwidth of the oscilloscope) and  $P = -19$  dBm (12.6  $\mu$ W), the resultant SNR value is given by:

$$\text{SNR} = \frac{(0.4 \times 12.6 \times 10^{-6})^2 \times 50}{(4 \times 1.381 \times 10^{-23} \times 293 + 2 \times 1.602 \times 10^{-19} \times 0.4 \times 12.6 \times 10^{-6}) \times 400 \times 10^6 \times 50}$$

$$\Rightarrow \text{SNR} = 3.92$$

If expressed in dB, then the SNR becomes  $10 \log_{10} \text{SNR} = 5.9 \text{ dB}$

The measured signal and noise power is given in Fig 4.4 which was obtained from an Advantest TR4131 Spectrum Analyser. The resolution bandwidth of this spectrum analyser was 10 kHz, and the average signal power was -26.2 dBm. From 0 to 280 MHz, the average noise power was -77 dBm (20 pW) and from 280 MHz to 400 MHz (the selected bandwidth of the oscilloscope), the noise power was -73 dBm (50 pW). Thus the total noise power was

$$10 \log_{10} \left[ 20 \times 10^{-9} \times \frac{280 \times 10^6}{10 \times 10^3} + 50 \times 10^{-9} \times \frac{(400 - 280) \times 10^6}{10 \times 10^3} \right]$$

$$= -29.4 \text{ dBm}$$

Therefore the measured SNR was  $-26.2 \text{ dBm} - (-29.4 \text{ dBm}) = 3.2 \text{ dB}$

This SNR is too low to obtain a good quality signal, but since the chirp frequency for the Type 9036 VCO (section 5.5) was from 226 MHz to 271 MHz, a bandpass filter was used to improve it (section 5.8.1). The filter's 3 dB bandwidth was from 170 MHz to 330 MHz which enabled the bandwidth to be halved. Thus there should be a corresponding increase in SNR. The measured SNR is given in Fig 4.5, with an average signal power of -26.2 dBm. The noise power, from 170 MHz to 330 MHz, was -74 dBm (40 pW), and elsewhere -87 dBm (2 pW). By using a similar approach, the noise power was calculated to be -31 dBm, and the measured SNR was improved to 4.8 dB.

An Avantek VTO-9032 VCO (section 5.5) was also used to chirp the laser diode's modulation frequency over the range 300 MHz to 680 MHz. A 1 GHz bandwidth was chosen when using the oscilloscope. A second bandpass filter corresponding to this frequency range was required (section 5.8.1) whose 3 dB bandwidth was from 200 MHz to 700 MHz. According to Eqn. 4.18, the SNR should now be 4.96 dB and the measured SNR is given in Fig 4.6 which shows an average signal power of -26.2 dBm. The noise power, from 200 MHz to 700 MHz was -74 dBm (40 pW), whilst elsewhere it was -87.5 dBm (1.8 pW). Thus the total noise power was -27 dBm, and so the measured SNR was only 0.8 dB.

#### 4.3.4 Summary

From the calculations and the measurements above, it can be seen that the SNR is insufficient to obtain a good quality signal even when a bandpass filter is used. The signals on the oscilloscope from the photodetector and the bandpass filter are given in Fig 5.22(a) and Fig 5.22(b) respectively and can be seen to have poor SNR. To overcome this an electrical signal processor was developed, and this is described in section 5.8.3. When processed in this way, a beat frequency was produced, and by appropriate filtering, the SNR was greatly improved (section 5.8).

The disagreement between the calculated and the measured SNR values arises from the photodetector's amplifying circuit which introduced additional noise not included in the calculations.

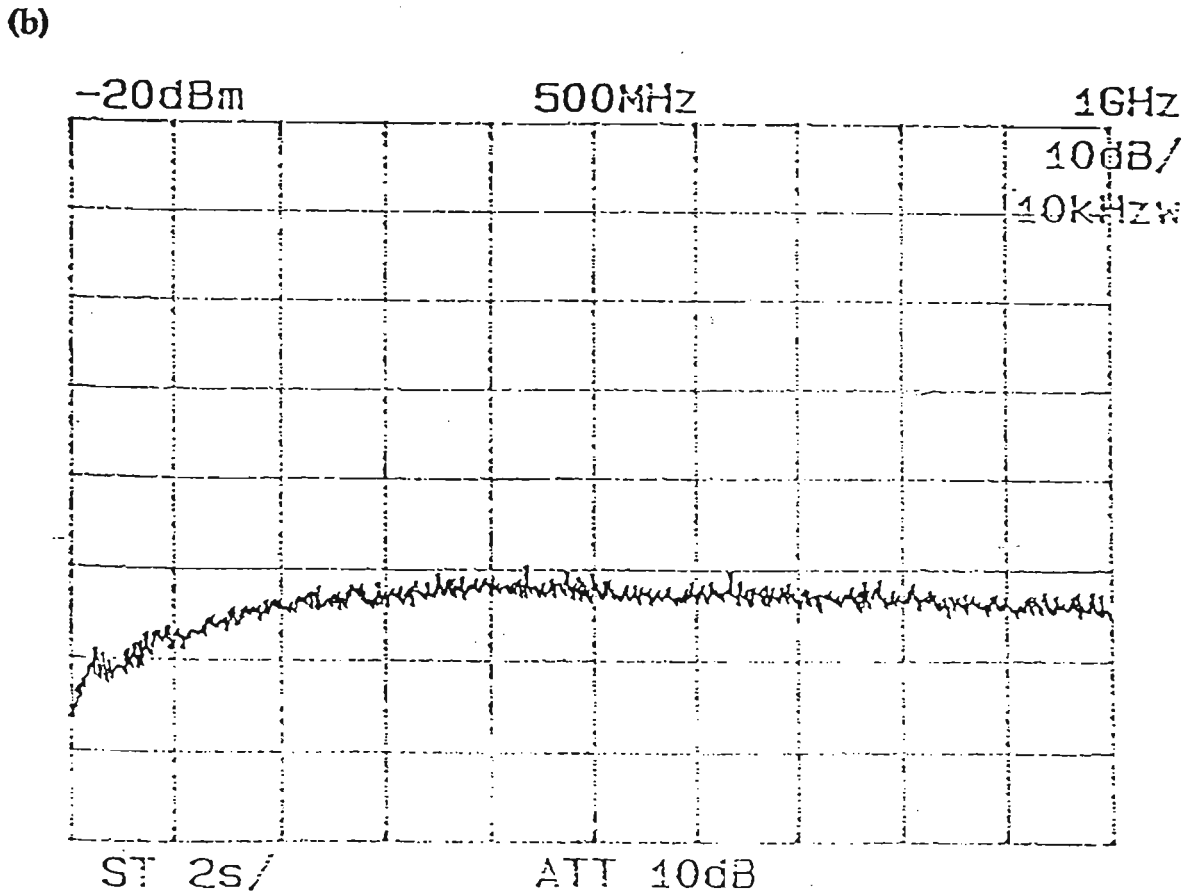
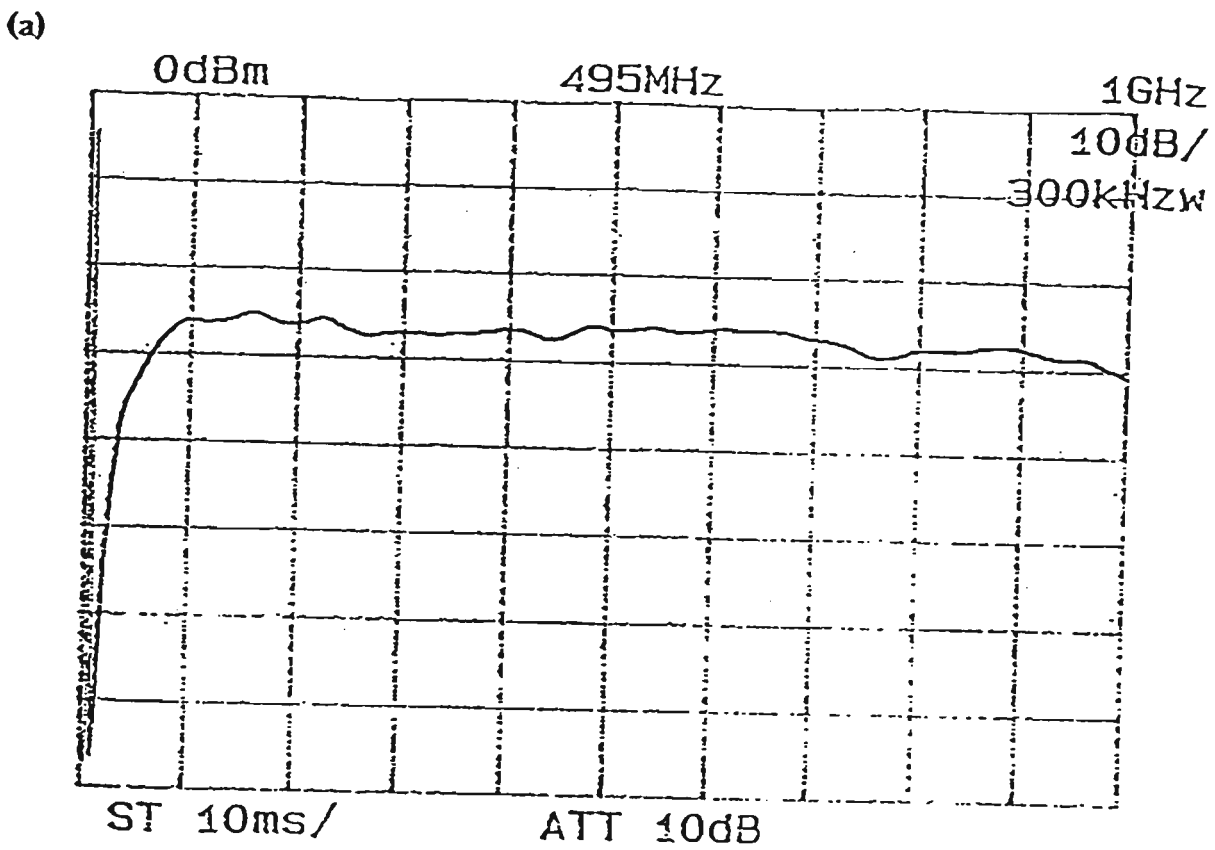


Fig 4.4 (a) signal and (b) noise spectra of the detection system

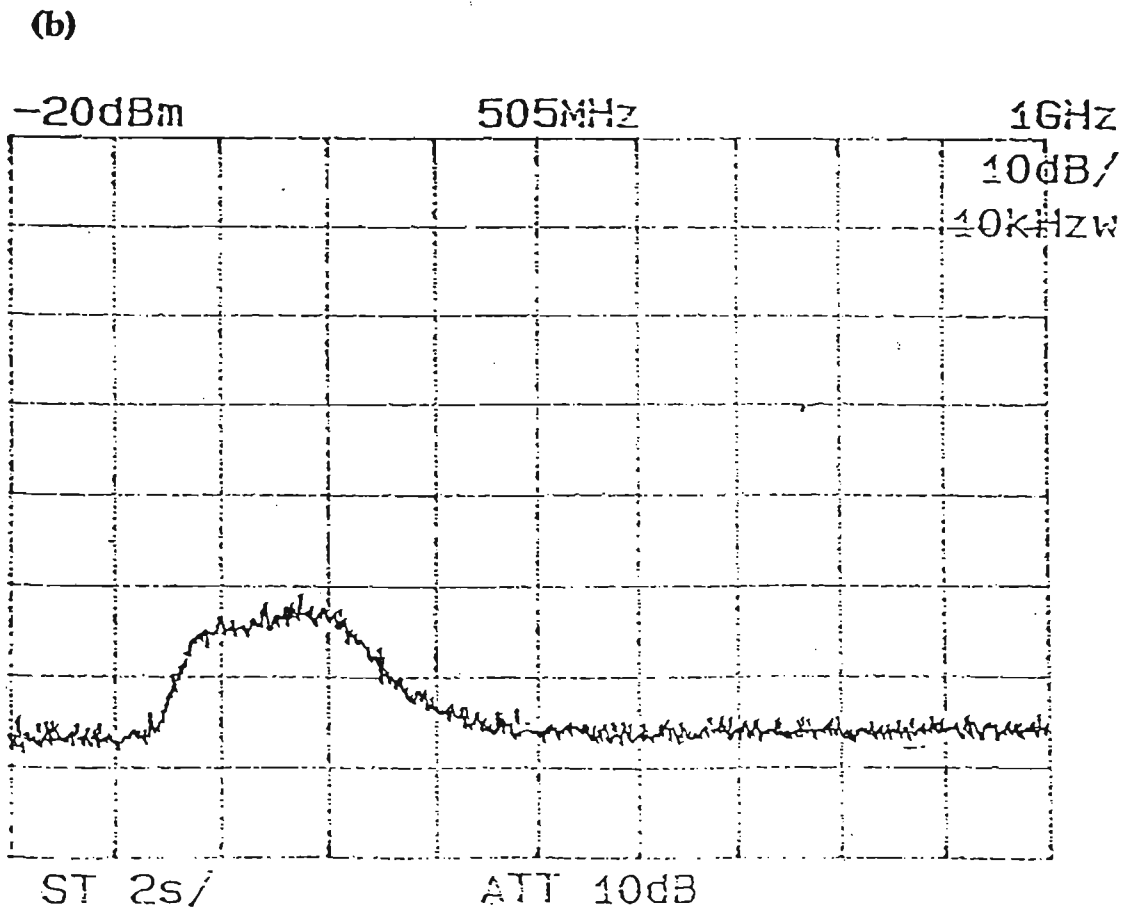
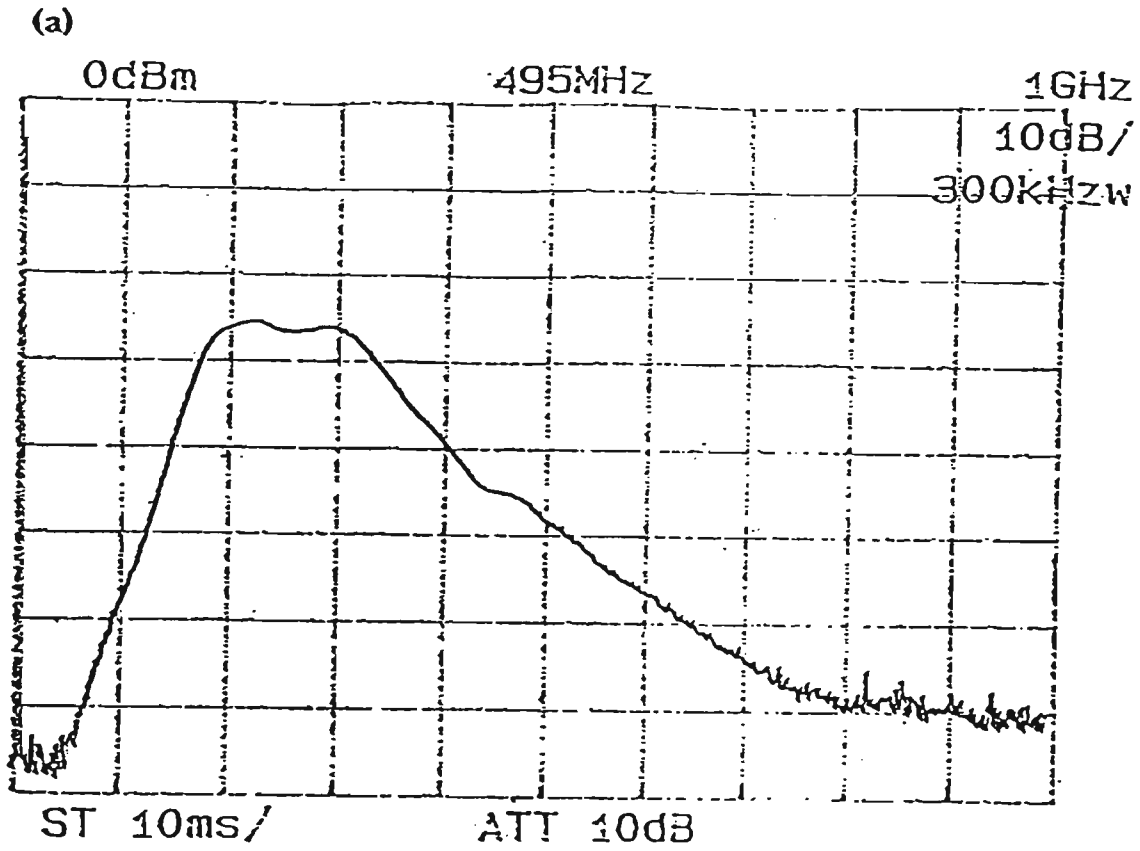


Fig 4.5 (a) signal and (b) noise spectra of the detection system after the bandpass filter whose 3 dB bandwidth is 170 MHz to 330 MHz

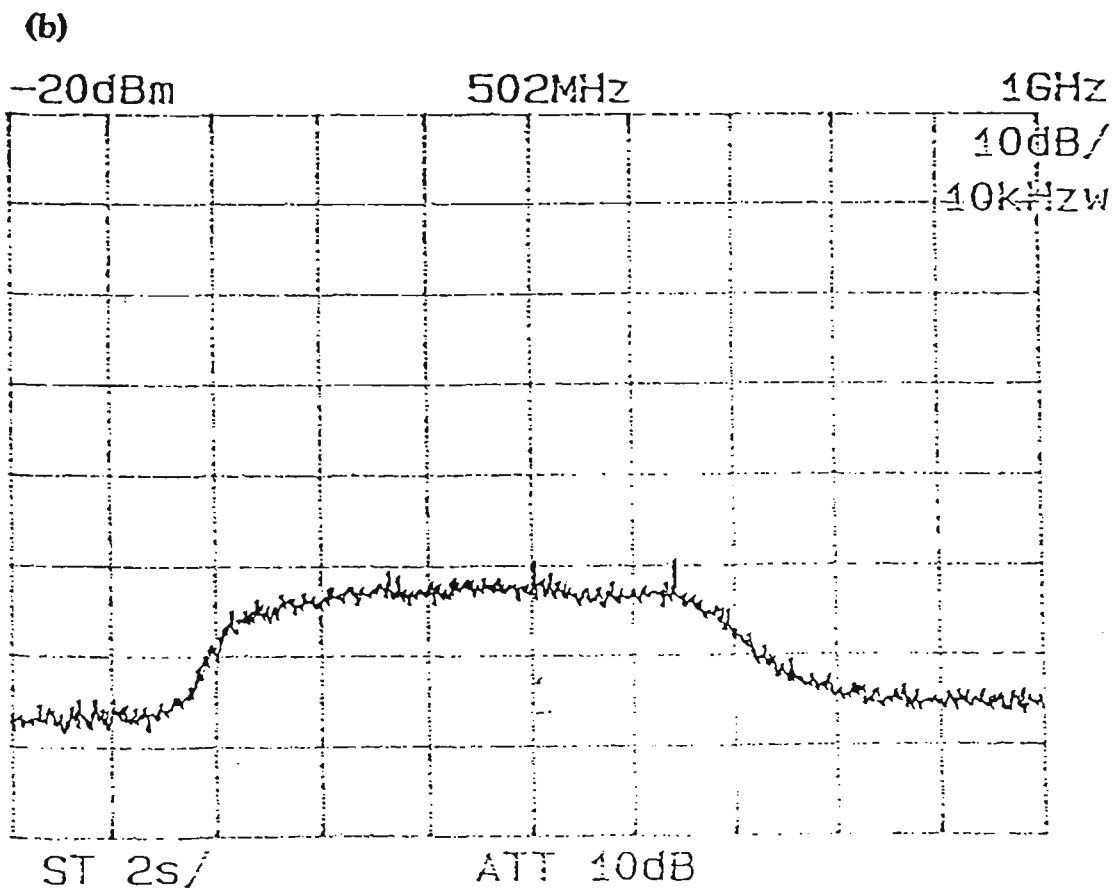
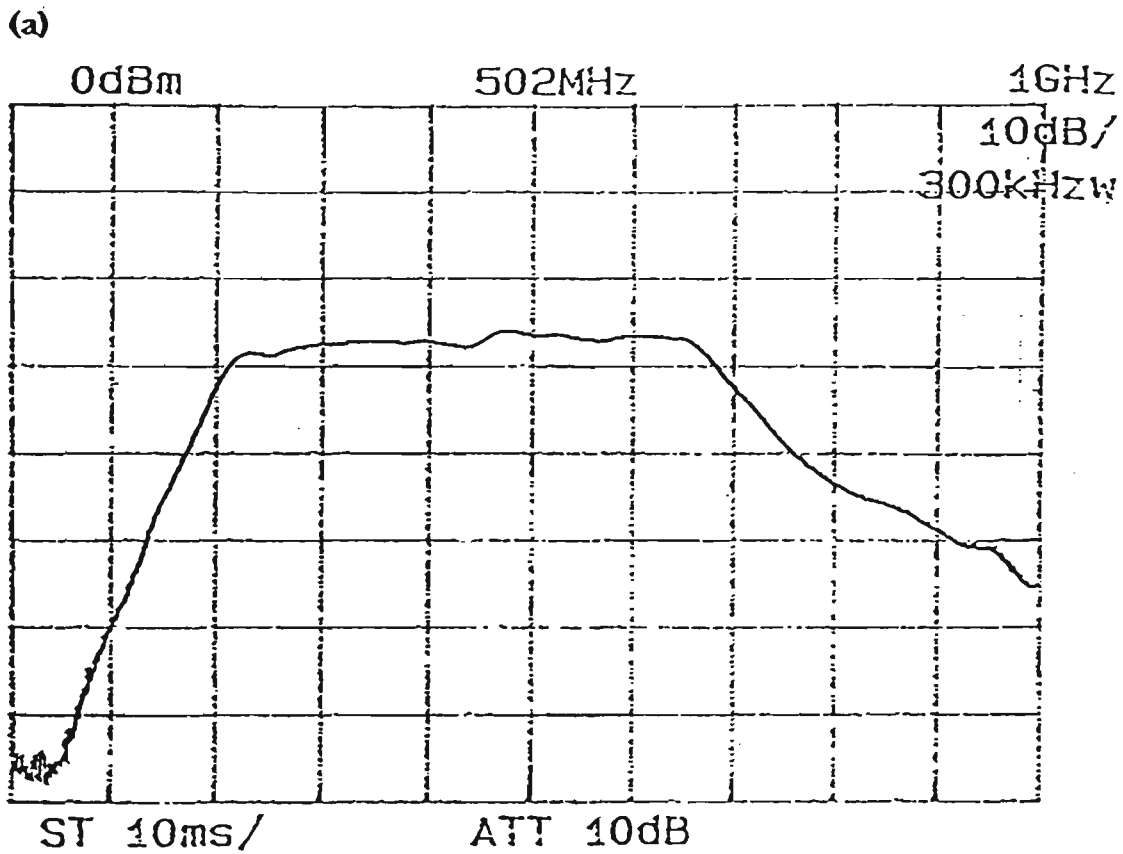


Fig 4.6 (a) signal and (b) noise spectra of the detection system after the bandpass filter whose 3 dB bandwidth is 200 MHz to 700 MHz

# Chapter 5 Experimental details

## 5.1 Introduction

The basic experimental configuration for incoherent FMCW (section 3.4.4) is shown in Fig 5.1 (similar to a Michelson interferometer). A sawtooth waveform from a function generator controlled the output frequency of a voltage controlled oscillator (VCO) (section 5.5). This VCO was used to modulate the drive current of a laser diode (section 5.2.1) and thus intensity modulate its output as a linear frequency chirp (Fig 3.4). The modulated optical signal from the laser diode was coupled into 50/125  $\mu\text{m}$  graded index multimode optical fibre (by butting to the diode lens) and split by a 50:50 fused directional coupler (section 5.6.2) into two paths. Light entering the reference path was returned by a reflector (section 5.7.2) at the fibre end. Light entering the target path travelled some distance through a fibre before being launched into air and directed through a collimator (section 5.7.1) onto a remote reflector (target) (section 5.7.2), from where it was recoupled into the same fibre. The reflected signals from both the reference and the target paths entered the fourth arm of the coupler and were directed onto a silicon PIN photodiode (section 5.3). These two signals have the same frequency chirp but are displaced in time from each other, as described in section 4.2.1. Therefore there is a frequency difference between the two signals and thus a beat waveform results. A signal processor (section 5.8) was used to combine these two detected signals, amplify the beat waveform and filter out the unwanted high frequency carrier signal. This beat signal was analysed using a digital oscilloscope (section 5.9).

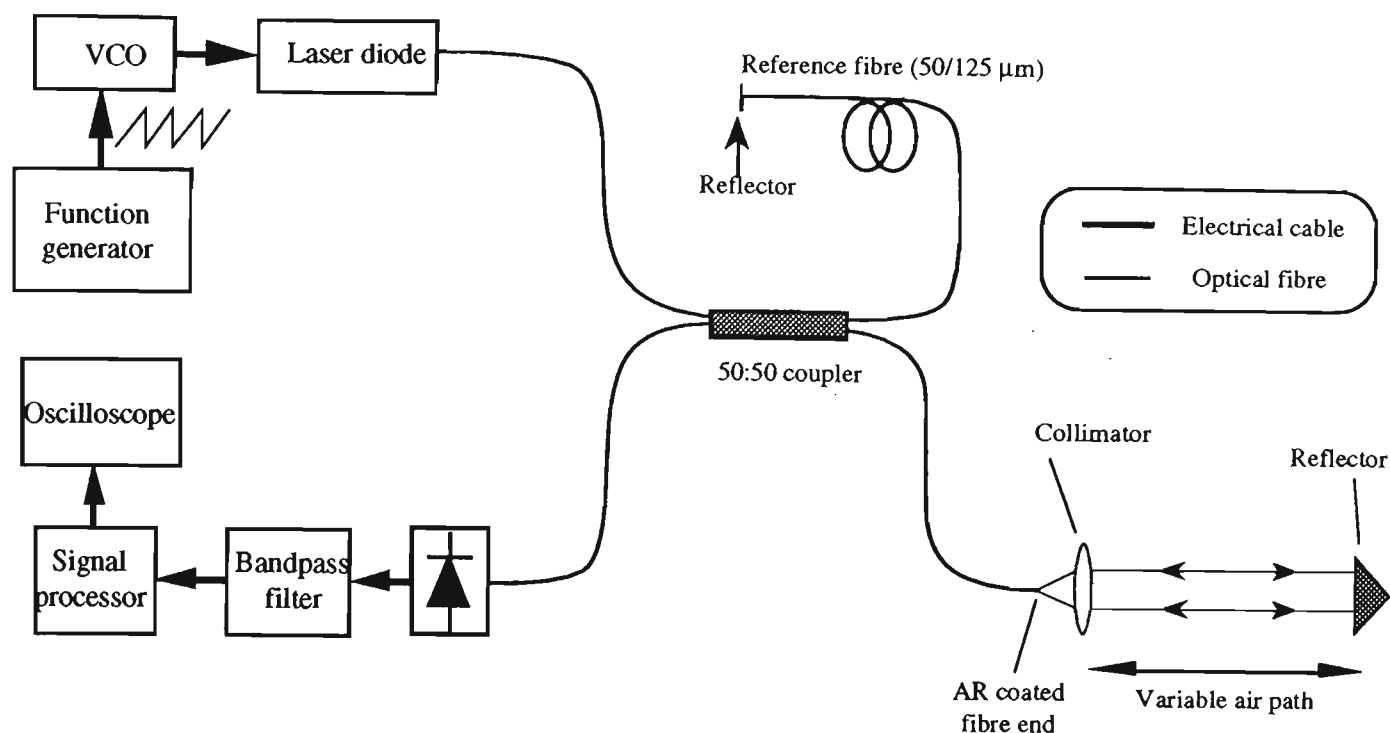


Fig 5.1 Experimental arrangement

## 5.2 Laser diode source

### 5.2.1 Laser diode source and modulation circuit

As mentioned in section 2.2.1, the laser diode selected was the inexpensive 5 mW Sharp LTO22PS (less than A\$ 10). It has a single transverse mode and is a compact, low noise device with an SNR of about 60 dB and a central wavelength of 780 nm (at 22°C). Its temperature dependence and radiation pattern were given in Fig 2.3 and Fig 2.4 respectively. Within the laser diode package, a built-in feedback photodiode was used for stability control, and in the modulation circuit (Fig 5.2) (Shelamoff, 1992), a Sharp IR3C07 laser diode driver was used for automatic power control. The bias optical power was set to 1.5 mW at room temperature (22°C). An AT01635 silicon bipolar transistor was used to modulate the output power of the laser diode. The modulation circuit was designed to intensity modulate the optical power over the range of 0 to 3

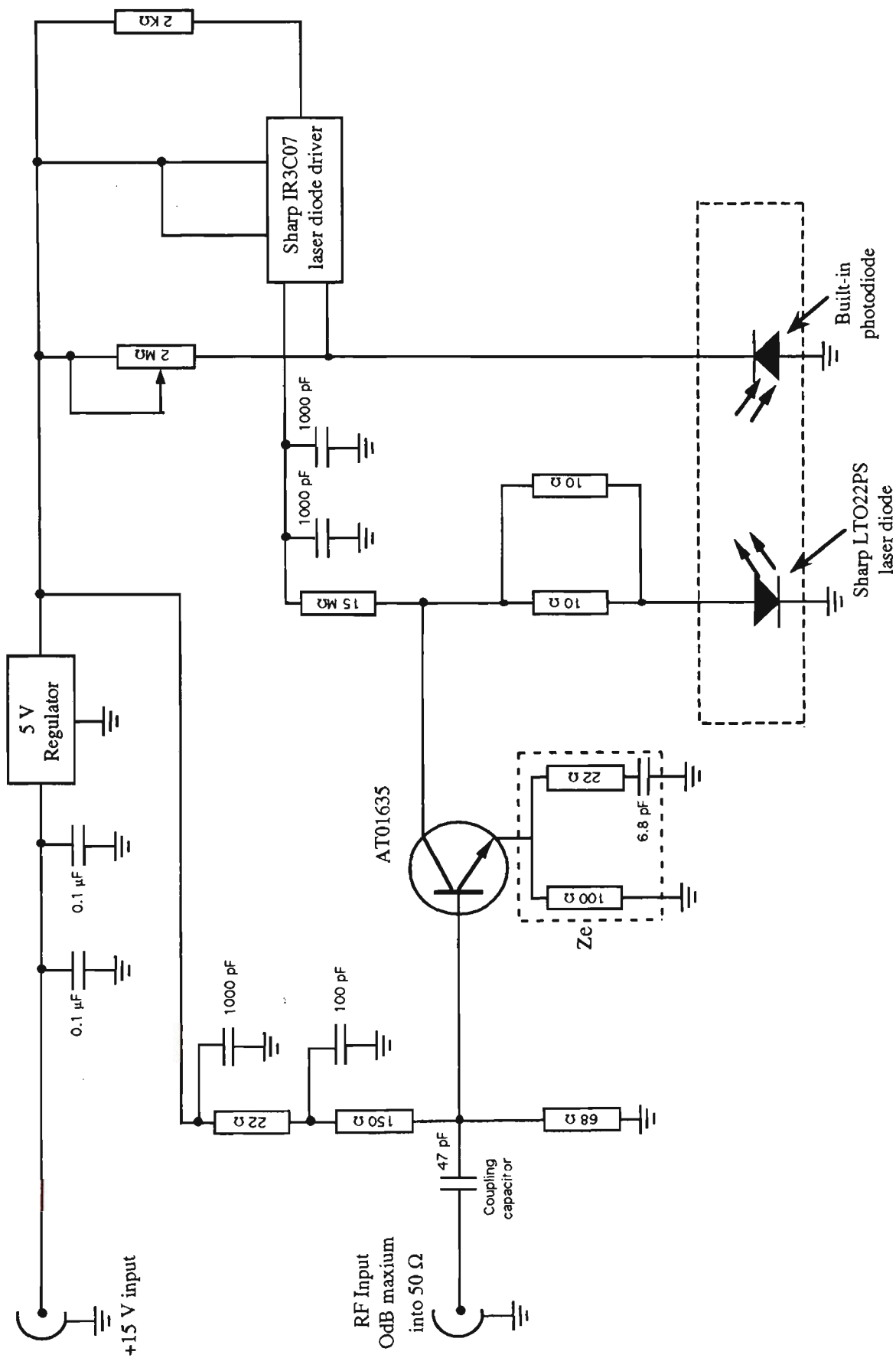


Fig 5.2 Laser diode modulation circuit

mW, which implies a modulation depth of 100%. The maximum modulation power allowed for the laser diode was 0 dBm. However, since this circuit lacks a temperature control system, the DC output power, modulation depth and output mode might vary. Since only the beat frequency formed by the chirped intensity modulation is of interest, any temperature change is not expected to have a significant effect on the final result. This circuit is effective for modulation frequencies from ~10 MHz to 1 GHz and has an input impedance of 50  $\Omega$ . A lens was bonded at the focal point of the laser diode radiation area in order to enhance the coupling of light from the laser diode to the butted optical fibre. The continuous working output power coupled into a 50/125  $\mu\text{m}$  graded index multimode fibre was -2.4 dBm.

### 5.2.2 Modulation optimisation for the laser diode circuit

The depth of optical modulation (section 5.2.1) is an important factor affecting signal quality (Oppenheim et al, 1983), and for an analogue drive current for an LD, the maximum modulation is shown in Fig 5.3 (note for analogue modulation, the DC current is set to  $I_{\text{bias}}$ ). The best SNR should occur when the modulation depth is as high as possible, and this happens when the peak-to-peak modulation current is double  $I_{\text{bias}}$  (Fig 5.3), which is difficult to achieve in practice.

In order to measure the depth of modulation of the laser diode output, a DC coupled detector was employed. However, since this detector's response was slow (with a bandwidth of only several megahertz), the coupling capacitor in the modulation circuit (Fig 5.2) had to be altered from 47 pF to 0.1  $\mu\text{F}$ . Thus using the arrangement shown in Fig 5.4, the laser diode's output was measured at a modulation frequency of 2 MHz.

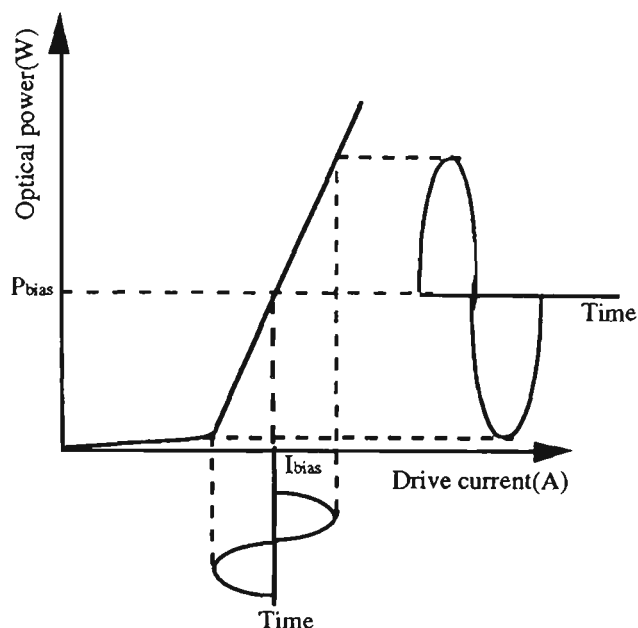


Fig 5.3 Maximum analogue modulation for a laser diode

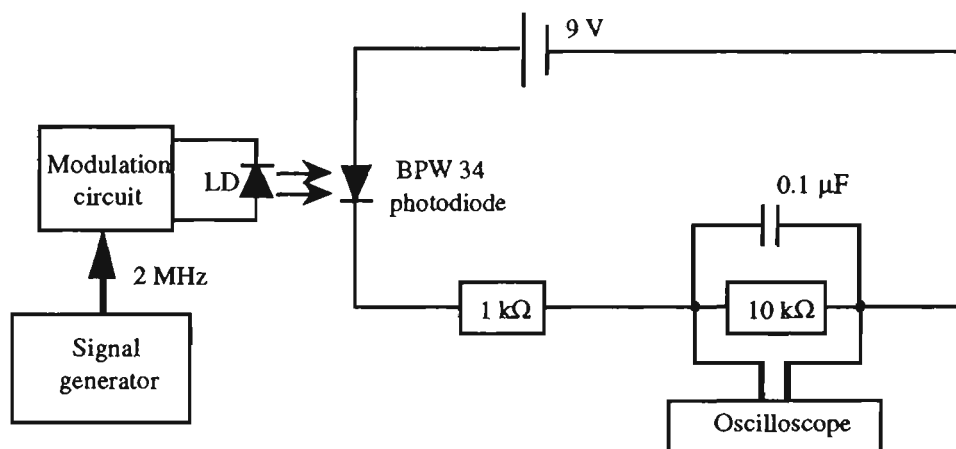


Fig 5.4 Arrangement used to measure the depth of modulation of the LD

The depth of modulation can be optimised by changing the emitter impedance ( $Z_e$ ) of the ATO1635 transistor (Fig 5.2) (Horowitz and Hill, 1989), although any change will also affect the frequency response of the circuit. To optimise the depth of modulation while maintaining a relatively flat frequency response (Fig 4.4(a)), several trials with different  $Z_e$  were conducted before a suitable value was found. The optimum modulation signal shown in Fig 5.5 has a DC voltage of 262.1 mV and a half peak-to-peak voltage of 166 mV, and therefore a modulation depth of 63%.

Although the modulation depth was measured at 2 MHz, rather than at the modulation frequencies employed in this experiment, this should still be a reliable estimate of the actual depth of modulation. The figure obtained, of 63% is a reasonable value to work with.

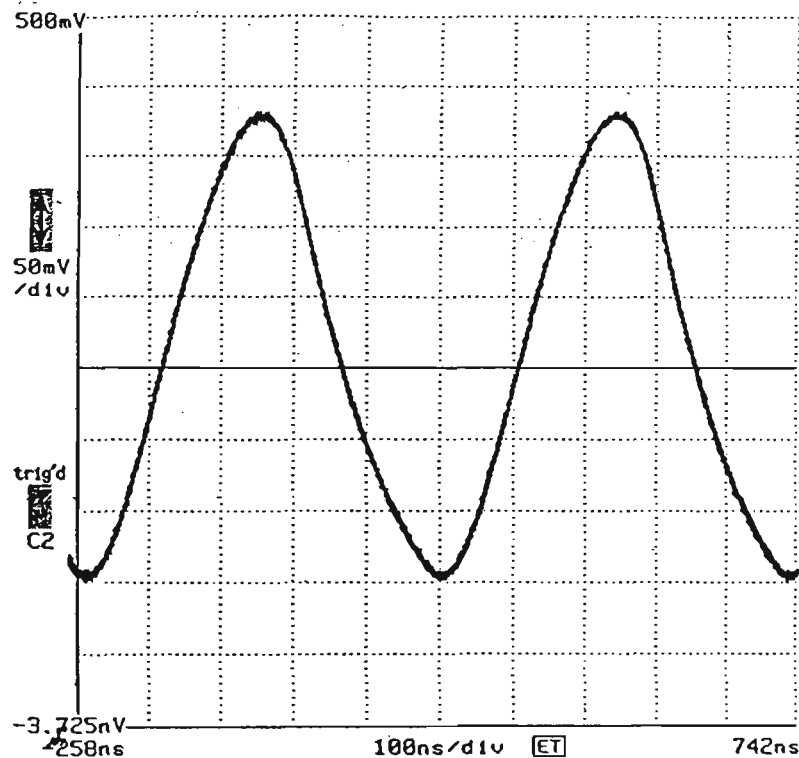


Fig 5.5 Intensity modulation of the laser diode output

### 5.3 Photodetector circuit

A silicon PIN photodiode (008 UDT) was selected because of its good responsivity, low dark current and large bandwidth (section 2.2.3). Its typical responsivity at 780 nm is 0.4 A/W, and its response time of 0.25 ns is fast enough to detect signals up to several hundred megahertz. The dark current is 0.02 nA. The photodetector's transconductance amplifier circuit is shown in Fig 5.6 (Shelamoff, 1992). Two wide bandwidth amplifiers were used, namely an Avantek ITA-12318 transimpedance amplifier which has high gain (72.5 dB)

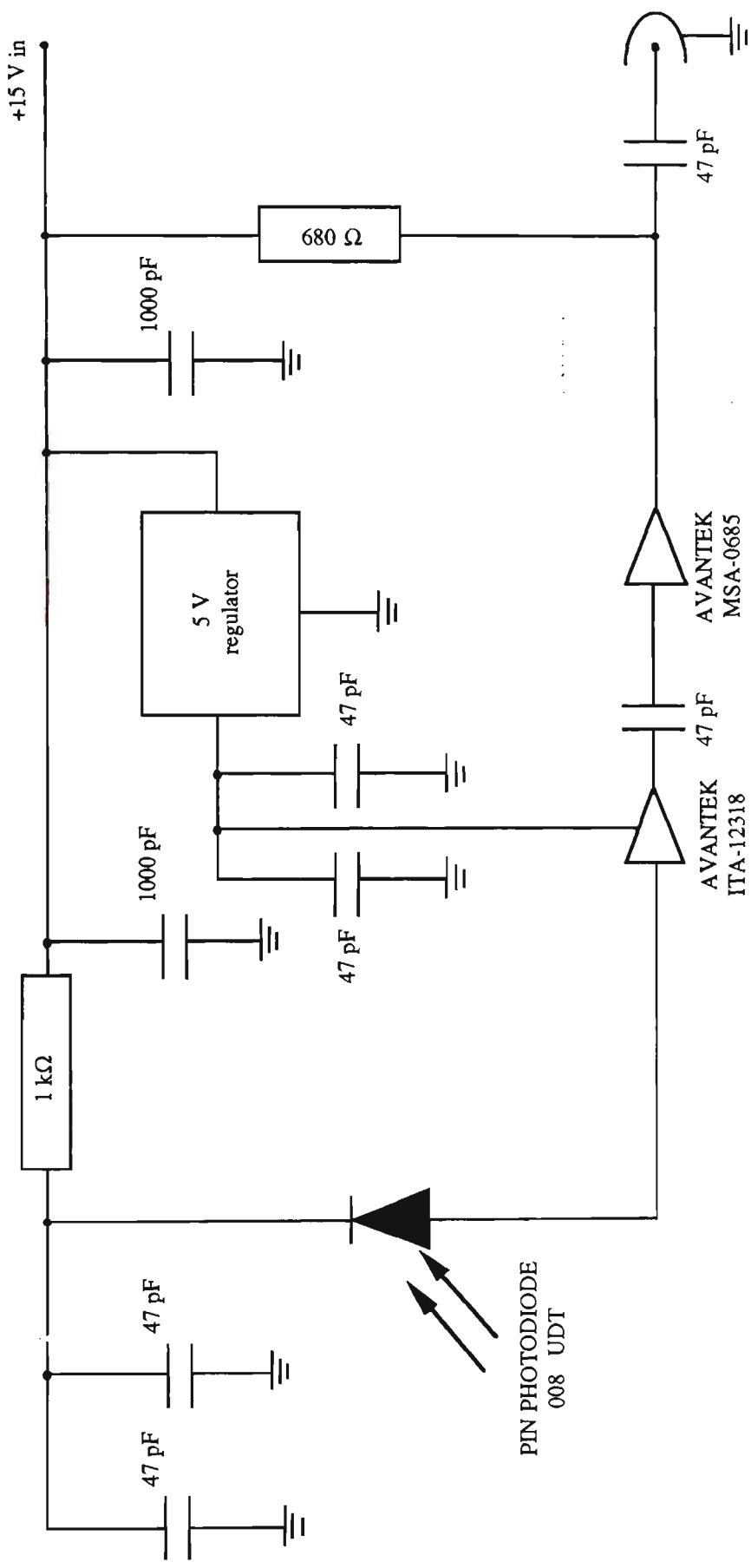


Fig 5.6 Detector circuit

and a bandwidth of 750 MHz, and an Avantek MSA-0685 integrated amplifier whose gain is 18.5 dB around 500 MHz with a bandwidth of 800 MHz. Thus the total gain of this amplifying circuit is 91 dB, but to ensure a linear response, the maximum optical power into the photodetector was limited to -9 dBm.

#### 5.4 Frequency response of the combined source and detector system

The arrangement used to measure the system's frequency response is shown in Fig 5.7. Since the maximum optical input power allowed by the detector is -9 dBm (section 5.3), and the power from the laser diode is -2.4 dBm (section 5.2.1), a variable optical attenuator was required. An Advantest TR4153A tracking generator with 0 dBm output was employed to modulate the laser diode, and the detector circuit output was displayed on an Advantest TR4131 RF spectrum analyser. This RF spectrum analyser has a wide adjustable bandwidth from 100 kHz to 4 GHz .

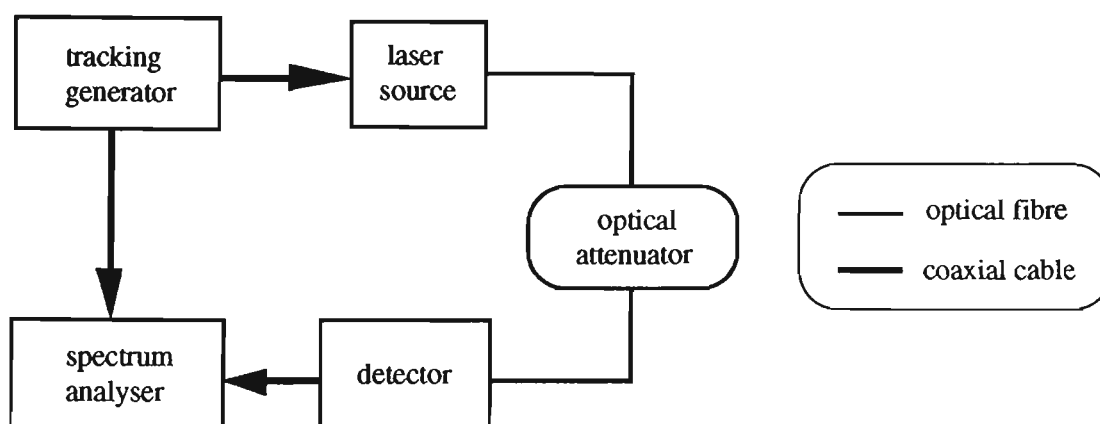


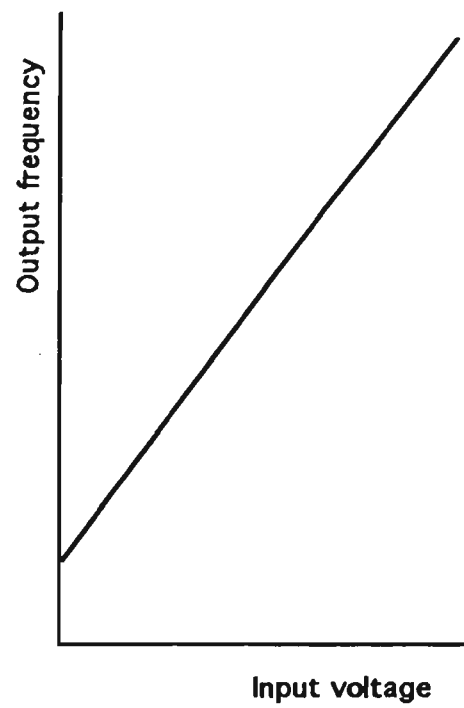
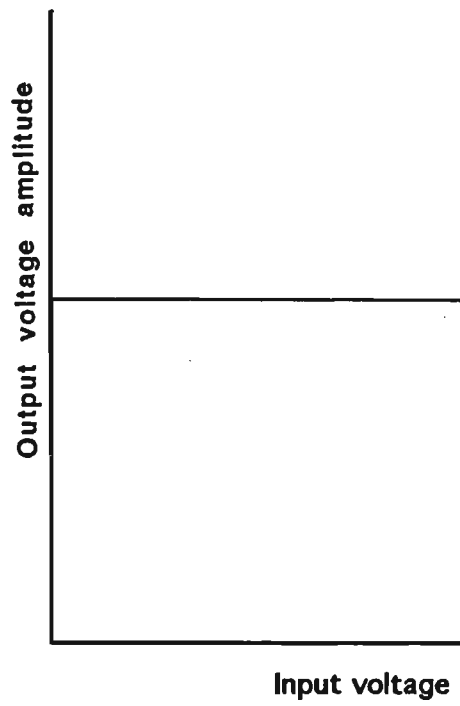
Fig 5.7 Measurement of the system's frequency response

In order to attain a uniform spectral response, several components in the detector's circuit were found to have a significant effect. These component values were varied in an attempt to optimise the spectral response. The best

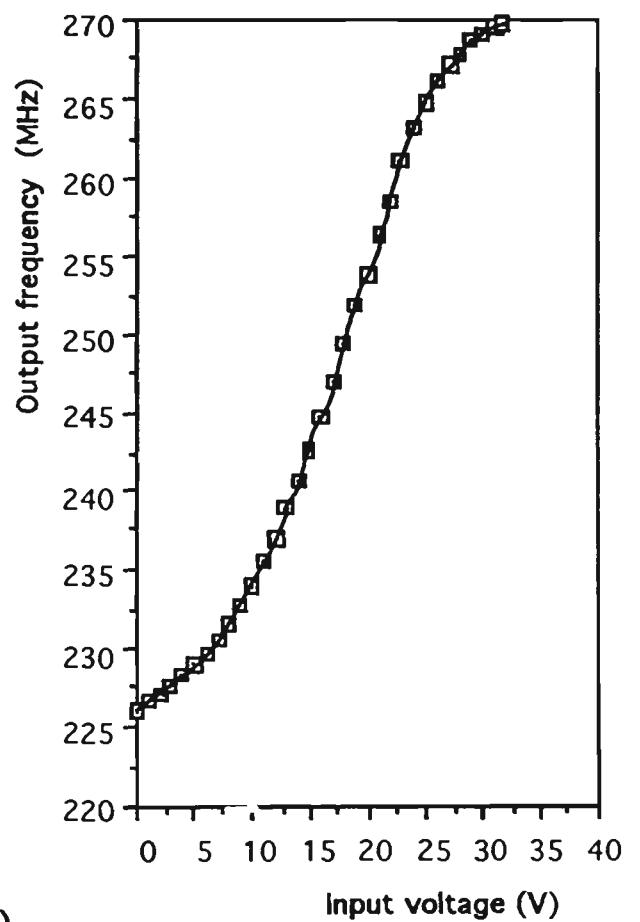
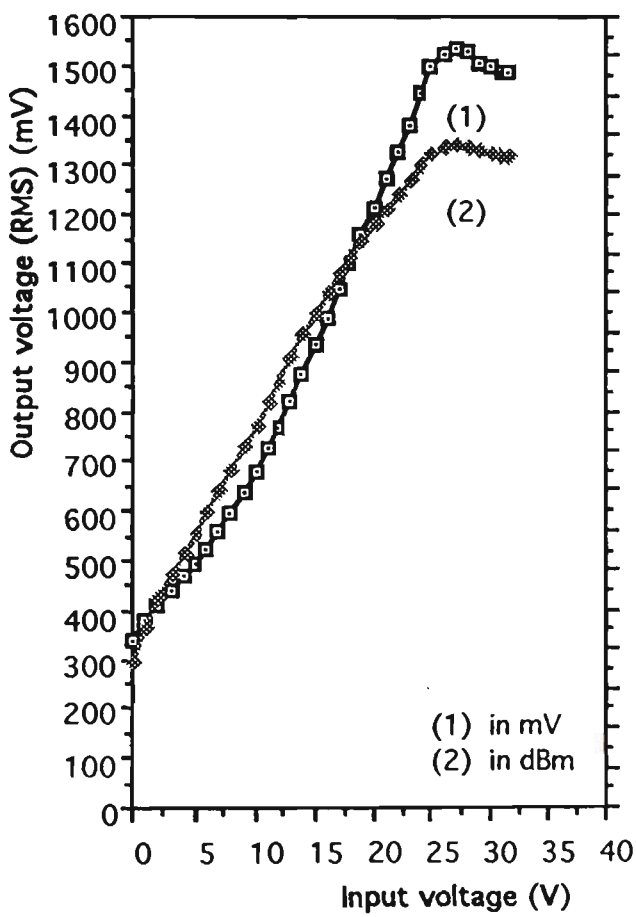
spectral response is illustrated in Fig 4.4(a), which shows that the system 3 dB bandwidth covered the band 75 to 975 MHz. This figure was compatible with the modulation frequencies obtained from the VCOs (section 5.5), namely 226 to 271 MHz and 300 to 680 MHz.

## 5.5 Voltage-controlled oscillators (VCOs)

Two VCOs were used in these experiments. The Type 9036 VCO (Research Communications Ltd.) has a sweep frequency range from 226 MHz to 271 MHz corresponding to the voltage range of 0 to 32 V and has a gain control to adjust the output power. For an ideal VCO the dependence of the output voltage amplitude and output frequency upon the input voltage should be as shown in Fig 5.8(a). Unfortunately, the response for this VCO was far from ideal (Fig 5.8(b)). A second VCO (Avantek VTO-9032) has a sweep frequency range from 300 MHz to 680 MHz corresponding to the voltage range of 0 to 20 V, and its output characteristics are shown in Fig 5.9. It should be noted from Fig 5.8(b) and Fig 5.9 that the output powers were not constant and the output frequencies were not in a linear relationship with the input voltage. These factors explain why the observed beat signal amplitudes and beat frequencies (sections 6.4, 6.5, 6.6) were not uniform over the ramp as anticipated from Fig 4.1(b). Furthermore the measurements of these VCO characteristics were under static conditions whereas both VCOs were employed under dynamic conditions. However, since the ramp frequency selected to drive the VCO was very low (100 Hz), there should be no difference between the static and the dynamic state.



(a)



(b)

Fig 5.8 Output characteristic of (a) an ideal VCO and (b) the Type 9036 VCO

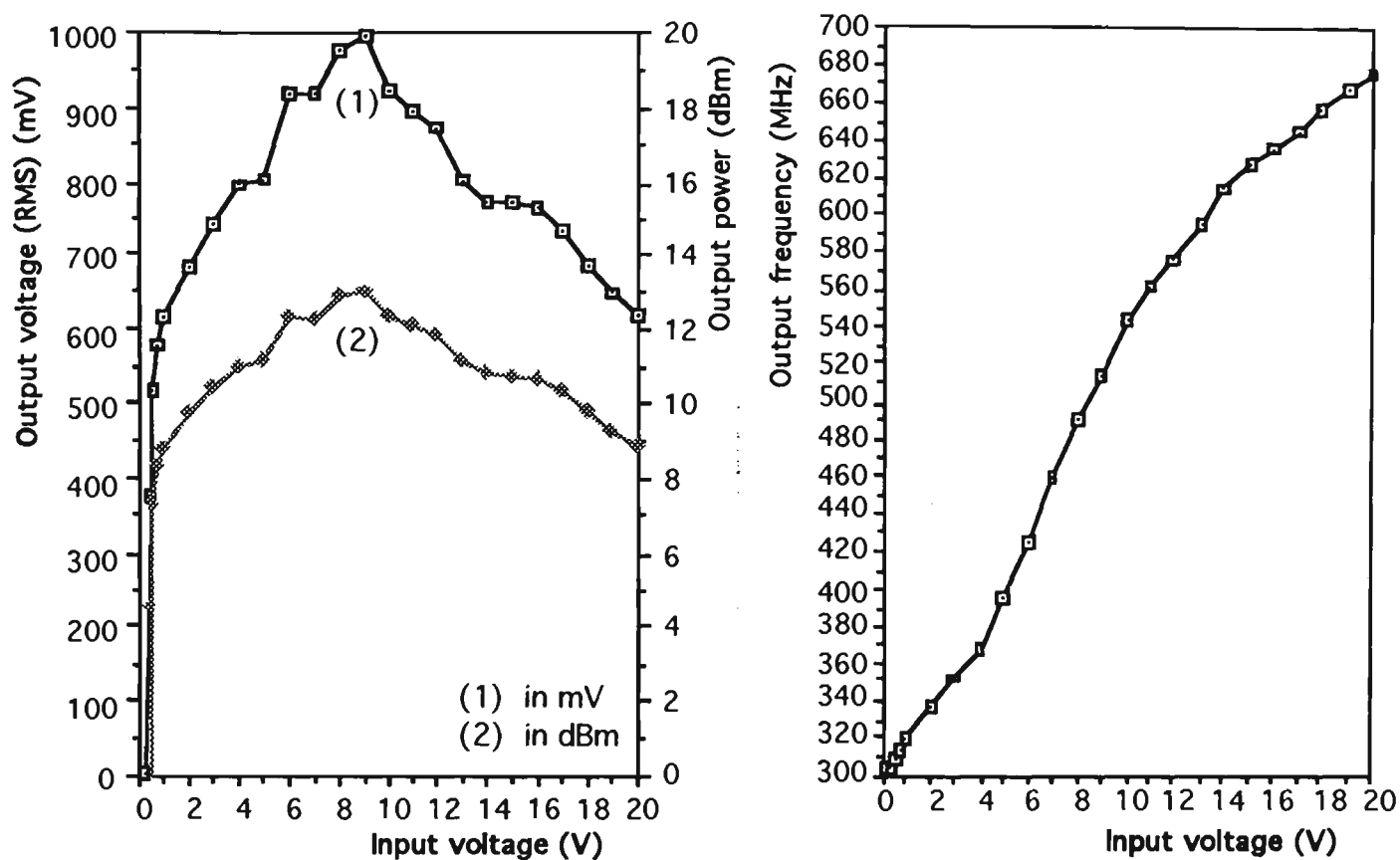


Fig 5.9 Output characteristics of the VTO-9032 VCO

### 5.5.1 Attenuators for the VCO output

The maximum input modulation power allowed for the laser source (section 5.2.1) was specified as 0 dBm, whilst the maximum output power from the Type 9036 VCO was, in fact, 17 dBm (Fig 5.8(b)). Therefore a 17 dB attenuator with 50  $\Omega$  input and output impedance, shown in Fig 5.10, was constructed. When the Type 9036 VCO's output was connected through this attenuator, the suitable characteristics shown in Fig 5.11 were obtained. The output voltage amplitude is thus reduced to the required amount, whilst the frequency response is unaffected.

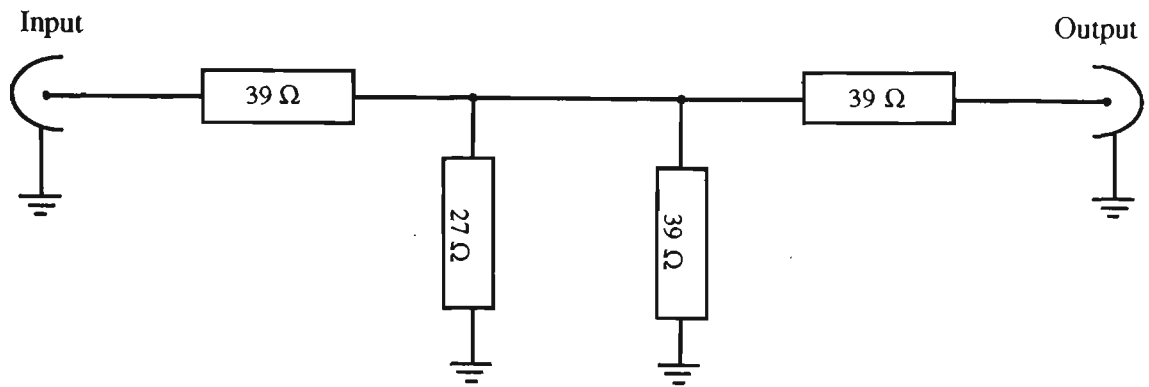


Fig 5.10 17 dB attenuator

The characteristics for the Avantek VTO-9032 VCO (Fig 5.9) show that its maximum output power is 13 dBm, so a commercial 13 dB attenuator was acquired. When using this attenuator in conjunction with this VCO, the output static characteristics shown in Fig 5.12 were obtained, and indicate that the overall output voltage amplitude has been suitably reduced without affecting the frequency response.

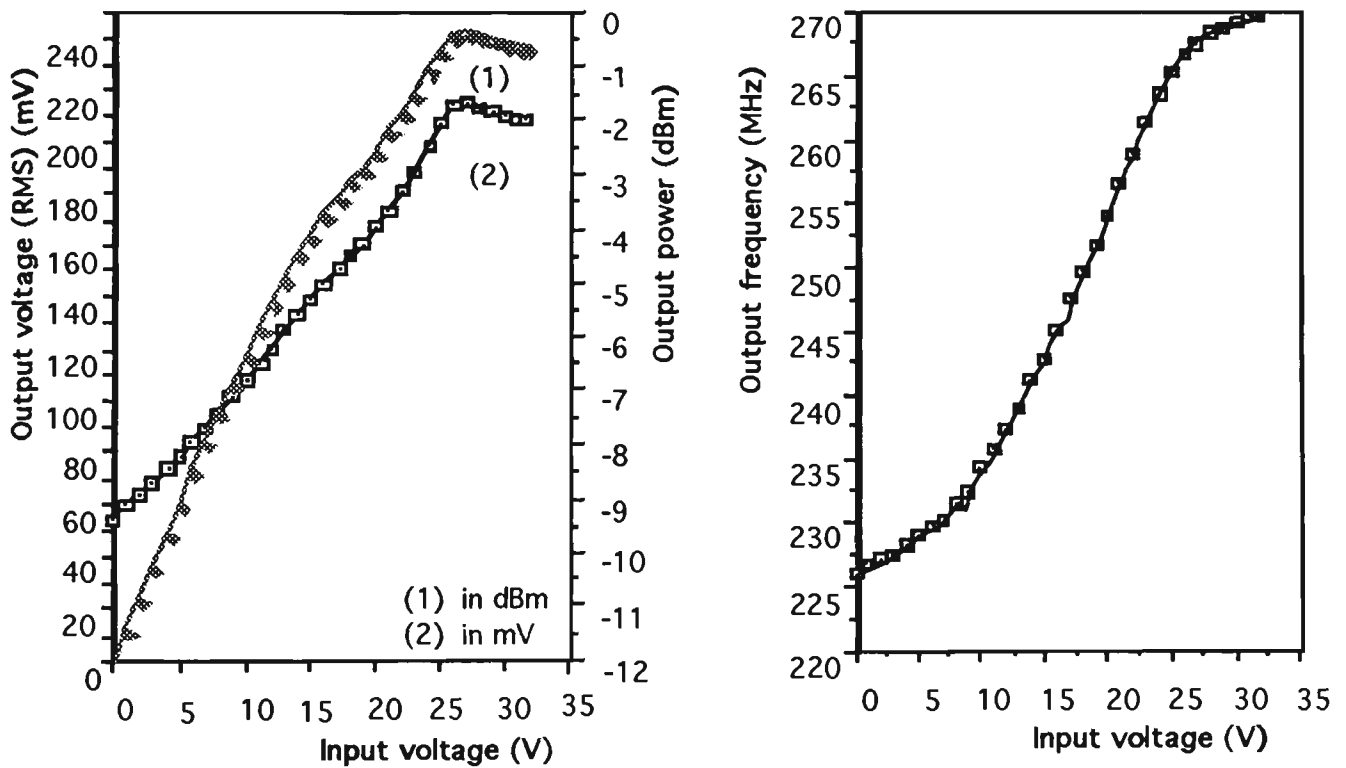


Fig 5.11 Output characteristics of Type 9036 VCO plus 17 dB attenuator

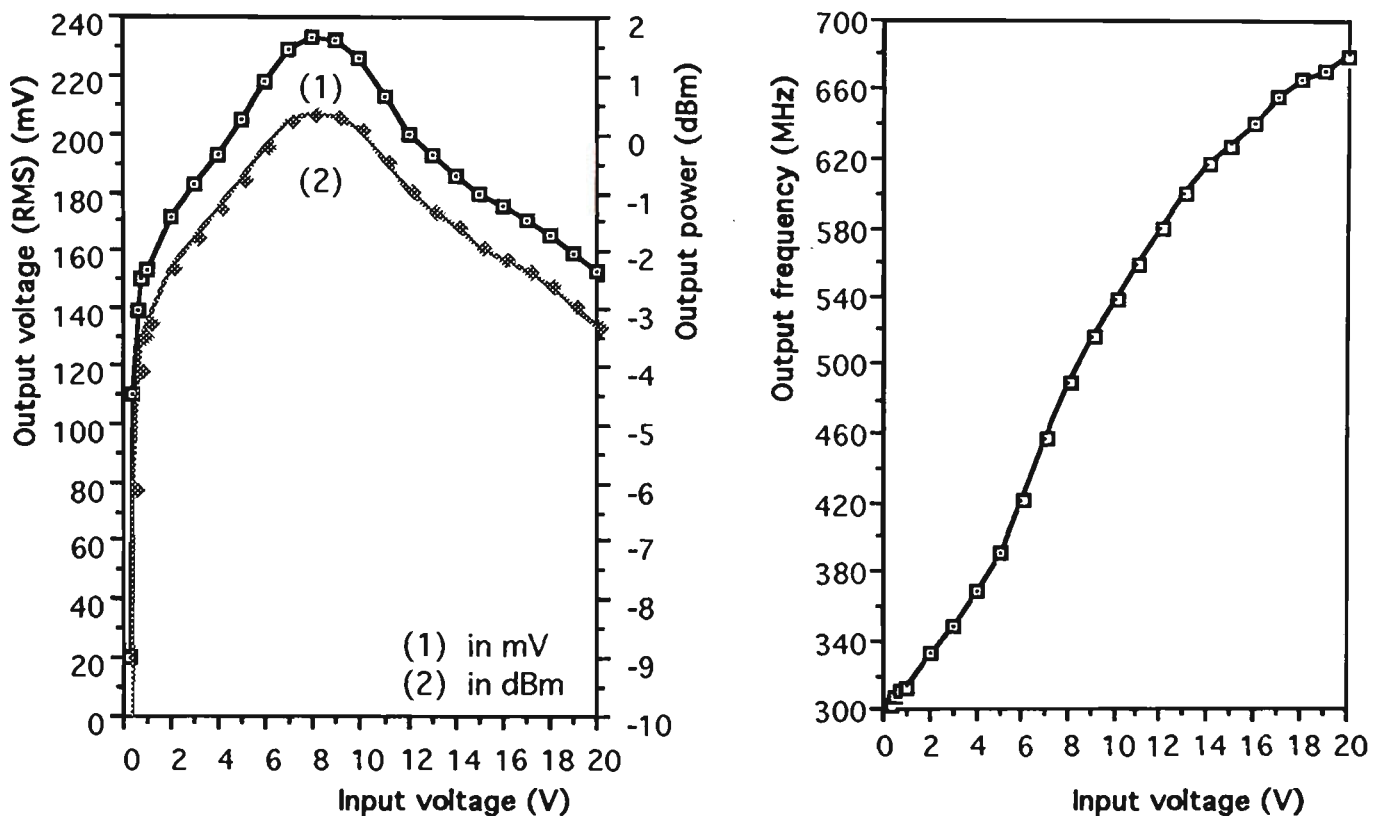


Fig 5.12 Output characteristics of VTO-9032 VCO plus 13 dB attenuator

## 5.6 Optical fibres and directional coupler

### 5.6.1 Optical fibres

50/125  $\mu\text{m}$  graded index multimode optical fibre (section 2.2.2) was used throughout these experiments. Two pigtailed were used to connect the laser diode to the coupler and the coupler to the photodetector. A length of around 25 metres of fibre was used for the reference path. Two GTE Fastomeric mechanical splices (Fibre Optic Products) and a number of fusion splices were used for necessary connections (section 2.3). The typical losses through the mechanical splice and fusion splice were about 0.5 dB and 0.1 dB, respectively.

### 5.6.2 Directional coupler

A 2×2 fused biconically-tapered directional coupler (Fig 5.13) was selected to split the light from the laser source into the two required paths (Palais, 1984). It was designed to provide low loss coupling with a range of splitting ratios. The splitting ratio of the coupler is 50:50 at a central operating wavelength of 850 nm. The characteristics of this coupler operating at 780 nm were obtained by using the arrangement given in Fig 5.14. It was found that the power distribution between the paths was equal, with some loss in the coupler. Assuming the loss in the mechanical splice was 0.5 dB and the loss in the fusion splice was 0.1 dB, then the excess loss of the coupler was 0.5 dB.

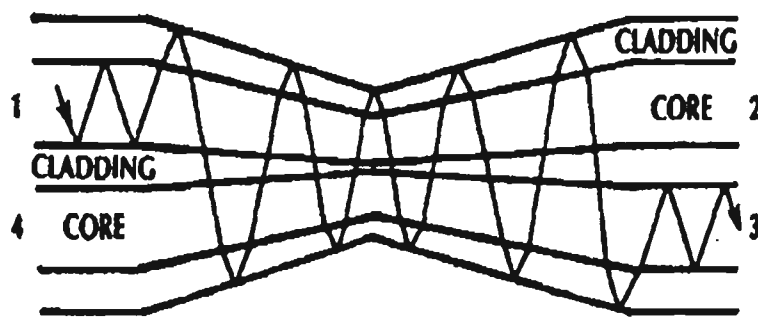


Fig 5.13 Fused biconically-tapered directional coupler

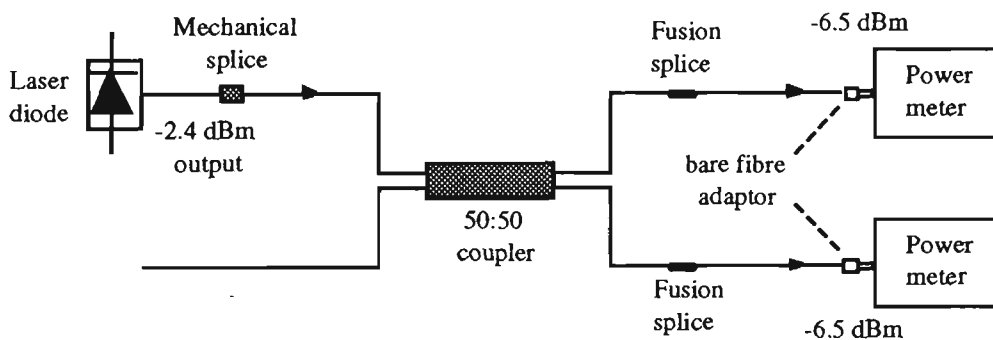


Fig 5.14 Testing of coupler splitting ratio

## 5.7 Other optical components

### 5.7.1 Collimators

Two lenses were selected for collimating the light launched into the air from the optical fibre end. A single microscope objective with magnification of  $\times 20$  and a 4 mm focal length was used initially. However as a microscope objective is designed for short distance collimation only, it did not perform well over long distances ( $\sim 5$  m). A 1 m focal length thin lens was used in addition to the microscope objective in order to improve the collimation, but even then the results were still far from ideal (section 6.3).

As a different approach, an 8 cm focal length concave mirror was used as a collimator, with the optical fibre end located at its focus. The collimated light spot was larger than that obtained with the lenses but, more importantly, provided greatly improved collimation (section 6.3).

### 5.7.2 Reflectors

Three types of reflectors were used in this work. The first was a thin film ( $TiO_2$ ) reflector which was deposited onto one end of a fibre using vacuum coating techniques (Stuart, 1983), the second was a simple front-coated mirror and the third was a corner cube (Smith, 1970). A very high reflectance (up to 90%) can be achieved with a thin film coating, but the film degrades with time, so a good quality reflection signal can not always be guaranteed. Front-coated mirrors are lower in cost and suitable when high reflectivity is not demanded. Corner cubes are designed to reflect any ray or beam entering the prism face back in the same direction, but with an offset, regardless of the orientation of the prism

(Edmund Scientific Co., 1989). Since a mirror will only do this at normal incidence, corner cubes are ideal when precision alignment is difficult or time-consuming. There are three total internal reflections within the corner cube (Smith, 1970) as shown in Fig 5.15.

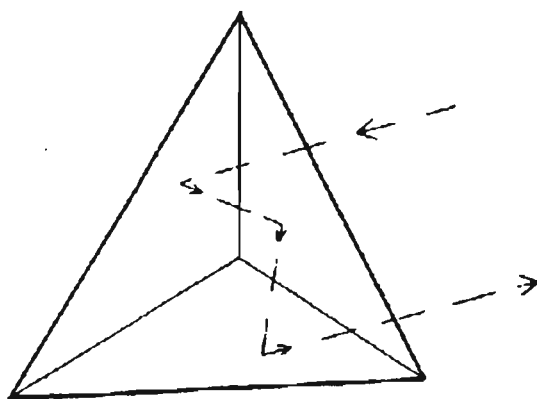


**Fig 5.15** Corner cube reflection

## 5.8 Electrical processing of detector output

The output of the basic experimental arrangement shown in Fig 5.1 was an RF carrier being modulated at the beat frequency (section 3.5 and Fig 6.9). A variety of circuits were built in an attempt to demodulate the output and obtain a more useful signal from the sensor. Whenever circuits involving high frequencies were required, special care was taken to ensure that unwanted capacitive or inductive effects on circuit boards were minimised (Bowick, 1991).

### 5.8.1 Bandpass filters

For the Type 9036 VCO, the output sweep frequency range is from 226 MHz to 271 MHz (section 5.5). A bandpass filter corresponding to this frequency range was designed (Bowick, 1991) in order to reduce the output noise level (section

4.3.3), and is given in Fig 5.16. However, mutual inductance between components resulted in several unexpected resonances, and was reduced by placing two copper shielding plates between the components. With the filter included (Fig 5.17), the system's response spectrum was as shown in Fig 4.5(a). The resultant 3 dB bandwidth was from 170 MHz to 330 MHz, and the insertion loss was very small which can be seen by comparing the maximum response shown in Fig 4.4(a) and Fig 4.5(a).

For the Avantek VTO-9032 VCO, the sweep frequency range was 300 MHz to 680 MHz (section 5.5). Another bandpass filter was designed (Fig 5.18) (Bowick, 1991) for which the 3 dB bandwidth was from 200 MHz to 700 MHz, with a small insertion loss. The system's response spectrum, with the bandpass filter included, is shown in Fig 4.6(a).

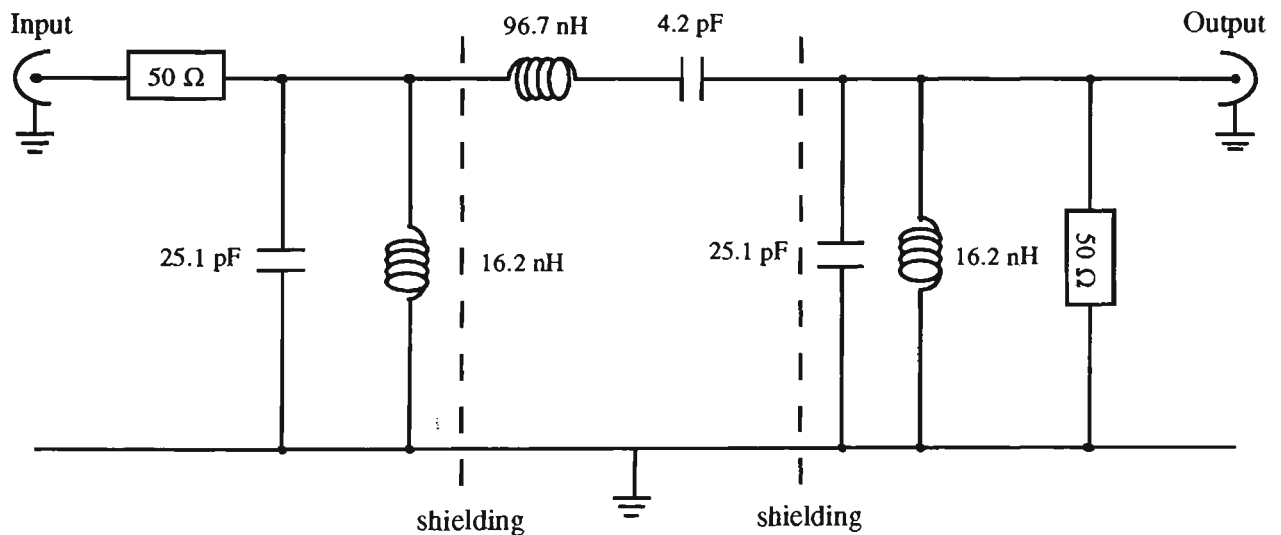


Fig 5.16 Bandpass filter circuit (170 MHz - 330 MHz)

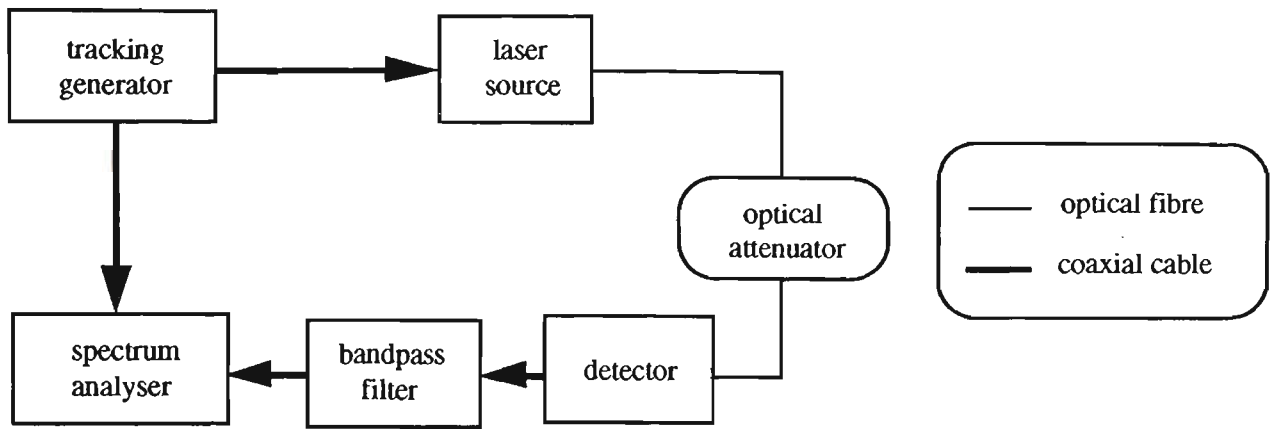


Fig 5.17 Measurement of the frequency response including the bandpass filter

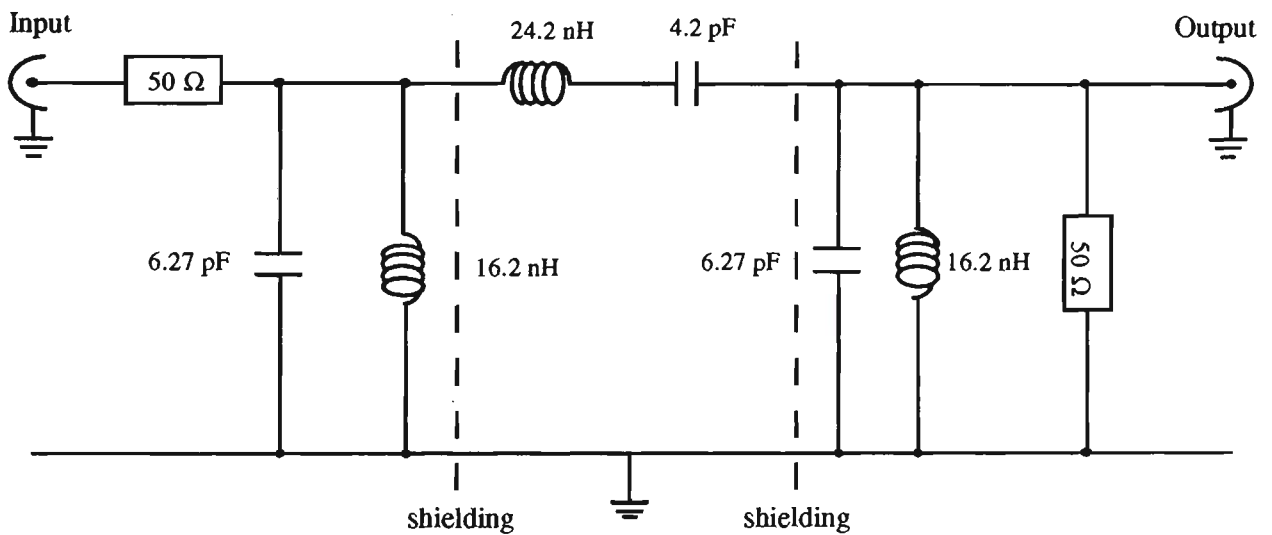


Fig 5.18 Bandpass filter circuit (200 MHz - 700 MHz)

### 5.8.2 Pre-amplifier

The photodetector was operating in a linear mode and so the two optical signals from the different paths were simply superposed upon one another at the photodetector and converted into an electrical signal, which had the form of an RF carrier being modulated at the beat frequency (Fig 6.9). In order to achieve a beat signal as a distinct frequency component, a non-linear circuit component, such as a diode, was required. However, the signal from the

photodetector was too small for a diode because of the usual cut-in voltage (Fortney, 1987). Therefore, a pre-amplifier circuit was designed (Fig 5.19), using a fast response Avantek MSA-0185 amplifier with 17.5 dB gain. Thus a sufficiently large signal voltage ( $\sim 200$  mV peak-peak) was obtained for use by the non-linear circuit.

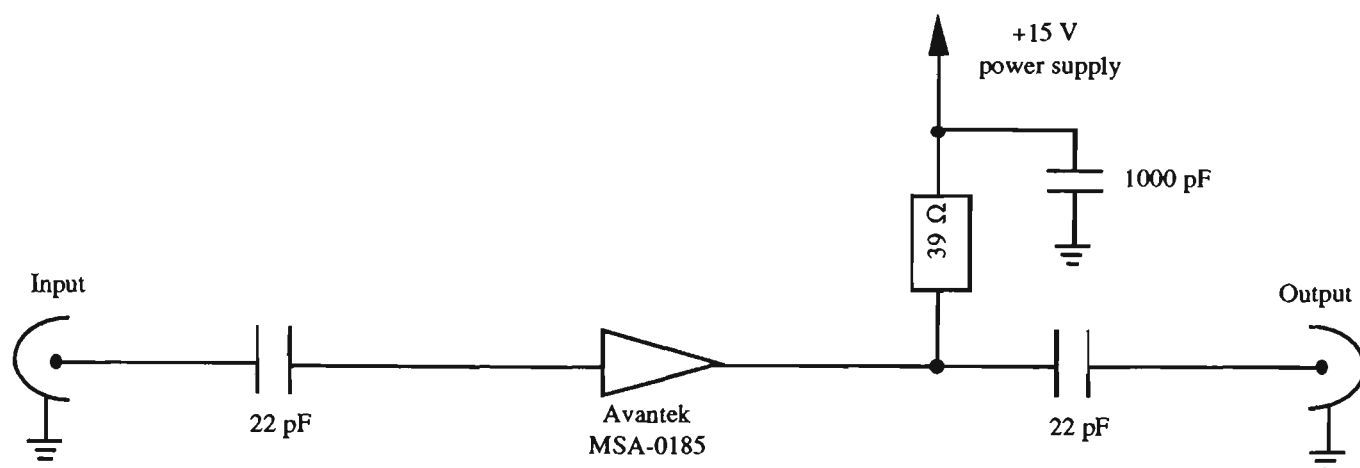


Fig 5.19 Pre-amplifier circuit

### 5.8.3 Electrical signal processor

A signal processor (Fig 5.20) was designed (Shelamoff, 1993) to analyse the output electrical signal from the photodetector. Firstly, to produce a beat frequency between the returned signals from the two optical paths, the signal was processed by a non-linear circuit in which a Sharp IN4148 high speed diode was used. In order to generate a signal at the beat frequency, the input signal must coincide with the non-linear part of the diode's forward voltage versus forward current curve. A variable resistor ( $R_1$ ) (Fig 5.20) allowed the DC bias voltage on the diode to be adjusted, and 460 mV was chosen as the operating point.

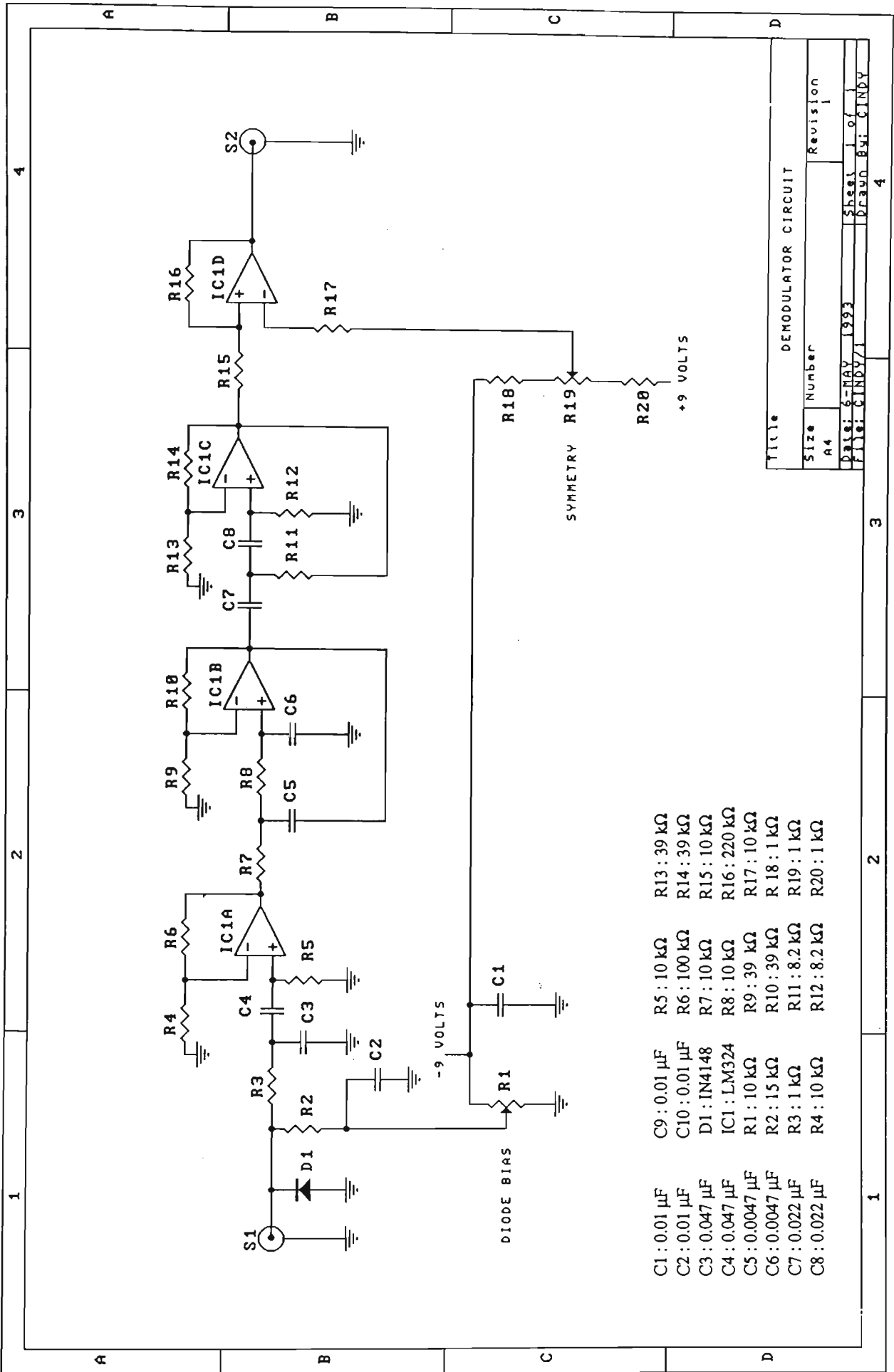


Fig 5.20 Signal processing circuit

The role of the non-linear circuit can be understood as follows (Horowitz and Hill, 1989):

When the input voltage (from the pre-amplifier (section 5.8.2)) lies within the non-linear part of the diode's forward voltage-forward current curve, the output current (I) will change with the input voltage (V) as below:

$$I = a + bV + cV^2 + dV^3 + \dots$$

where a, b, c, d ...are constants determined by the curve shape. The input voltage  $V = V_1 \sin\omega_1 t + V_2 \sin\omega_2 t$  (where  $V_1 \sin\omega_1 t$  and  $V_2 \sin\omega_2 t$  are the voltages due to the reference and target paths, and  $\omega_1$  and  $\omega_2$  are chirped and differ by a constant amount because of the path difference).

A simpler analysis than the Fourier analysis of the beat signal given in section 4.2 will be described here. Assuming cubic and higher order terms of I can be neglected, the output current will be

$$\begin{aligned} I &= a + b(V_1 \sin\omega_1 t + V_2 \sin\omega_2 t) + c(V_1 \sin\omega_1 t + V_2 \sin\omega_2 t)^2 \\ &= a + b(V_1 \sin\omega_1 t + V_2 \sin\omega_2 t) + c(V_1^2 \sin^2\omega_1 t + V_2^2 \sin^2\omega_2 t \\ &\quad + 2V_1 \sin\omega_1 t \times V_2 \sin\omega_2 t) \end{aligned}$$

Note that the terms  $V_1^2 \sin^2\omega_1 t$  and  $V_2^2 \sin^2\omega_2 t$  only have Fourier components at  $2\omega_1$  and  $2\omega_2$  respectively. The cross term may be rewritten as:

$$\begin{aligned} &V_1 \sin \omega_1 t \times V_2 \sin \omega_2 t \\ &= V_1 \sin \omega_1 t \times V_2 \sin (\omega_1 + 2\alpha\tau)t \\ &= \frac{1}{2} V_1 V_2 [ \cos (\omega_2 - \omega_1)t - \cos (\omega_2 + \omega_1)t ] \\ &= \frac{1}{2} V_1 V_2 [ \cos (2\alpha\tau)t - \cos (\omega_2 + \omega_1)t ] \end{aligned} \tag{5.1}$$

where  $2\alpha\tau$  is the beat angular frequency ( $750 \text{ Hz} \leq 2\alpha\tau \leq 4 \text{ kHz}$ ) defined in section 4.2.4. Using typical values,  $\Delta f = 100 \text{ MHz}$  and  $T_S = 0.01 \text{ s}$ , according to Eqn. 3.3, this frequency span restricts  $R$  to values between 11 m and 60 m. However, with the present arrangement, the air path is related to  $R$  according to Eqn. 6.2, and so by suitable choice of reference path length, the minimum and maximum air paths can be adjusted.

Apart from the first term in Eqn. 5.1, the other terms in  $I$  involve the frequencies  $(\omega_1, \omega_2, \omega_2 + \omega_1, 2\omega_1, 2\omega_2)$  which are in the RF region, and can be eliminated by a suitable filter, so that only the beat frequency  $(2\alpha\tau)$  remains.

After the non-linear circuit, circuitry using an LM324 quad operational amplifier (National Semiconductor Corporation) provided amplification, low pass and high pass filtering. The first op-amp circuit provided 20 dB gain, the second operated as a 4 kHz low pass filter with 3 dB gain, and the third as a 750 Hz highpass filter with a further 3 dB gain. (These frequency cut-offs were selected so that the signal processor would be compatible with the VTO-9032 VCO when its sweep range was from 424 MHz to 539 MHz.) The fourth op-amp circuit was a Schmitt trigger which transforms a sinusoidal beat signal into a square waveform for possible further processing. The overall signal processing scheme is summarised in Fig 5.21, and the corresponding signals of each processing stage are illustrated in Fig 5.22.

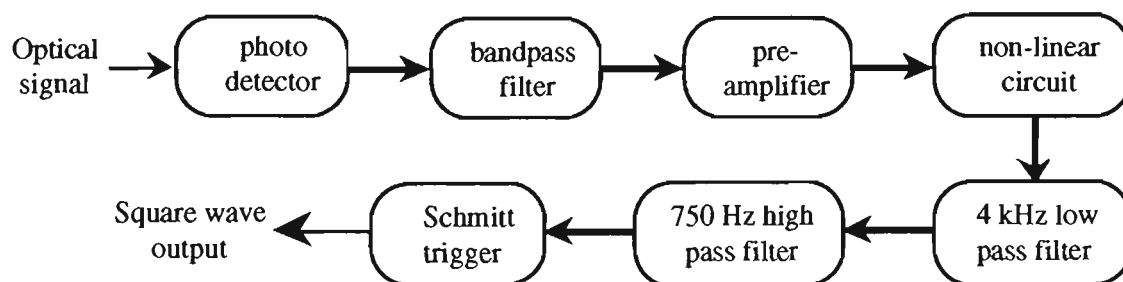


Fig 5.21 The overall signal processing scheme

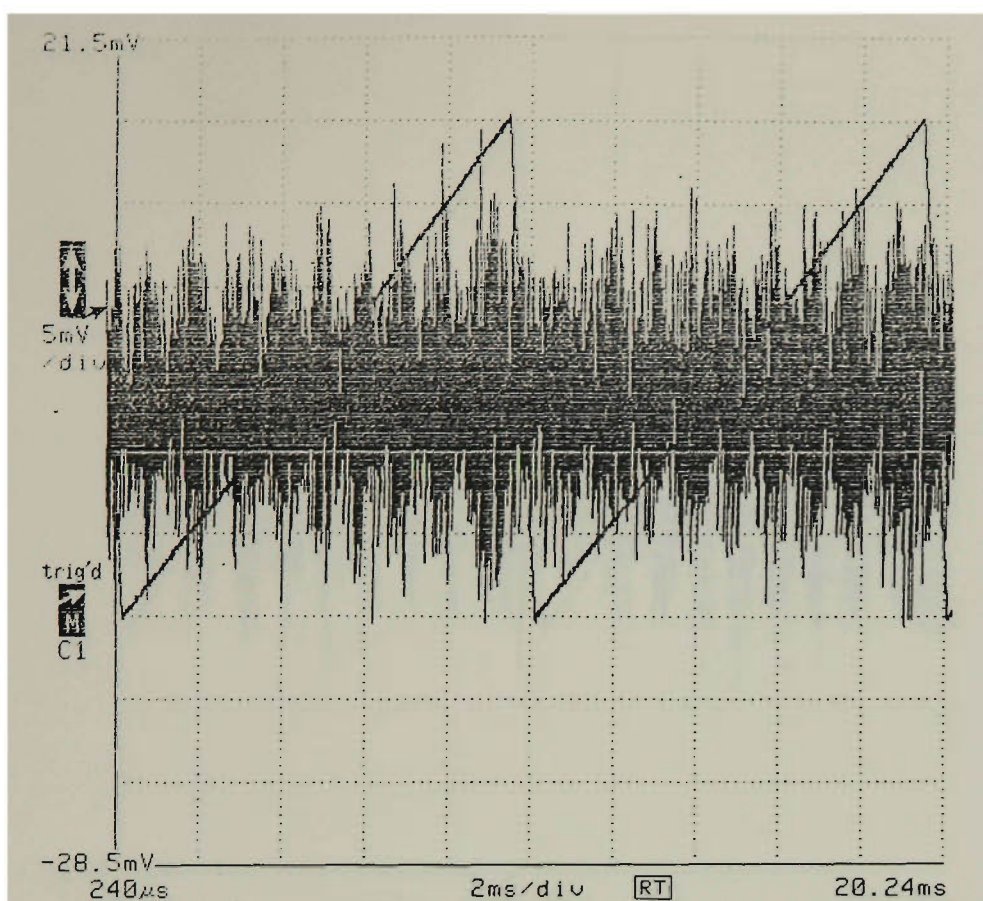


Fig 5.22 (a) Output of the photodetector

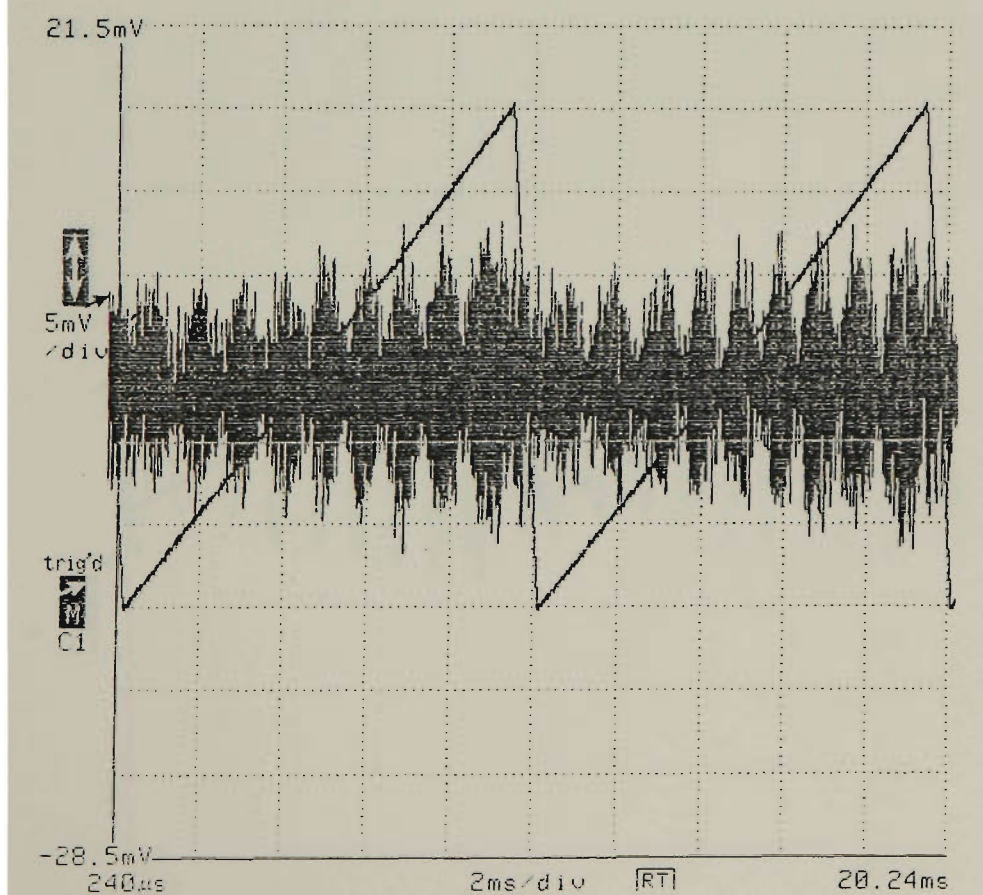


Fig 5.22 (b) Output of the bandpass filter

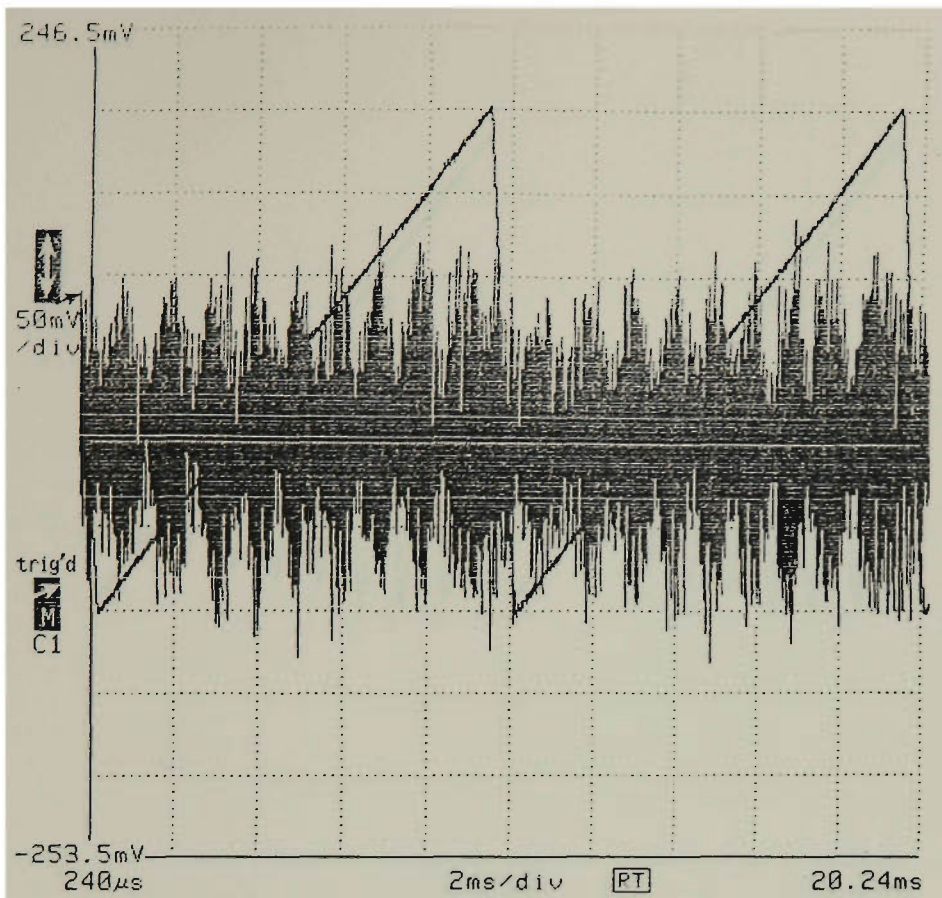


Fig 5.22 (c) Output of the pre-amplifier circuit

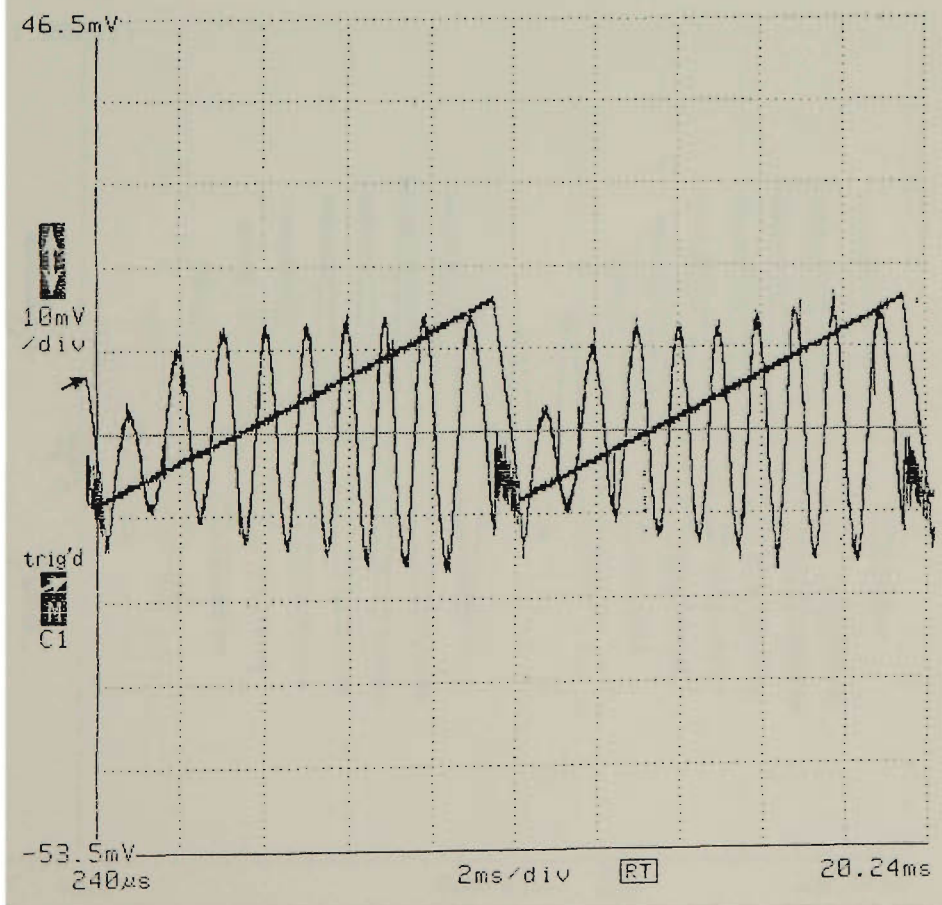
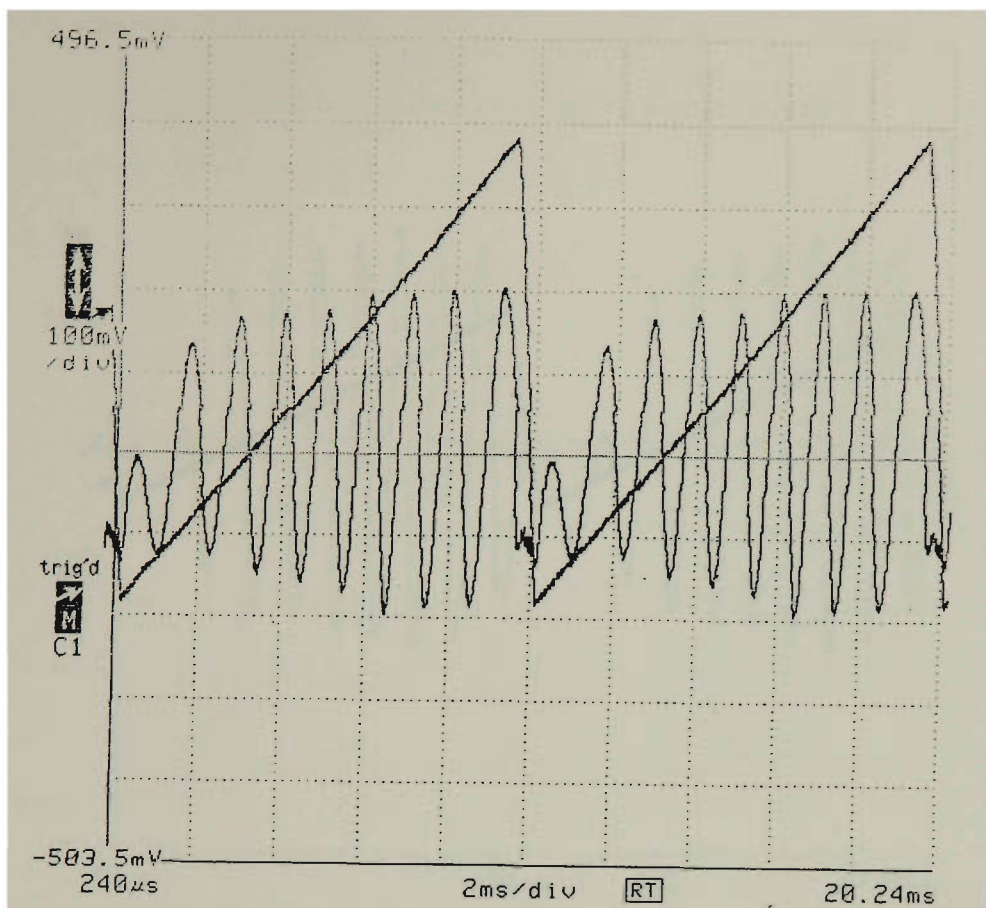
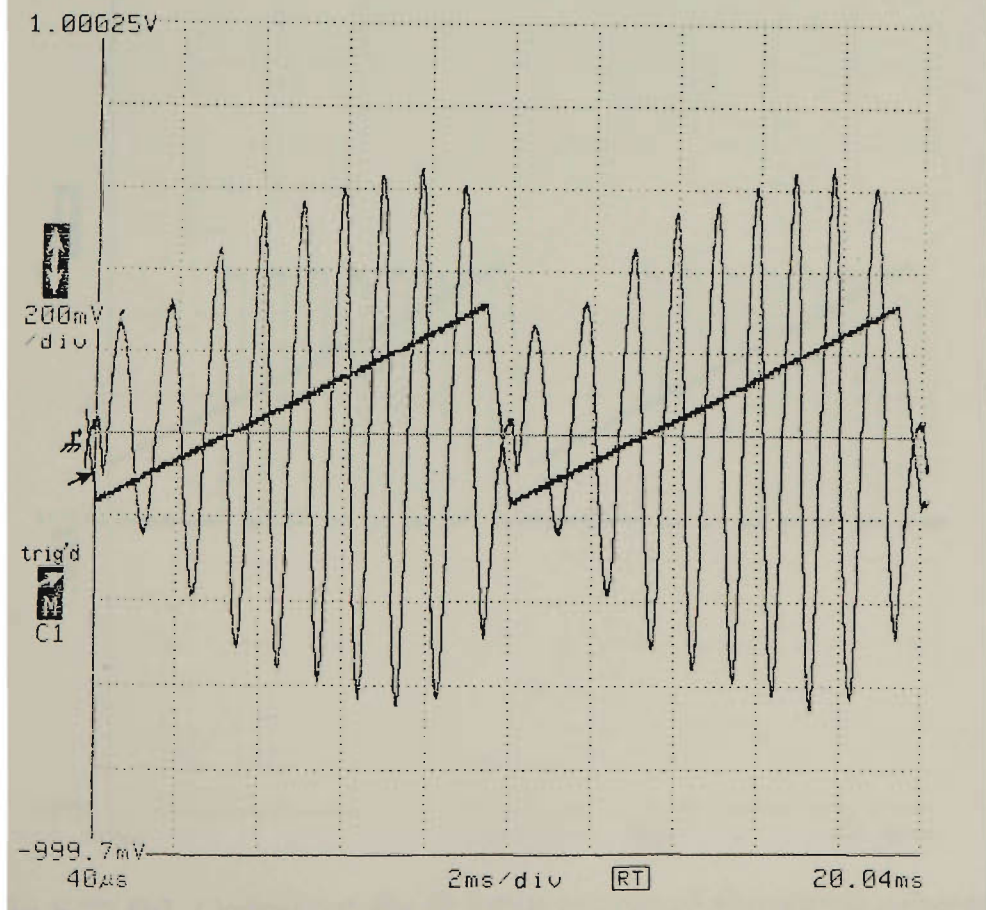


Fig 5.22 (d) Output of the non-linear part of the signal processor



**Fig 5.22 (e)** Output of the amplifier of the signal processor



**Fig 5.22 (f)** Output of the 4 kHz low pass filter of the signal processor

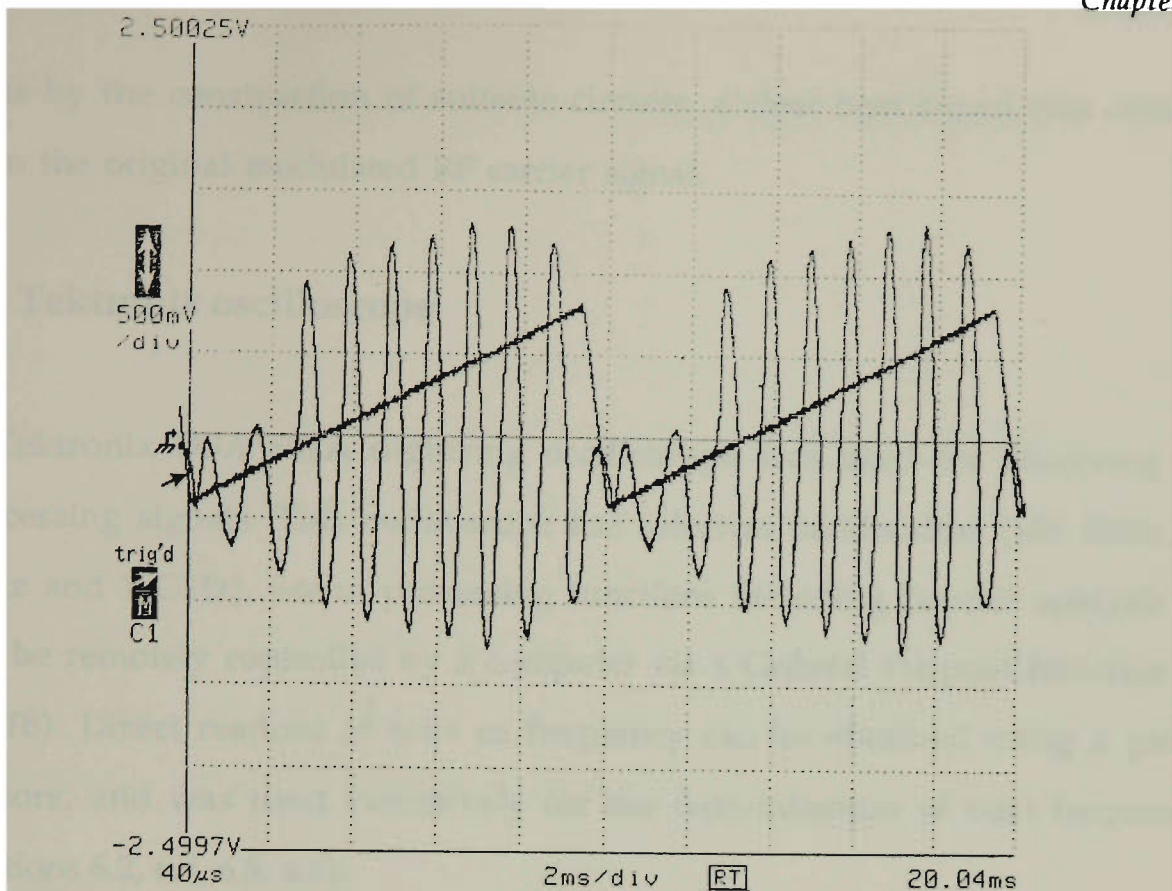


**Fig 5.22 (g)** Output of the 750 Hz high pass filter of the signal processor

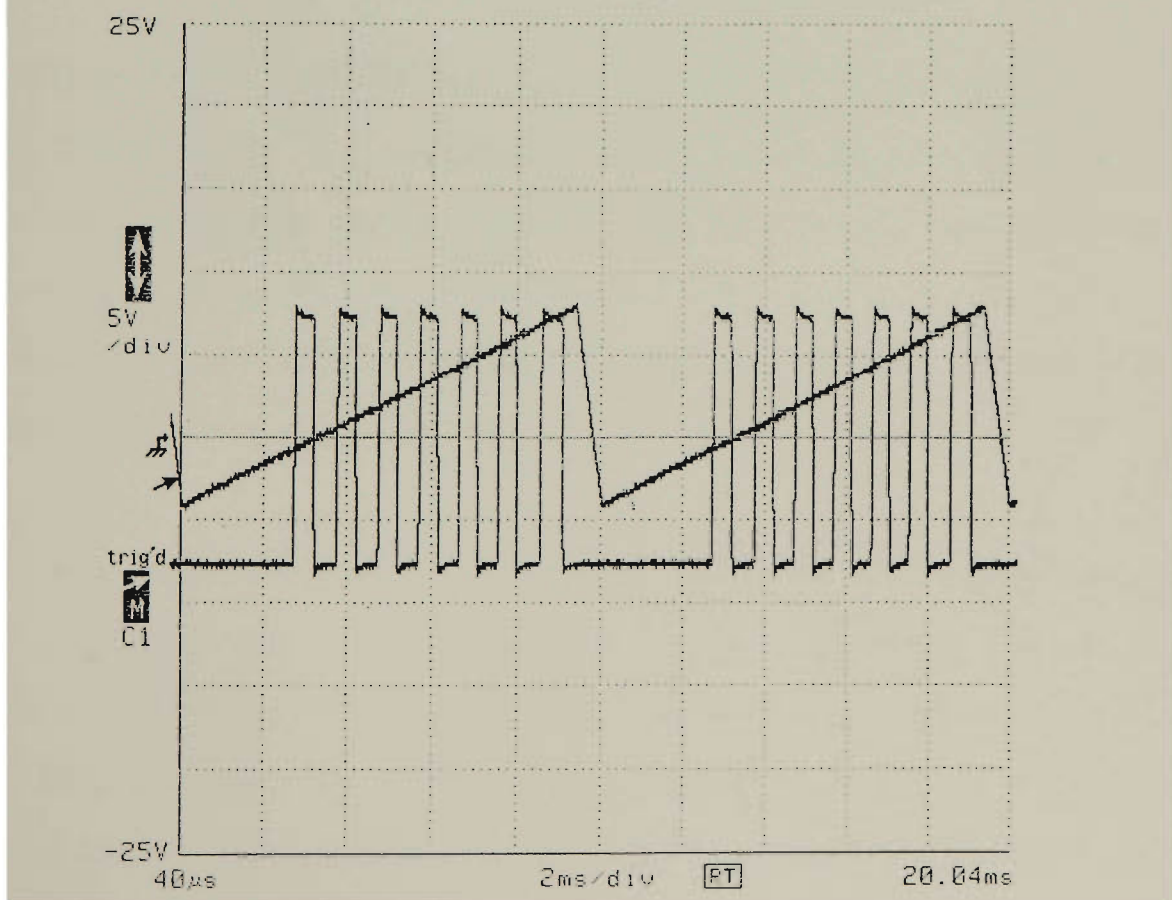


**Fig 5.22 (h)** Output of the Schmitt trigger of the signal processor

Thus by the construction of suitable circuits, a clear beat signal was obtained from the original modulated RF carrier signal.

## 5.9 Tektronix oscilloscope

A Tektronix DSA 602A digitising oscilloscope was used for observing and processing signals. This oscilloscope has selective bandwidths (100 MHz, 400 MHz and 1 GHz), useful processing functions including Fourier analysis and can be remotely controlled by a computer via a General Purpose Interface Bus (GPIB). Direct readout of time or frequency can be obtained using a pair of cursors, and was used extensively for the determination of beat frequencies (sections 6.2, 6.4, 6.5, 6.6).

## Chapter 6 Experimental results

### 6.1 Introduction

In this chapter the major experimental results are presented. Initially, by an electrical simulation the principle of FMCW was demonstrated (section 6.2). In order to optimise the optical coupling efficiency, various system alignments were tried and the best arrangement was selected (section 6.3). Several methods for the extraction of the beat frequency were also investigated and compared (sections 6.4, 6.5, 6.6). An anti-reflection (AR) coating was employed to minimise the unwanted Fresnel reflection (section 2.3).

### 6.2 Electrical simulation

In order to demonstrate the principle of FMCW (section 3.3) and to evaluate the suitability of the VCOs selected (section 5.5), an electrical simulation was performed. Here two coaxial cables of different length were used as the reference and test path. The chirped signals from each path were fed into an electrical multiplier (mixer) to form a beat signal which was displayed on the Tektronix oscilloscope (section 5.9).

The experimental configuration is shown in Fig 6.1. A 100 Hz sawtooth signal was used to modulate each VCO's output frequency (section 5.5). For the Type 9036 VCO, the sweep voltage was from 0 V to 29.2 V corresponding to the sweep frequency range from 226 MHz to 269 MHz (Fig 5.8(b)). Two different test cable lengths (14 m and 14.8 m) were used whilst the reference cable length was 1.03 m. The beat waveforms obtained and the input sawtooth wave are shown in Fig 6.2. There is no RF carrier present because it was eliminated by the mixer

circuit (Horowitz and Hill, 1989). The beat waveform is clearly evident, but since the output frequency of this VCO did not change linearly with the input voltage (Fig 5.11), the beat frequency was not constant over the duration of the ramp.

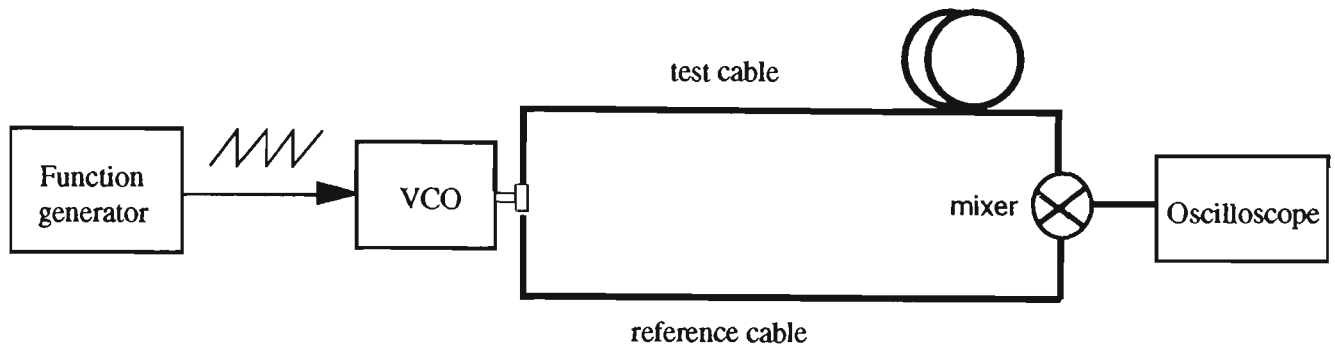
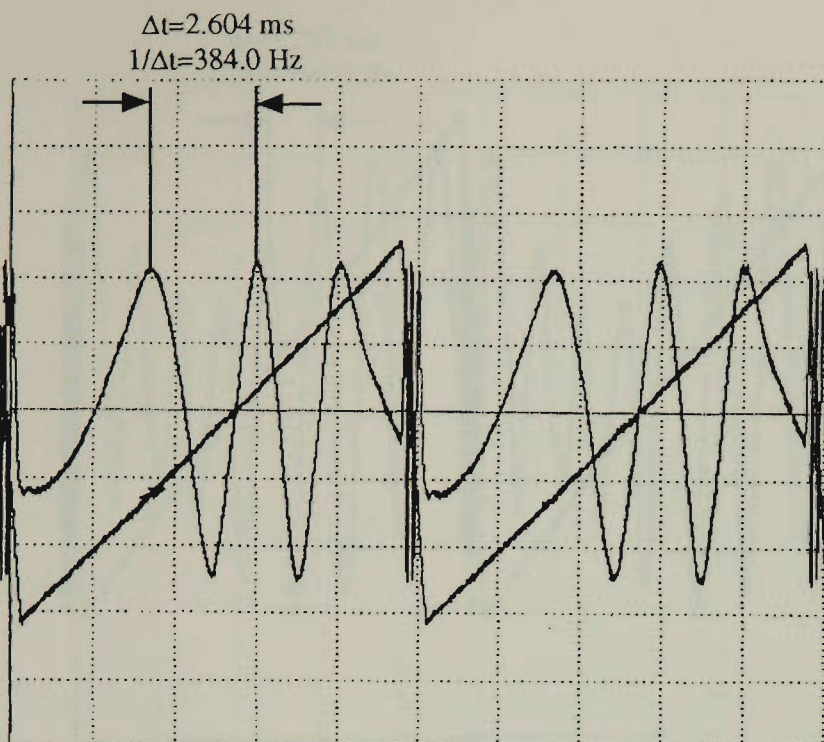
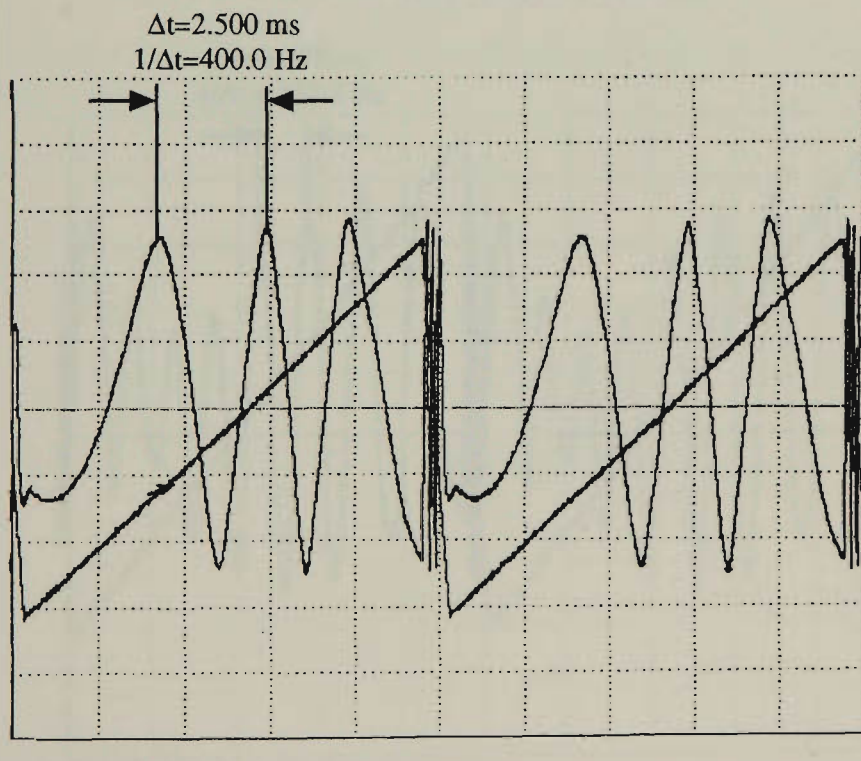


**Fig 6.1** Electrical simulation

The beat frequencies shown in Fig 6.2 were obtained from the portion of the ramp corresponding to the relatively linear part of the VCO's frequency response curve (Fig 5.11). However, when the expected beat frequency was calculated using Eqn. 3.3, differences between the measured and calculated values were apparent (384 Hz versus 277.5 Hz and 400 Hz versus 294.8 Hz). These mismatches occur because the sweep rate used in the calculation differed from that used in the measurement. These mismatches may be reduced by restricting the sweep voltage to a relatively linear sweep region. The minimum sweep voltage range is limited by the cable length difference in order that there be a sufficient number of cycles present (from Eqn. 3.3, number of beat cycles =  $\frac{f_{\text{BEAT}}}{f_{\text{ramp}}} = \frac{2\Delta f \times R}{c}$ ; here  $c = 2 \times 10^8$  m/s for coaxial cables). However, the difference between the two calculated values (294.8 Hz - 277.5 Hz = 17.3 Hz) is about the same as the difference between the two measured values (400 Hz - 384 Hz = 16 Hz), which suggests that despite the VCO's non-linearity, the beat frequency change could still be used to determine displacement.

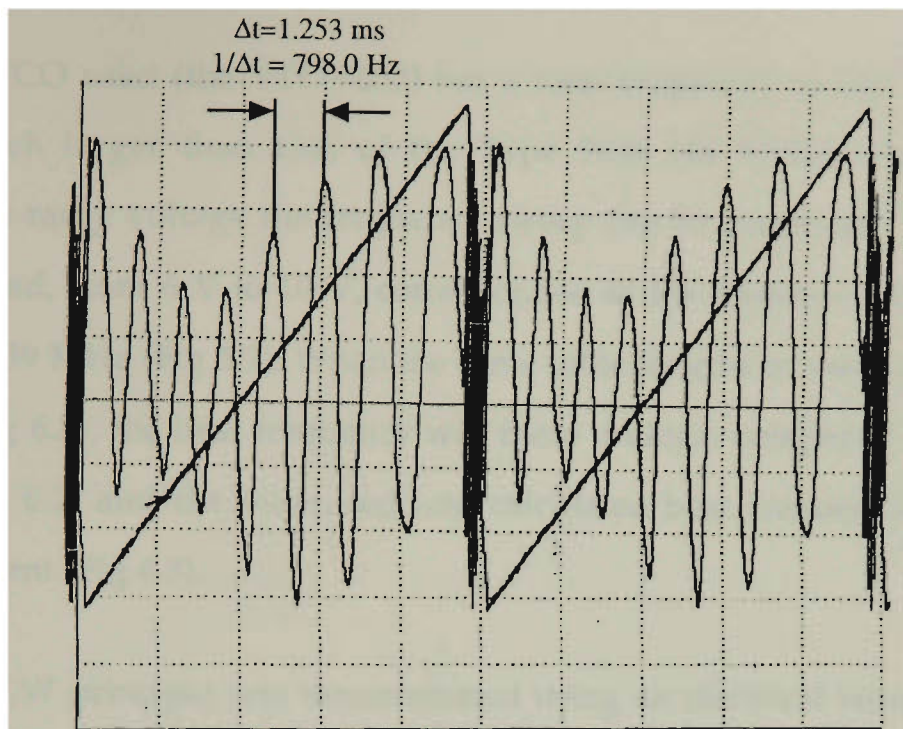


- (a) Cable length difference = 12.97 m  
 Measured beat frequency = 384.0 Hz  
 Calculated beat frequency = 277.5 Hz

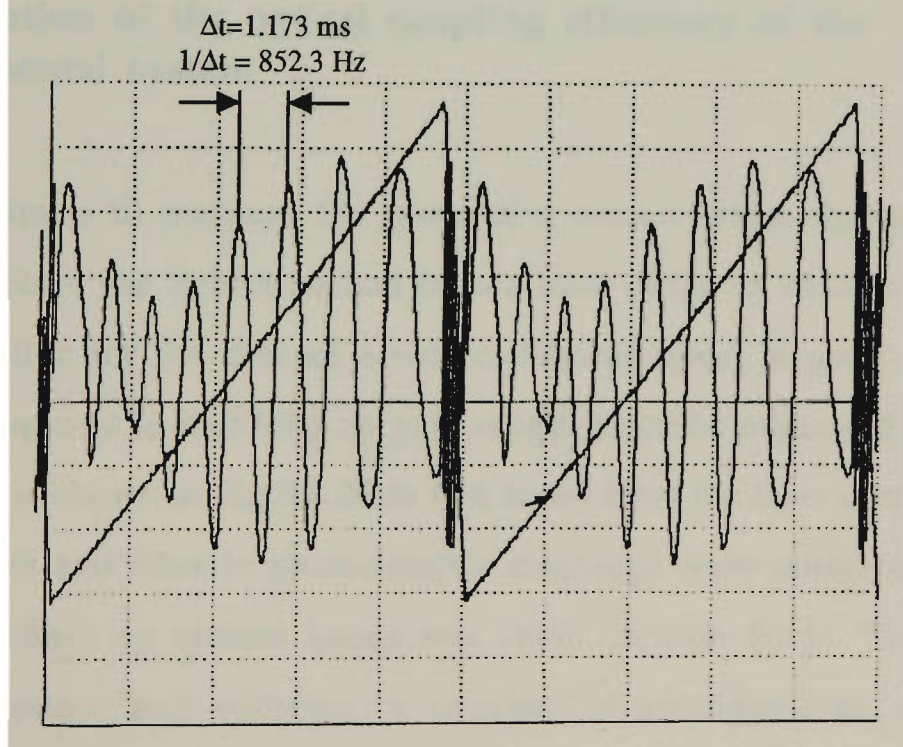


- (b) Cable length difference = 13.77 m  
 Measured beat frequency = 400.0 Hz  
 Calculated beat frequency = 294.8 Hz

Fig 6.2 Cable length measurements using the Type-9036 VCO



- (a) Cable length difference = 12.97 m  
 Measured beat frequency = 798.0 Hz  
 Calculated beat frequency = 750.3 Hz



- (b) Cable length difference = 13.77 m  
 Measured beat frequency = 852.3 Hz  
 Calculated beat frequency = 796.5 Hz

**Fig 6.3** Cable length measurements using the Avantek VTO-9032 VCO

The second VCO used (the VTO-9032) has a total frequency sweep (380 MHz) which is much larger than that of the Type 9036 (44 MHz). Therefore by restricting the ramp voltage the frequency sweep can be linearised. The sweep voltage selected, from 6 V to 10 V, corresponded to the frequency sweep from 424 MHz to 539 MHz (Fig 5.9). When the same cable lengths as used above were measured (Fig 6.3), the beat frequency was more uniform compared with those shown in Fig 6.2, and the measured and calculated beat frequencies were in better agreement (Fig 6.3).

Thus the FMCW principle was demonstrated using an electrical simulation. By using two different VCOs, the importance of a linear frequency sweep was clearly shown.

### **6.3 Optimisation of the optical coupling efficiency of the experimental system**

The project aim is to measure the range of a remote target through the air (section 1.2). Since the light launched from a laser diode or an optical fibre is diverging (unlike for the case of a well-collimated laser), a good alignment system was required so that long air path ranges could be measured. The basic system set-up is shown in Fig 5.1. Note that losses from the laser diode to fibre, coupler to fibre and fibre to photodetector couplings were minimised and so their overall effect on system losses was small (section 5.6.1). To choose a suitable collimator and reflector, a number of arrangements, using the components discussed in section 5.7, were investigated.

The first set-up is shown in Fig 6.4 (set-up 1), in which a 4 mm focal length microscope objective was used as a collimator and a front coated mirror was

used as a reflector. The numerical aperture of the fibre was 0.2. The diameter of the light spot 4 mm from the fibre end was 1.6 mm, and since the diameter of the lens was around 6 mm, all the light from the fibre was accepted. The microscope objective itself did not collimate light well and so divergence was evident over a few metres. Clearly the reflectance (the optical power reflected back to the fibre compared to the optical power emerging from the fibre) will reduce as the air path increases.

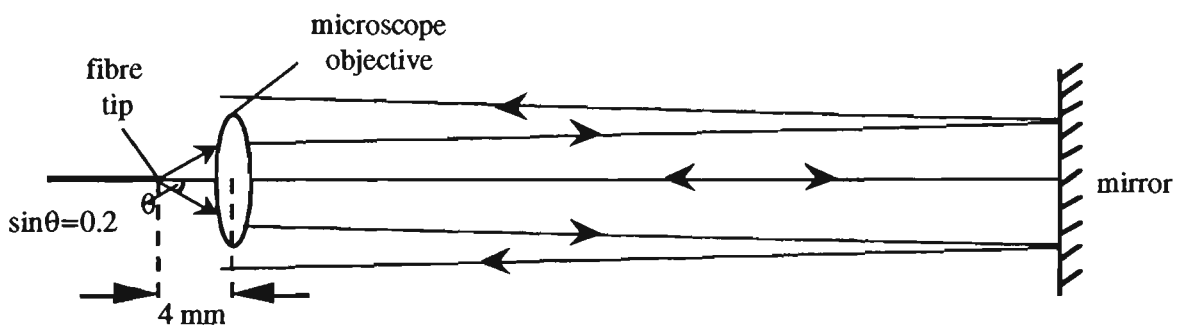


Fig 6.4 System set-up 1: a lens and a mirror

In order to improve collimation, a long focal length (1 m) thin lens was inserted after the microscope objective (Fig 6.5, set-up 2). Using an IR detection card, it was found that the spot size over a few metres was smaller than for set-up 1. However the light still diverged and for a sufficiently large range, only a fraction of the reflected light was collected by the optical fibre. Furthermore the additional lens introduced an extra insertion loss.

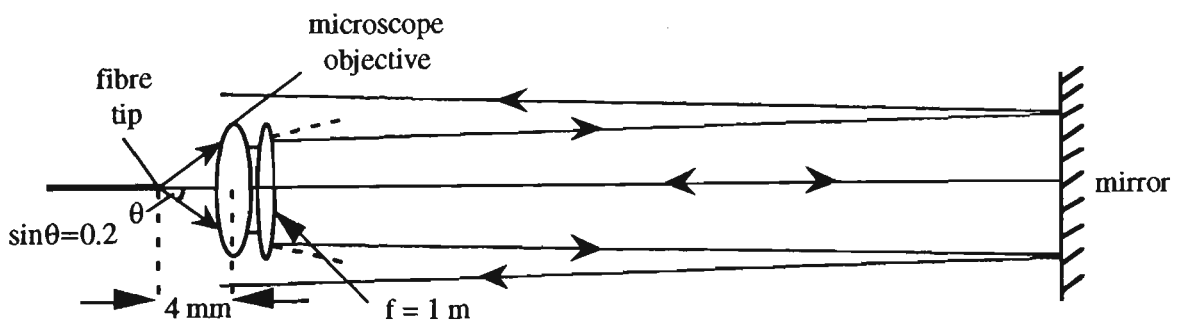


Fig 6.5 System set-up 2: two lenses and a mirror

As a variation to set-up 2, a corner cube was used (Fig 6.6) instead of the front-coated mirror (set-up 3). Corner cubes (section 5.7.2) reflect any ray back in the same direction, so even if the light is diverging, any light which hits the corner cube will be reflected back through the lens and thus into the optical fibre.

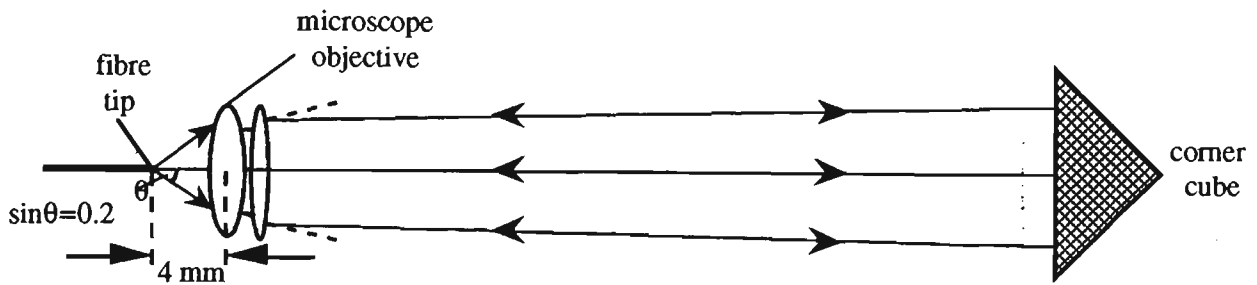


Fig 6.6 System set-up 3: two lenses and a corner cube

After numerous trials with set-ups 1 to 3, the optical power reflected back into the fibre over a long distance (10 m) was still insufficient to be detected. As an improvement, an alternative reflective arrangement was investigated (set-up 4), in which the lenses were replaced by a concave mirror (focal length around 8 cm) which reflected and collimated the light from the fibre (Fig 6.7). A very small optical fibre stand was constructed to minimise shadow effects. It was noted that although the light spot being reflected was larger in this case, its size was much more constant over ranges of interest. Thus this arrangement provided an improved reflectance over a wide range of distances (Fig 6.8).

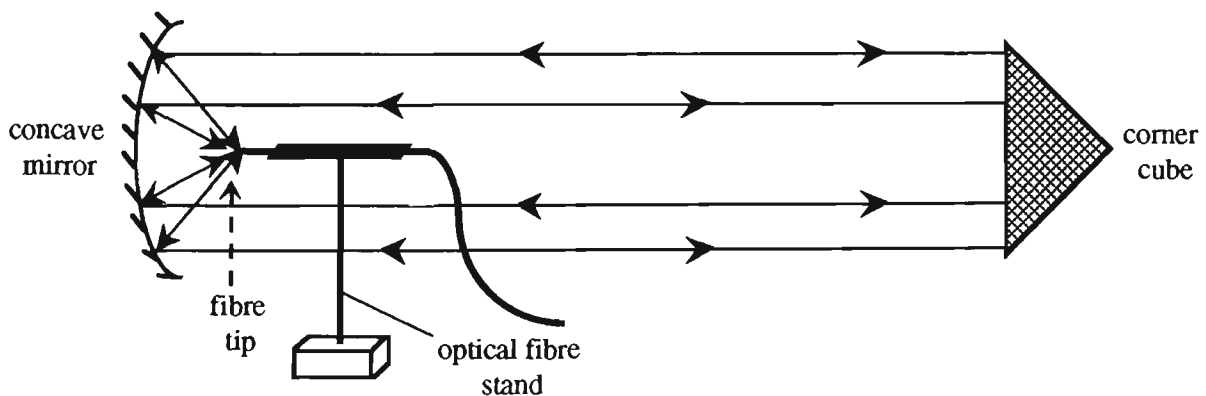


Fig 6.7 System set-up 4: a concave mirror and a corner cube

The measured reflectance as a function of air path for the four set-ups is plotted in Fig 6.8. It can be seen that with lenses (set-ups 1 to 3), reflectances are high at small distances, but decrease rapidly as the distance increases. Thus over air paths of several metres or longer, the reflectance will be too small to be practical. However, when the concave mirror was used (set-up 4), the reflectance is reduced close-in, but remains relatively constant as the distance increases, thus providing the possibility of long air path measurements.

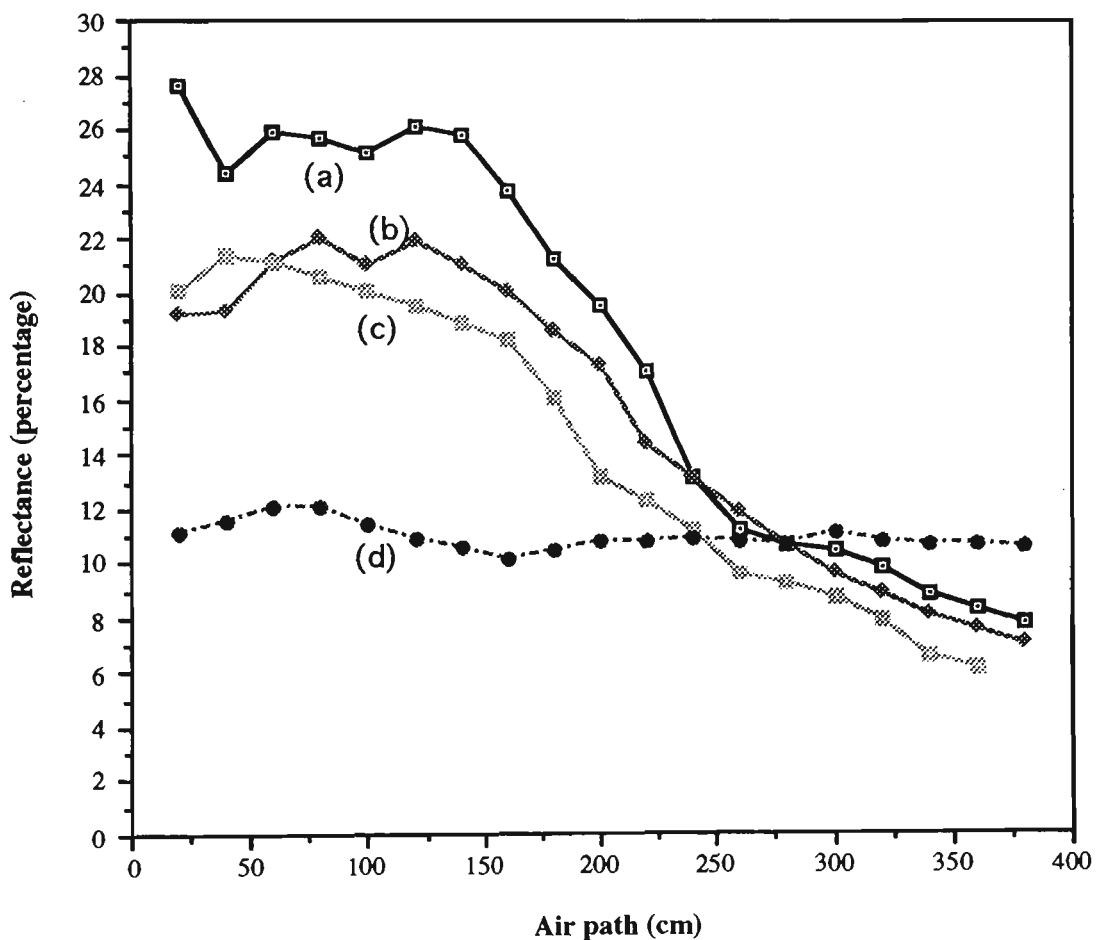


Fig 6.8 Optical reflectance of different set-ups:

- (a) Set-up 1    (b) Set-up 2  
 (c) Set-up 3    (d) Set-up 4

## 6.4 Range determination from the modulation envelope

The simplest way to obtain range information is by monitoring the signal from the photodetector through the bandpass filter on an oscilloscope (sections 5.3, 5.8.1, 5.9). Measurements were made using set-up 3 (Fig 6.6) over ranges up to 9 metres.

Firstly, the effect of equal or unequal reflectances from the two paths was considered. Let the instantaneous optical powers returned from the reference and target paths be  $I_1 \sin \omega_1 t$  and  $I_2 \sin \omega_2 t$  respectively, where  $I_1$  and  $I_2$  are their intensity amplitudes and  $\omega_1$  and  $\omega_2$  are their intensity modulation angular frequencies. Since one signal is delayed with respect to the other,  $\omega_1$  and  $\omega_2$  differ by a constant amount. If the time delay between the two paths is  $\tau$ , then  $\omega_2 = \omega_1 + 2\alpha\tau$  (if  $\tau \ll T_S$  and assuming  $\omega_2 > \omega_1$ ) for most of the ramp (section 4.2.1), where  $T_S$  is the ramp period and  $2\alpha$  is the frequency sweep rate (section 4.2.1). Upon detection they were superposed and the resulting output voltage was proportional to the input optical power, ie.  $V_{out} = c(I_1 \sin \omega_1 t + I_2 \sin \omega_2 t)$  where  $c$  is a constant whose value depends on the photodetector's amplifying circuit. Normally  $I_1 \geq I_2$ , because the reflector on the reference path was a thin-film coating whose reflectance can be as high as 90% (section 5.7.2) (Stuart, 1983), while the target path includes the air path whose reflectance was below 30% for any one of the four set-ups, as can be seen from Fig 6.8. Therefore,  $V_{out}$  is written as

$$\begin{aligned}
 V_{out} &= c(I_1 \sin \omega_1 t + I_2 \sin \omega_2 t) \\
 &= c[(I_1 - I_2) \sin \omega_1 t + I_2 (\sin \omega_1 t + \sin(\omega_1 + 2\alpha\tau)t)] \\
 &= c[(I_1 - I_2) \sin \omega_1 t + 2I_2 \sin(\omega_1 + \alpha\tau) t \cos(\alpha\tau)t] \quad (6.1)
 \end{aligned}$$

Here  $\omega_1$  and  $\omega_1 + \alpha\tau$  are both in the RF range, while  $\alpha\tau$  is normally a low frequency.

From Eqn. 6.1 it can be seen that the output voltage will be composed of two parts, an unmodulated high frequency signal  $c(I_1 - I_2)\sin\omega_1 t$ , and a high frequency signal  $2cI_2 \sin(\omega_1 + \alpha\tau)t$  which is modulated at the lower frequency  $\alpha\tau$ . If  $I_1 = I_2$ , the unmodulated term ( $c(I_1 - I_2)\sin\omega_1 t$ ) goes to zero and the output signal is 100% modulated.

These findings were confirmed experimentally as shown in Fig 6.9. When equal reflectances were used, the modulation was large as seen in Fig 6.9(a). By comparison, if  $I_1 \gg I_2$ , then the unmodulated part is larger than the modulated part, and so the signal of interest is difficult to discern (Fig 6.9(b)) which means that the modulation angular frequency,  $\alpha\tau$  can not be determined very well.

The output modulation frequency in Eqn. 6.1 is  $\frac{\alpha\tau}{2\pi}$  (half the beat frequency). However such a waveform (Fig 6.9(a)) exhibits two maxima for each cycle so the envelope frequency is the required beat frequency ( $f_{\text{BEAT}} = \frac{2\alpha\tau}{2\pi}$ ). From Eqn. 3.3, the range  $R$  is directly proportional to the beat frequency ( $R = \frac{f_{\text{BEAT}} T_s c}{2\Delta f}$ ). As  $\Delta f$ ,  $T_s$  and  $c$  are all constant during the measurement,  $R$  can be determined from the beat frequency.

Using a 37 MHz sweep of the Type 9036 VCO (section 5.5), an initial air path measurement was conducted over the range 0 m to 3.6 m, and typical output waveforms are shown in Fig 6.10. Unequal reflectances were used. For the experimental system used, the reference path was longer than the target path, so as the air path increased, the modulation frequency decreased. Clearly the

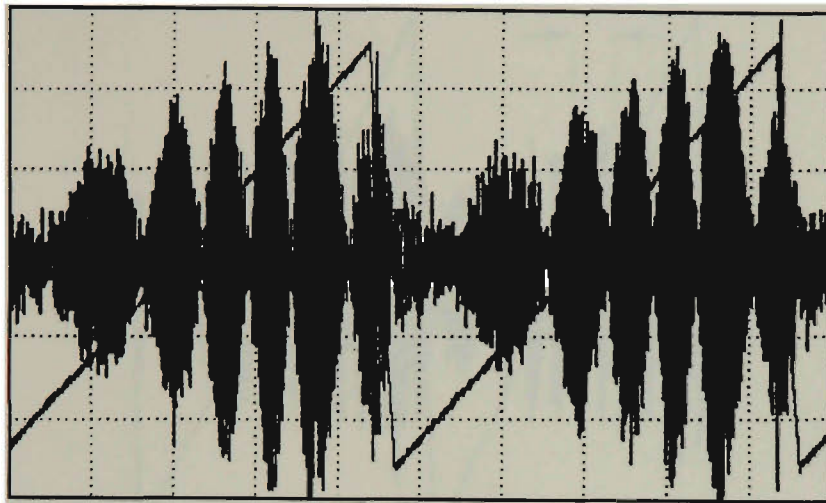
beat frequency is not constant over the duration of the ramp (Fig 6.10). For each air path the beat frequency was determined by measuring the duration (section 5.9) of two beat cycles at the centre of the ramp and averaging. This approach seemed reasonable since the VCO frequency sweep was at its most linear in this region. The resulting graph of beat frequency as a function of air path is shown in Fig 6.11(a). The beat frequencies were measured three times, and the points on the graph were their average values whilst the errors were obtained by using:

$$\text{Error} = (\text{maximum reading} - \text{minimum reading}) / 2$$

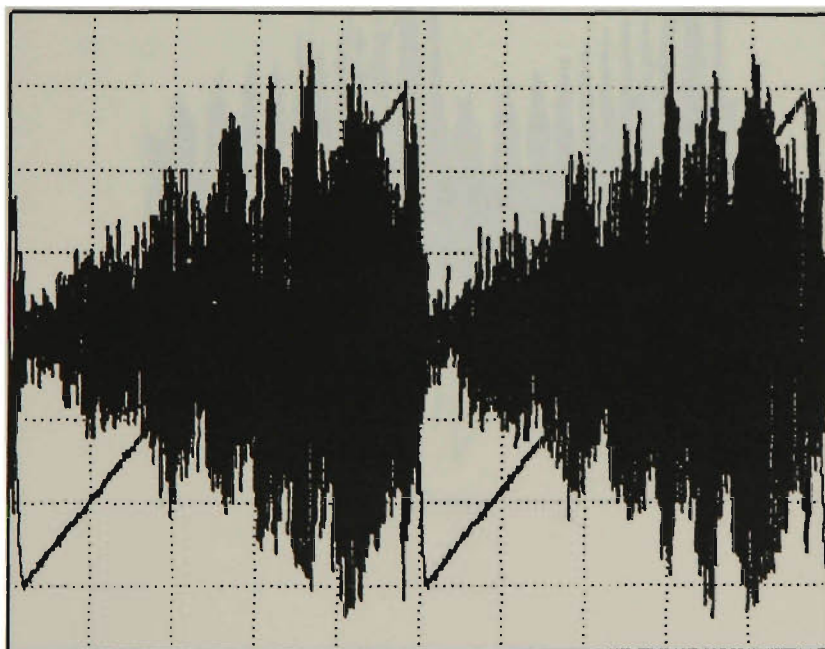
Similar measurements over a range of 9 metres were obtained and the results are shown in Fig 6.11(b). The errors used were the oscilloscope measurement errors. However as indicated in Fig 6.8, the optical reflectance for set-up 3 drops rapidly as the air path increases and so beyond this 9 metre range, the return power was too low to obtain a clear signal.

It can be seen from Fig 6.11 that in both instances the accuracy was poor (~ 20 cm and 1 m respectively). The reasons for this were the non-linear operation of the VCO (section 5.5) and also because of excessive electrical noise which made the identification of modulation maxima or minima difficult.

To overcome this excess noise, the overall SNR must be increased, and the most straightforward method is to raise the signal power (since a bandpass filter has already been used) (section 4.3.3). The beat frequency is best determined when the modulation depth of the output is optimised, which corresponds to equal reflectances in each path (Fig 6.9(a)). However this means a low reflectance for the reference path since the reflectance of the target path is so small (Fig 6.8), which then has the effect of reducing the overall signal level.



(a) Equal reflectances (both 17%)



(b) Reflectances are 72% from the reference path and 15% from the target path

**Fig 6.9** Modulated waveforms for (a) balanced reflectances and (b) unbalanced reflectances from reference and target paths

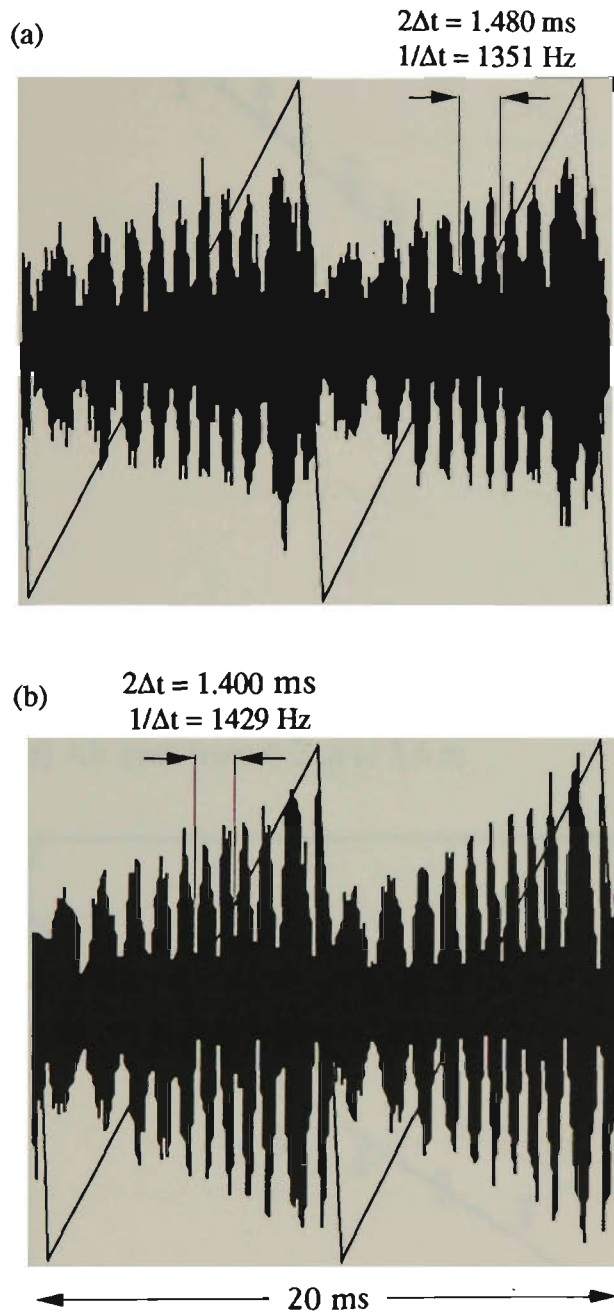
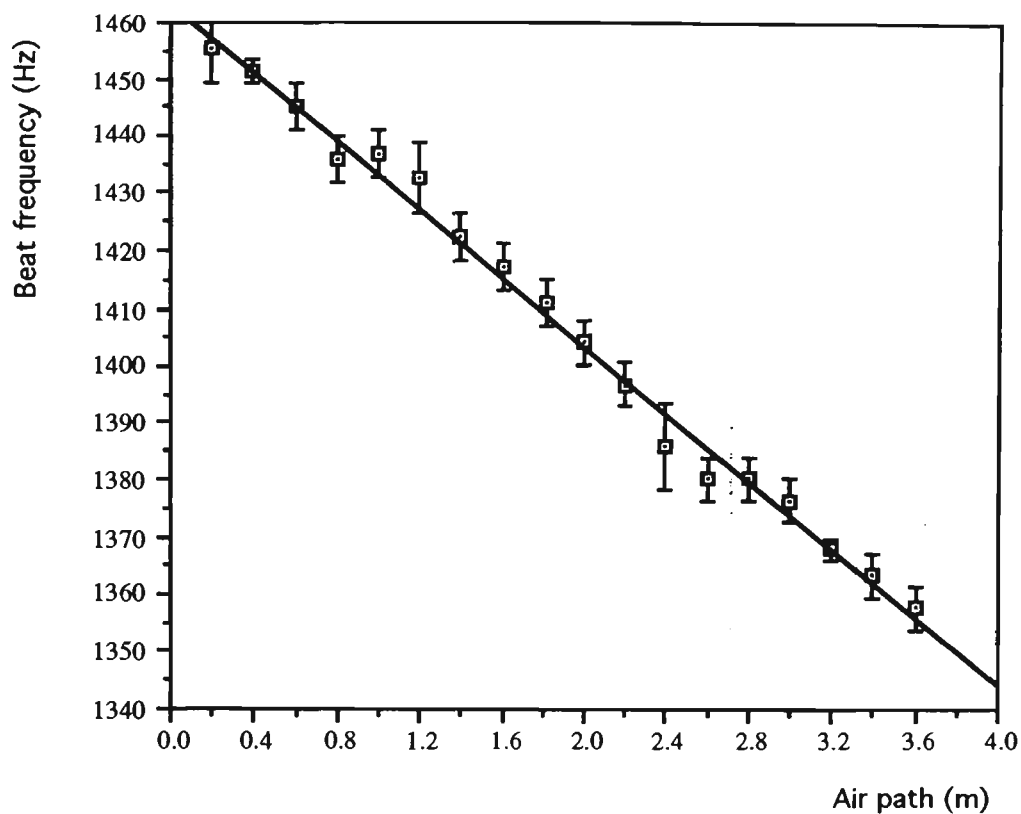
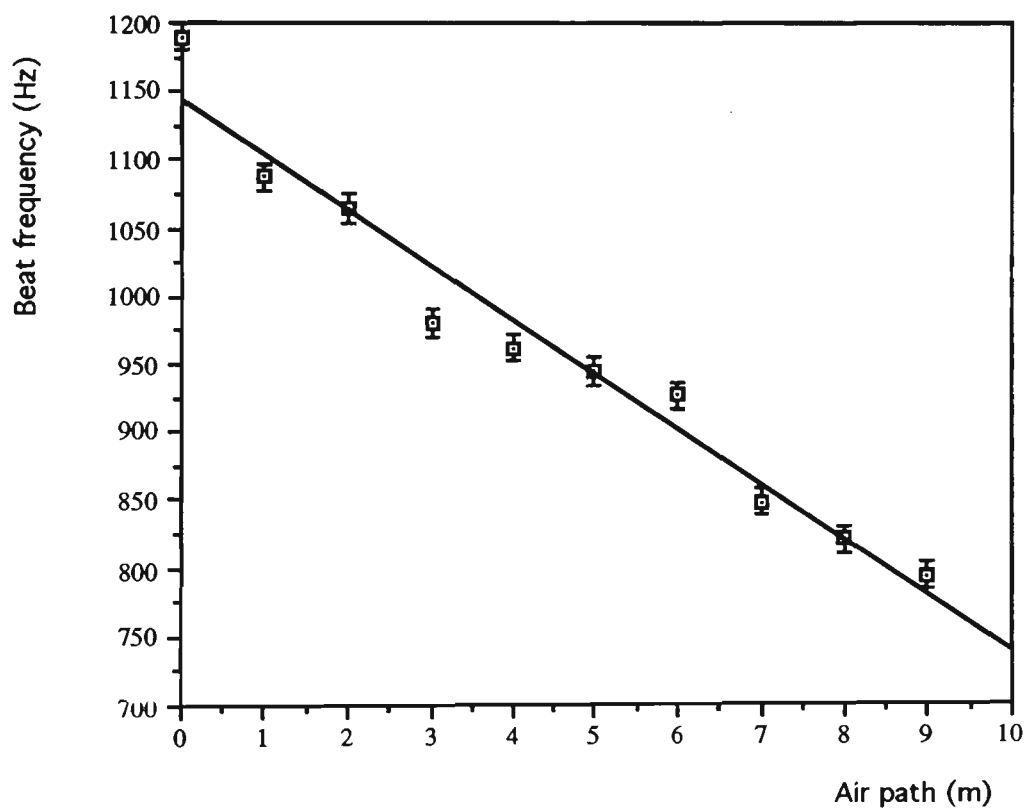


Figure 6.10 Modulated waveforms for an air path of (a) 3.6 m and (b) 0.2 m



(a) Air path from 0.2 m to 3.6 m



(b) Air path from 0 m to 9 m

**Fig 6.11** Distance measurement by measuring two beat cycles

## 6.5 Range determination from the beat frequency

Range measurement through interpretation of the modulation envelope is limited by low contrast, as described in the previous section (section 6.4). To overcome this, a signal processor (section 5.8.3) was used after the photodetector and the bandpass filter circuit, for demodulation. The signal processor comprised a non-linear circuit (a fast response diode). From Eqn. 5.1, the term of interest is the mixing term  $\frac{1}{2} V_1 V_2 \cos(2\alpha\tau)t$ . This signal from the non-linear circuit was fed into a 4 kHz low pass filter and then a 750 Hz high pass filter so that all the high frequency components and associated noise would be diminished. The resultant signal,  $cV_1 V_2 \cos(2\alpha\tau)t$ , was displayed on the Tektronix oscilloscope (section 5.9) ( $c$  is a constant determined by the demodulation circuit). Note that the signal quality can not be further improved by simply increasing  $c$  since this will also increase the noise power (Horowitz and Hill, 1989). However,  $I_1$  does not have to equal  $I_2$  in this case (section 6.4), and can be increased by applying a high reflectance thin-film coating on the end of the reference fibre (section 5.7.2). This resulted in a larger beat waveform amplitude at the output of the signal processing circuit (Fig 5.22(g)), even though the original signal exhibited a smaller modulation depth.

Thus the frequency observed on the oscilloscope was the beat frequency  $f_{\text{BEAT}}$ , where

$$f_{\text{BEAT}} = \frac{2\alpha\tau}{2\pi} = \frac{\Delta f}{T_s} \times \frac{2R}{c} = \frac{2\Delta f}{T_s c} R$$

This is the same as Eqn. 3.3, in which  $R$  represents the optical path difference in air. For the experimental arrangement in Fig 5.1,  $R$  can be rewritten in terms of the air path length and the optical path lengths in fibre of the target and reference paths, ie.

$$\begin{aligned} R &= \text{reference optical path length} - \text{target optical path length} \\ &= nL_{\text{ref}} - (nL_{\text{tar}} + \text{air path length}) \end{aligned}$$

where  $n$  is the refractive index of the fibre being used, and  $L_{\text{ref}}$  and  $L_{\text{tar}}$  are the optical fibre lengths of the reference and target paths respectively. Then  $f_{\text{BEAT}}$  can be rewritten as

$$f_{\text{BEAT}} = \frac{2\Delta f}{T_{\text{sc}}} [nL_{\text{ref}} - (nL_{\text{tar}} + \text{air path length})] \quad (6.2)$$

Eqn. 6.2 is written with the terms on the right in this order because the reference path was longer than the target path (section 6.4).

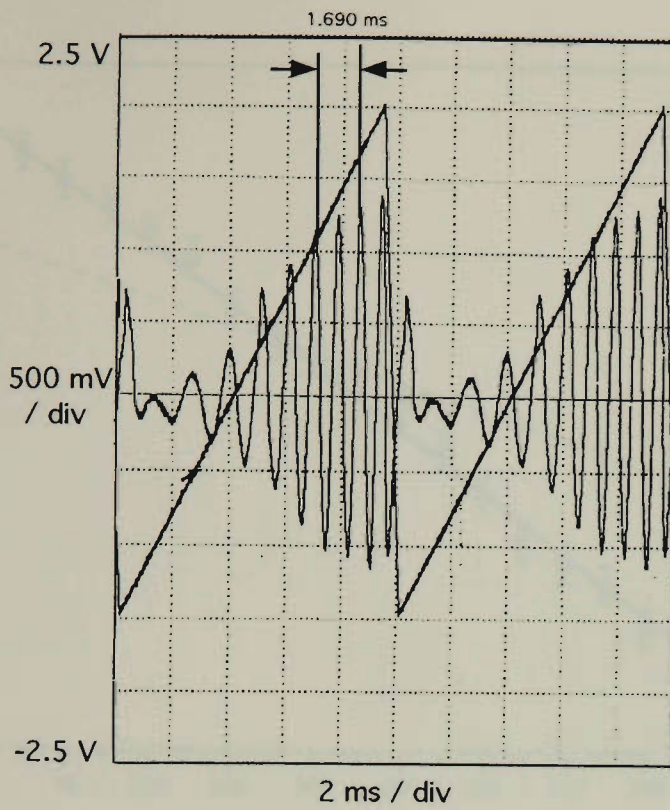
Since optical fibres without their buffer jacket are easy to break, the fibres of both paths had to be re-cleaved and re-spliced occasionally, and so the fibre lengths of both paths were not known exactly. Thus it was not possible to use Eqn. 6.2 to calculate the expected beat frequency. However the variation in beat frequency with air path length could be determined because the slope ( $\frac{2\Delta f}{T_{\text{sc}}}$ ) was predetermined. The air path range can be obtained by measuring the beat frequency change relative to a reference point. In this work, the reference point was chosen to be an air path equal to zero. The air path was measured using both the Type 9036 and VTO-9032 VCOs.

### 6.5.1 Range measurements using a Type 9036 VCO

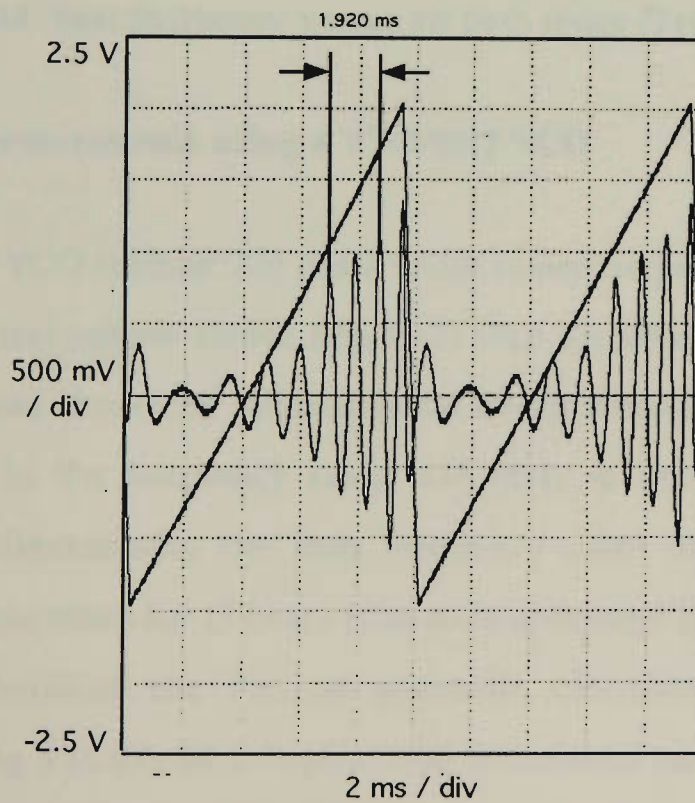
The sweep range used for a Type 9036 VCO (section 5.5) was restricted to between 8 V to 22 V for which the frequency sweep is relatively linear (Fig 5.11). The sweep frequency range was not further reduced to obtain a more linear working region because the ranging resolution is proportional to the sweep frequency range (Eqn. 3.4). The sweep range was chosen by considering both

these factors. Typical experimental beat waveforms are shown in Fig 6.12. Note from Fig 5.11 that the output electrical modulation power from this VCO increases as the input voltage increases, which explains why the amplitude of the beat signal also increased. Furthermore the beat frequency varied with the sweep voltage because the frequency chirp was not exactly linear, as was demonstrated for the electrical simulation (section 6.2). The beat frequency for each range was derived by considering the time duration for two cycles at the centre of the ramp in a similar manner to section 6.4. The error used is simply the oscilloscope measurement error.

The graph of beat frequency as a function of range is given in Fig 6.13, where it can be seen that the best-fit (least-squares) line passes through most of the points. The calculated slope of the change in beat frequency with range was obtained (Fig 6.13) from Eqn. 6.2 assuming  $\Delta f = 27$  MHz and  $T_s = 0.01$  s. It can be seen that the experimental slope is different from that calculated and is due to VCO non-linearities. This suggests that the actual frequency sweep rate over the portion of the ramp where these measurements were made was rather different to the average rate assumed. Nevertheless the experimental calibration curve could be used to determine the range with an accuracy of  $\sim 15$  cm.



(a) Air path  $R = 20$  cm Average beat frequency = 1185.6 Hz



(b) Air path  $R = 380$  cm Average beat frequency = 1042 Hz

**Fig 6.12** Beat waveforms using Type-9036 VCO

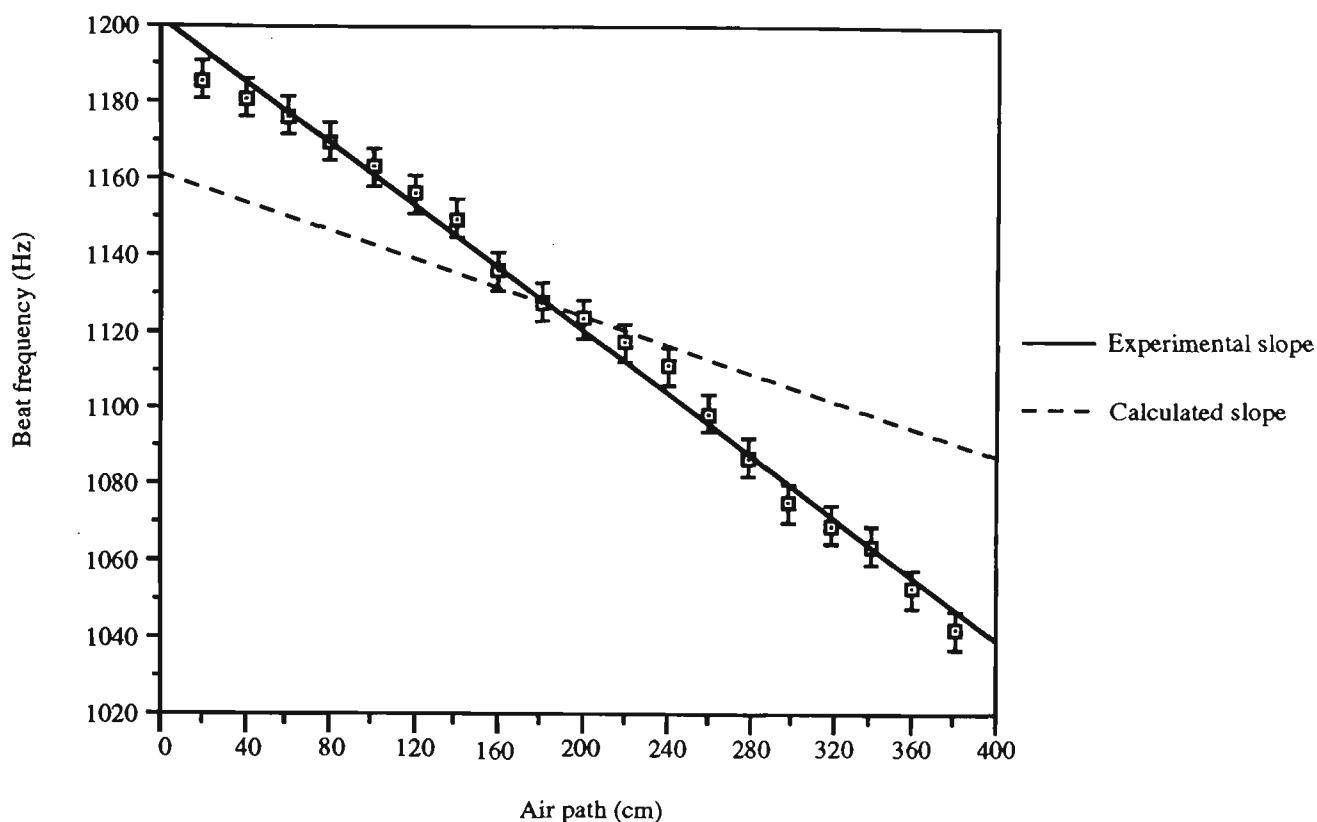


**Fig 6.13** Beat frequency versus air path range (Type 9036 VCO)

### 6.5.2 Range measurements using a VTO-9032 VCO

The VTO-9032 VCO (section 5.5) has a wider sweep frequency range and a more constant electrical output power (Fig 5.12) than the other VCO. A more linear sweep range was chosen by restricting the sweep between 7 V and 9 V, which corresponded to the frequency range 457 MHz to 516 MHz. Two different methods for determining the beat frequency were investigated. The first required the time taken for 17 beat cycles to be measured (Fig 6.14 (a), (c)), whilst the second involved the Fourier spectrum calculated by the Tektronix oscilloscope (Fig 6.14 (b), (d)). Typical beat waveforms are shown in Fig 6.14(a), (c) and it can be seen that the beat signals were much more uniform than those obtained with the other VCO (Fig 6.12). Since the beat frequency was nearly constant over the entire input voltage sweep range, the beat frequency was

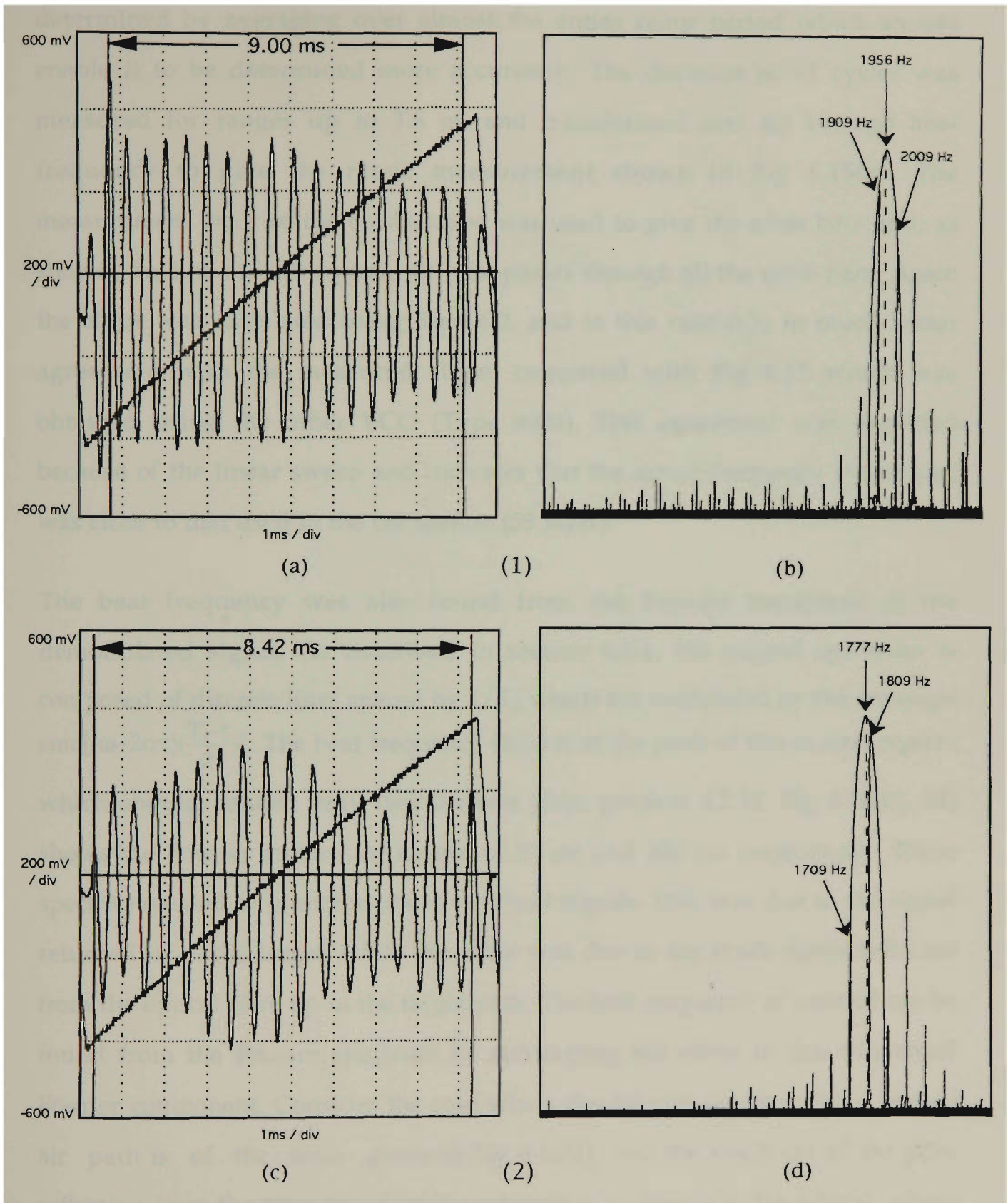


**Fig 6.14** Beat waveforms and their Fourier transforms at air path (1) 20 cm (2) 380 cm (VTO-9032 VCO)

determined by averaging over almost the entire ramp period which should enable it to be determined more accurately. The duration of 17 cycles was measured for ranges up to 3.8 m, and transformed into an average beat frequency to give the range measurement shown in Fig 6.15(a). The measurement error of the oscilloscope was used to give the error bars and, as shown, the line of least-squares fit now passes through all the error bars. Again the slope was calculated using Eqn. 6.2, and in this case it is in much better agreement with the measured slope, compared with Fig 6.13 which was obtained using the other VCO (Type 9036). This agreement was expected because of the linear sweep and indicates that the actual frequency sweep ( $\Delta f$ ) was close to that used in the calculation (59 MHz).

The beat frequency was also found from the Fourier transform of the demodulated signal. As described in section 4.2.4, the output spectrum is composed of discrete lines spaced by  $1/T_S$  which are modulated by the envelope  $\text{sinc}[(\omega - 2\alpha\tau)(\frac{T_S - \tau}{2})]$ . The beat frequency ( $2\alpha\tau$ ) is at the peak of this central region, which should contain only two discrete lines (section 4.2.5). Fig 6.14(b), (d) shows the Fourier spectra for ranges of 20 cm and 380 cm respectively. These spectra revealed information about two beat signals. One was due to the signal returned from the target, while the other was due to the small signal reflected from the optical fibre tip in the target path. The beat frequency of interest can be found from the Fourier spectrum by subtracting the effect of this unwanted Fourier component. Consider the case where the Fourier spectrum for a certain air path is of the form given in Fig 6.16(a), and the spectrum of the pure reflection from the fibre tip of the target path is as shown in Fig 6.16(b), where  $f_1, f_2, \dots, f_5, f_6$  are integer multiples of  $1/T_S$ . The actual Fourier components of the

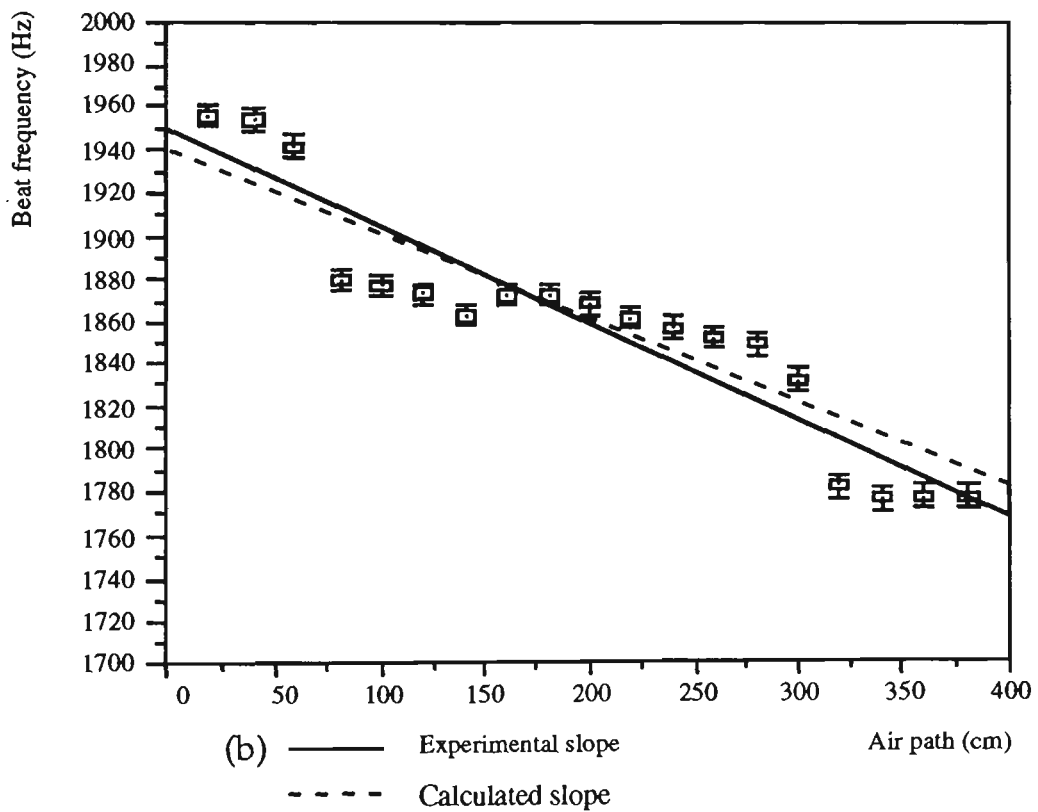
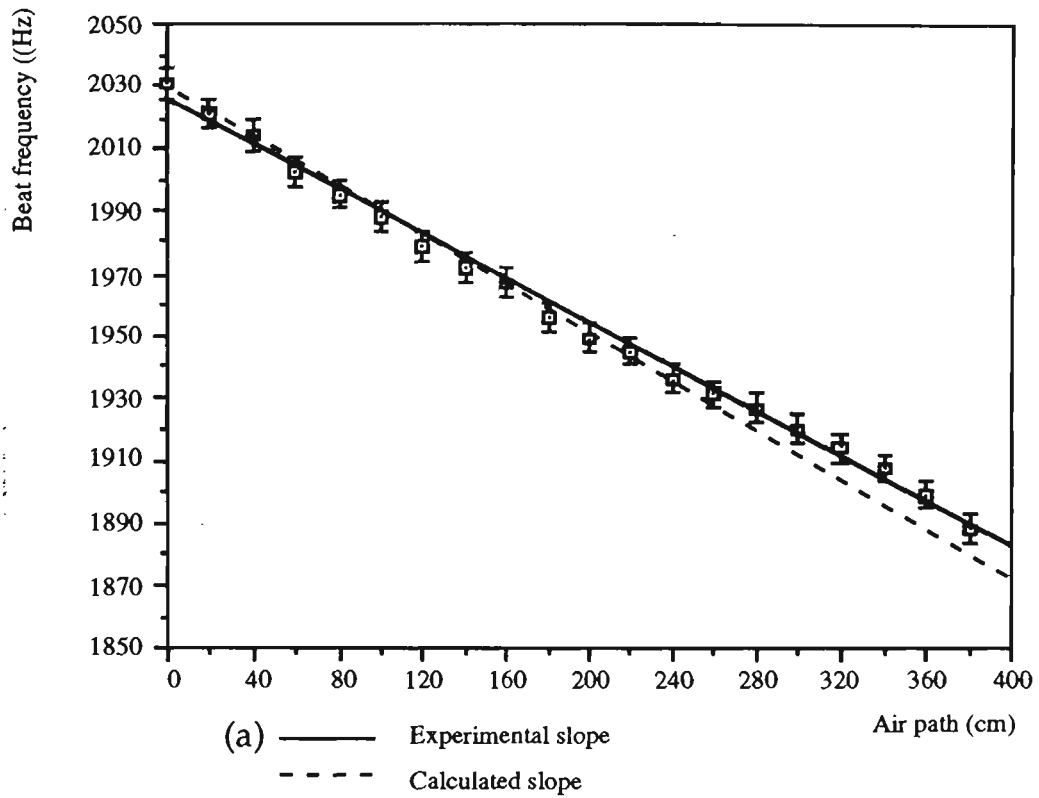


**Fig 6.15** Beat frequency versus air path range obtained from (a) 17 beat cycles and (b) using a Fourier transform (VTO-9032 VCO)

beat signal corresponding to the air path alone can be obtained by subtracting Fig 6.16(b) from Fig 6.16(a) to give Fig 6.16(c). The beat frequency ( $f$ ) can be calculated from the two significant lines as  $f = \frac{h_3 f_3 + h_4 f_4}{h_3 + h_4}$  (Eqn. 4.17).

Using this approach, the range measurement shown in Fig 6.15(b) is obtained. It can be seen that the results are not good which is not surprising because there were more than two strong lines evident in Fig 6.14(b), (d). However, it can be seen that the gradient of the best-fit line is close to that of the calculated line. The calculated slopes in Fig 6.15(a) and Fig 6.15(b) are the same because the frequency sweep range used in both sets of measurements was the same.

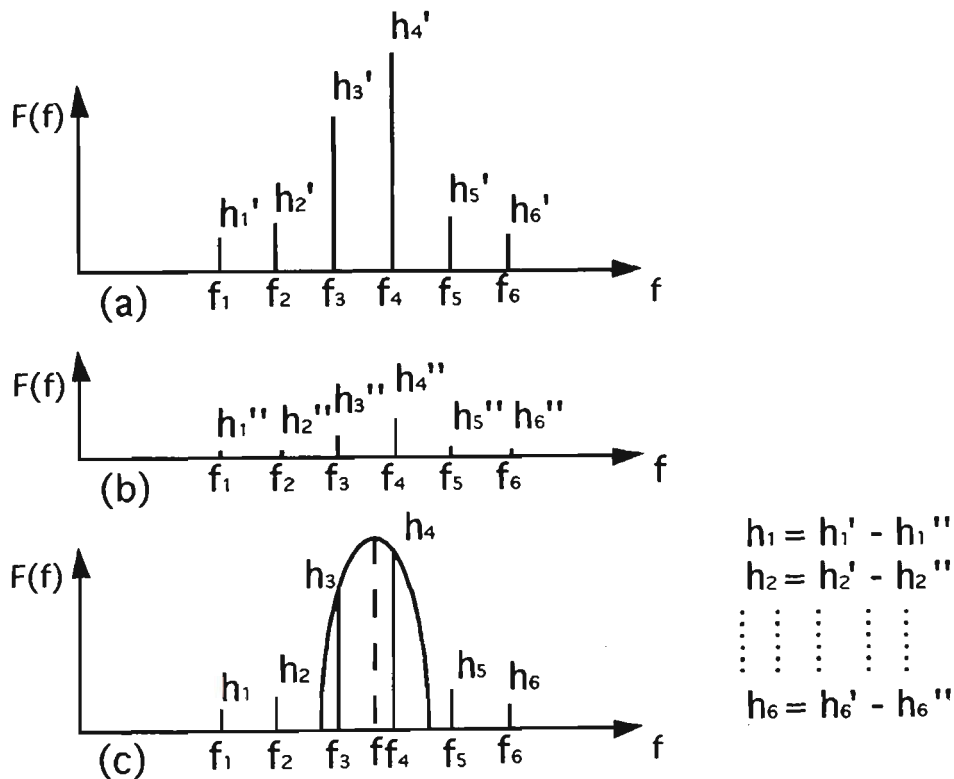


**Fig 6.16** Fourier spectra of beat frequency (a) on the oscilloscope, (b) due to the pure Fresnel reflection from the fibre tip of the target path and (c) due to the target only

## 6.6 Range measurements when an anti-reflection (AR) coating is present on the fibre tip in the target path

### 6.6.1 Effect of the signal returned from the fibre tip of the target path

When a light wave is incident on a plane boundary between two dielectrics (refractive indices  $n_1$  and  $n_2$ ), it is partially transmitted and partially reflected. The ratio of the reflected intensity to the incident intensity  $R$  (reflectance) is (Connor, 1986)

$$R = \left( \frac{n_1 - n_2}{n_1 + n_2} \right)^2$$

The optical fibres used in this experimental system were 50/125  $\mu\text{m}$  graded index multimode fibres with a refractive index 1.47 (section 2.2.2). Thus when the light inside the fibre ( $n_1 = 1.47$ ) emerges into the air ( $n_2 = 1$ ), the reflectance is 3.62%. The Fresnel reflection from the fibre tip (section 2.3) is an unwanted signal and affects the quality of the beat waveform due to the target. This reflected signal from the fibre tip will superpose on the signal returned from the reference path and their mixing forms another beat waveform. Therefore, the beat waveforms observed on the oscilloscope actually consist of two parts (section 6.5.2). Thus an anti-reflection coating was evaporated onto the fibre end to reduce this unwanted reflectance. The coating material used was transparent crystal  $\text{MgF}_2$  whose refractive index is 1.38, and the AR coating process was controlled by an optical fibre thin film thickness monitor (Caranto et al, 1993). The minimum reflectance ( $R_{\text{min}}$ ) was achieved with a coating whose thickness was a quarter of the wavelength (780 nm) and was calculated using the following formula (Stuart, 1983)

$$R_{\min} = \left\{ \frac{n_1 - \frac{n_f^2}{n_2}}{n_1 + \frac{n_f^2}{n_2}} \right\}^2$$

where  $n_1$  (=1),  $n_2$  (=1.47) and  $n_f$  (=1.38) are the refractive indices of air, optical fibre and coating material respectively. Thus the minimum reflectance was 1.41%. The effect of the applied anti-reflection coating was determined by removing the reflector from the target path. As shown in Fig 6.17, the AR coating reduced the reflectance by approximately half, which can be seen by comparing the amplitudes of the beat waveforms (now due to the fibre tip reflection only) for each case. By using system set-up 4 (Fig 6.7), the reflectance from the target (corner cube) was around 12%. Thus the intensity of the optical signal returned from the uncoated fibre tip was originally 30% of that from the target, and was reduced to 15% when an anti-reflection coating was applied. This can be seen by comparing the waveforms shown in Fig 6.18. The quality of the beat waveform was clearly improved when the coating was applied.

The effect of the signal returned from the fibre tip upon the detection system was analysed using a computer simulation for which the results are given in Fig 6.19. The beat frequency of the target corresponded to an air path of 3.8 metres. It can be seen from Fig 6.19 that the effect of the fibre tip Fresnel reflection on the overall beat waveform is to further modulate the amplitude. When the anti-reflection coating is present, the amplitude of the beat waveform becomes more constant which can be seen by comparing Fig 6.18(b) with Fig 6.18(a) and Fig 6.19(2c) with Fig 6.19(1c). Thus the beat waveform amplitude increased when an anti-reflection coating was applied, which improved the accuracy of the measurement of the beat frequency.

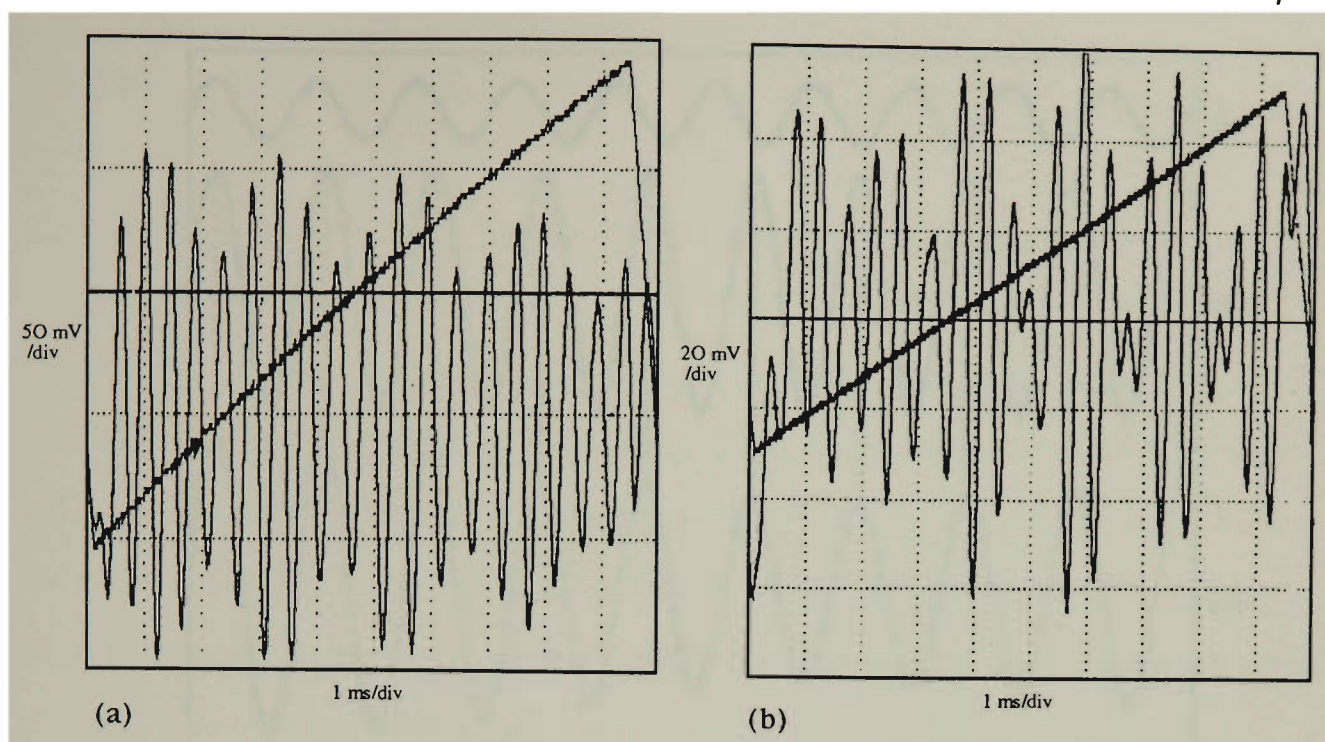


**Fig 6.17** Beat waveforms corresponding to the signal returned from fibre tip (a) without anti-reflection and (b) with anti-reflection coatings

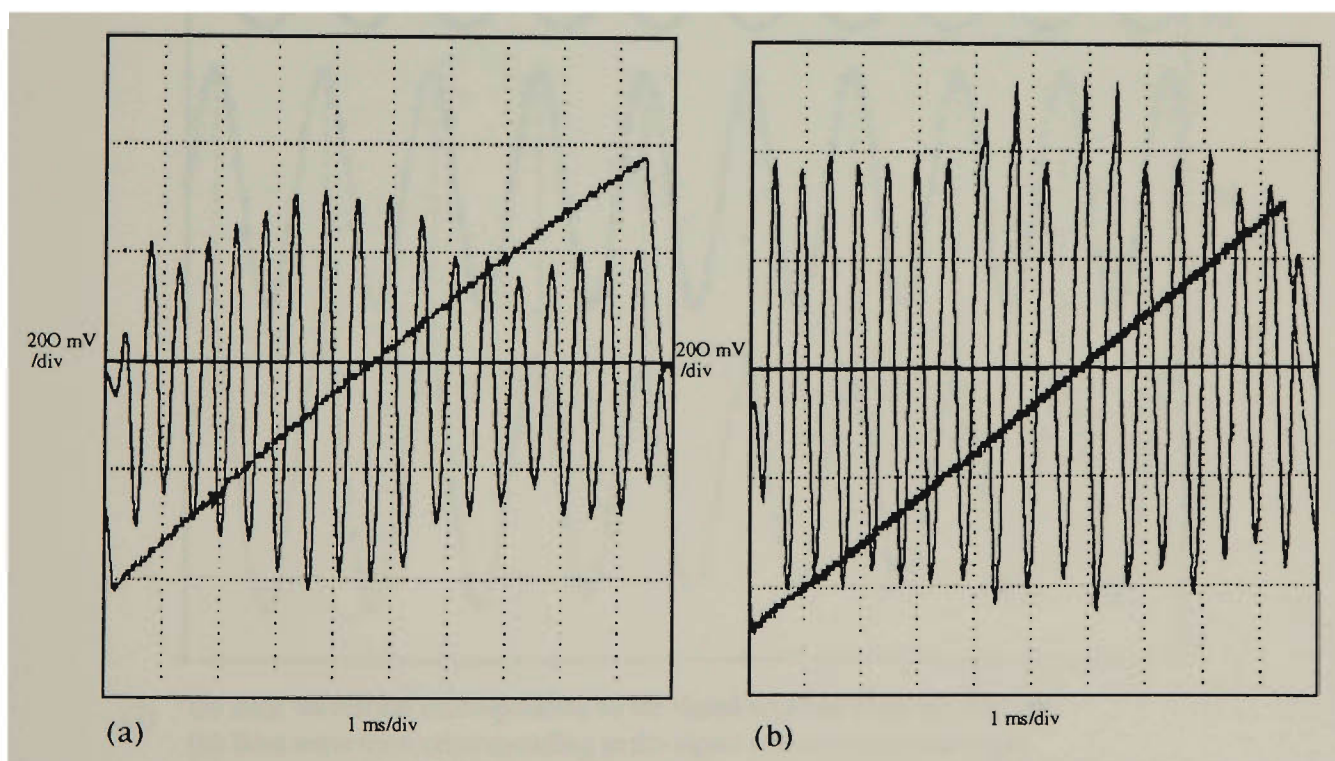
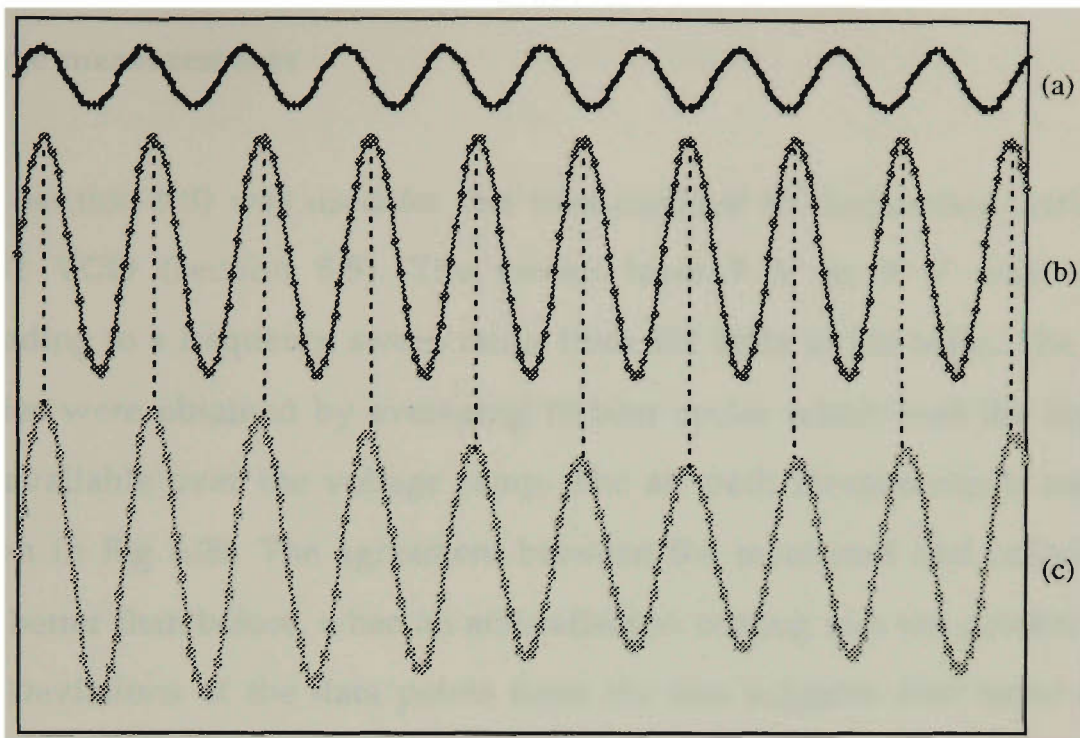
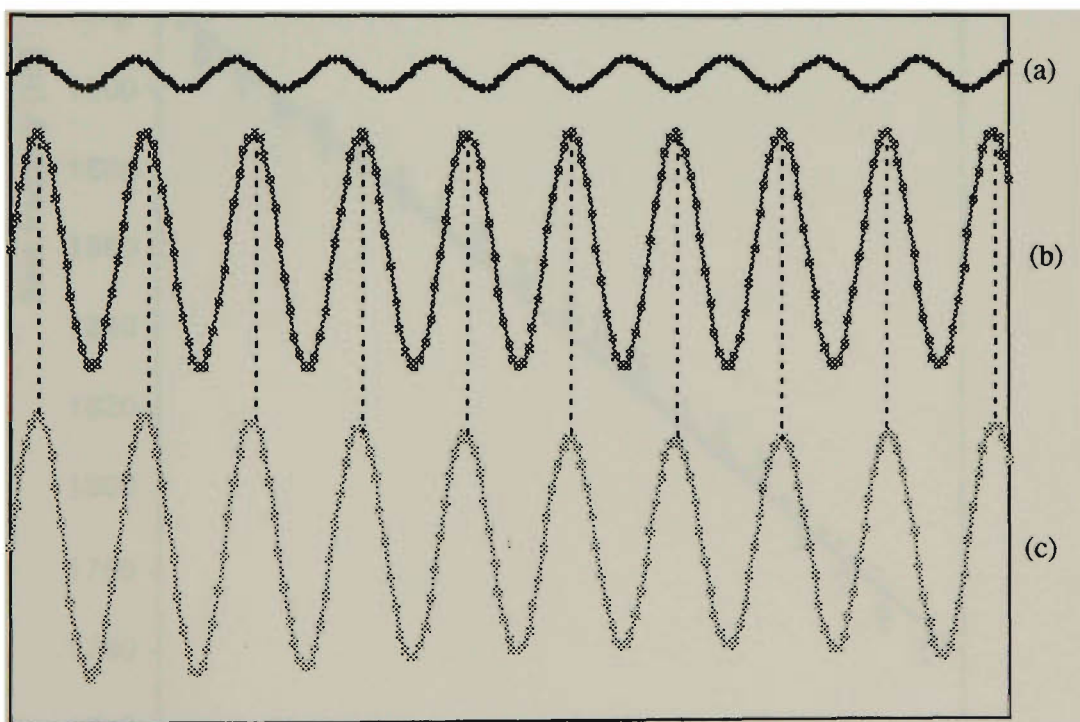


**Fig 6.18** Beat waveforms observed on the oscilloscope (a) without anti-reflection and (b) with anti-reflection coatings



- (1) (a) Beat waveform corresponding to the signal returned from the fibre tip  
 (b) Beat waveform corresponding to the signal returned from the target  
 (c) Beat waveforms obtained on the oscilloscope which is superposed by (a) and (b)



- (2) (a) Beat waveform corresponding to the signal returned from the fibre tip  
 (b) Beat waveform corresponding to the signal returned from the target  
 (c) Beat waveforms obtained on the oscilloscope which is superposed by (a) and (b)

**Fig 6.19** Simulation of the effect of the signal reflected from the fibre tip  
 (1) without anti-reflection and (2) with anti-reflection coatings

### 6.6.2 Range measurements

Set-up 4 (section 6.3) was used for this measurement in conjunction with the VTO-9032 VCO (section 5.5). The sweep from 7 V to 9 V was used, corresponding to a frequency sweep range from 457 MHz to 516 MHz. The beat frequencies were obtained by averaging 15 beat cycles which was the largest number available over the voltage ramp. The air path measurements results are shown in Fig 6.20. The agreement between the measured and calculated slopes is better than before, when an anti-reflection coating was not present (Fig 6.15(a)). Deviations of the data points from the line suggests that some non-linearity effects from the VCO are still evident (section 5.5).

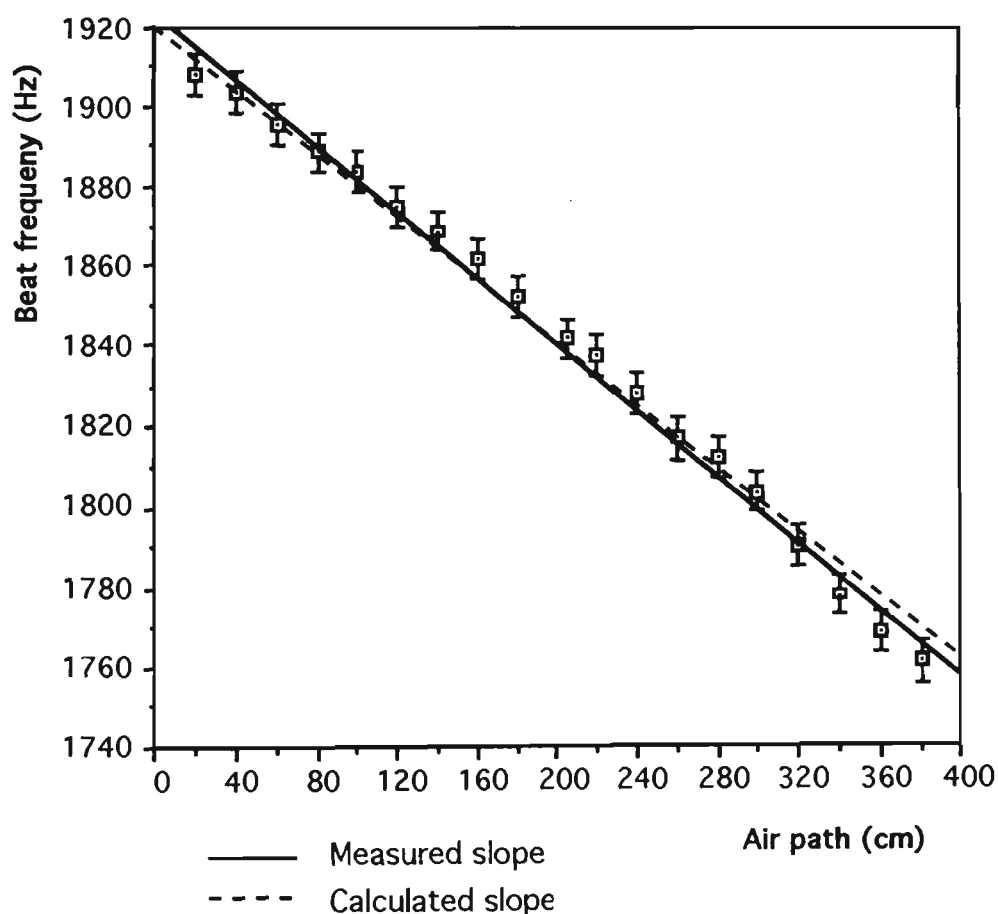


**Fig 6.20** Beat frequency measurements (with anti-reflection coating at the fibre tip) by averaging 15 beat cycles

In these results (Fig 6.20) the measured beat frequency corresponds closely to the expected beat frequency when many cycles are considered. Thus the frequency sweep range was increased (from 424 MHz to 539 MHz corresponding to a sweep voltage from 6 V to 10 V), which was still within a relatively linear region. The beat frequencies displayed in Fig 6.21 were higher because of the wider sweep range, and so the number of beat cycles were nearly double compared with Fig 6.14(a), (c). The beat frequencies were obtained by averaging over 30 cycles and the results are shown in Fig 6.22(a), with the corresponding deviations given in Fig 6.22 (b). Clearly these results exhibit improved linearity than those obtained by averaging over 15 cycles and all the measured points lie close to both the best-fit line and calculated line.

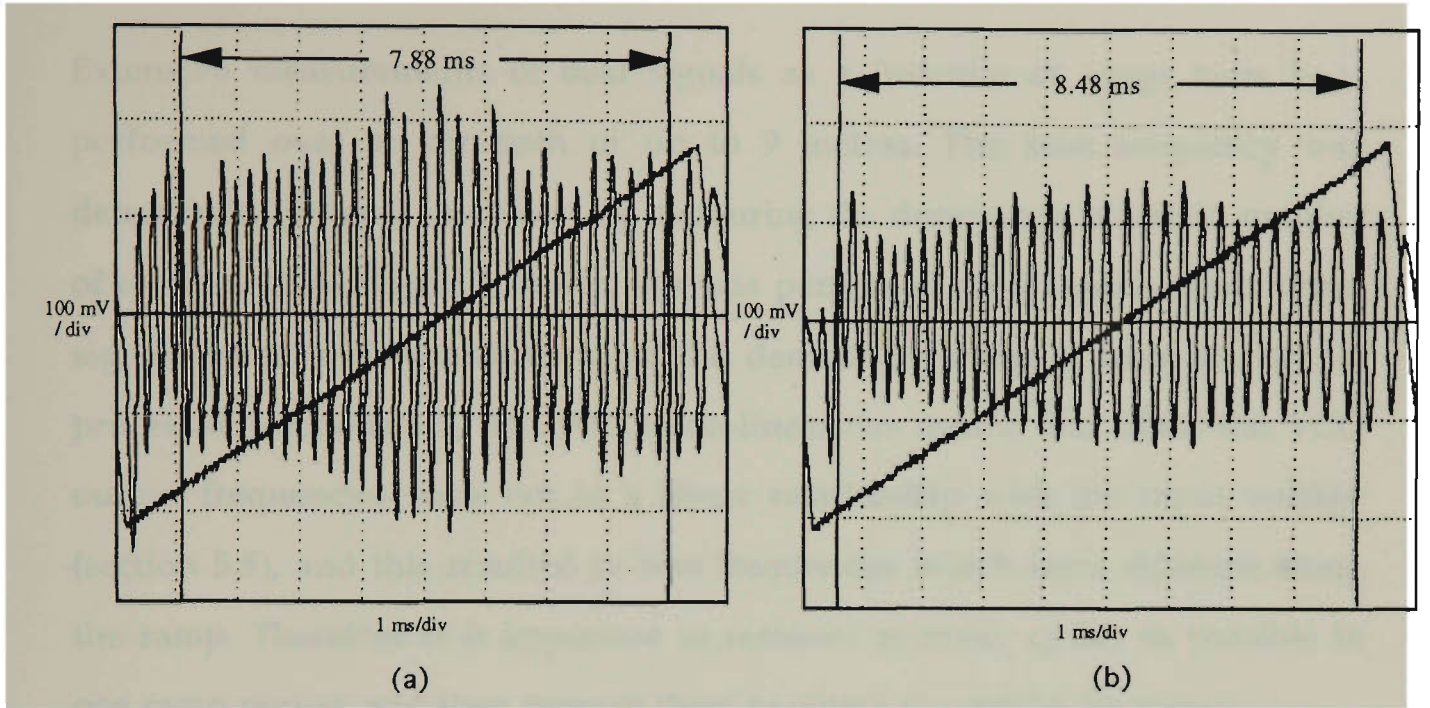


Fig 6.21 Beat waveforms at (a) air path = 20 cm and (b) air path = 380 cm

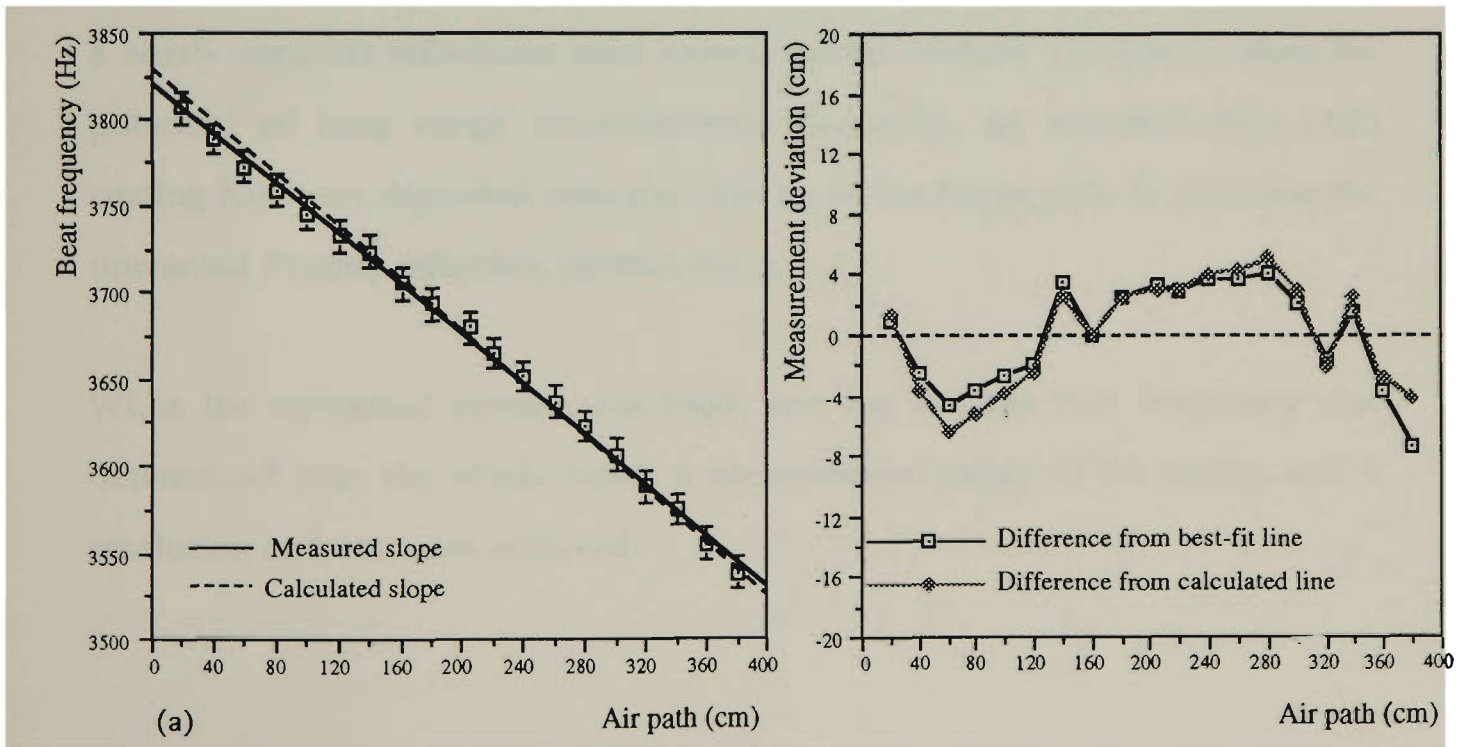


Fig 6.22 (a) Beat frequency versus air path range by averaging 30 beat cycles  
(b) Measurement deviation versus air path

## 6.7 Conclusion

Extensive measurements of beat signals as a function of range have been performed over an air path of up to 9 metres. The beat frequency was determined (in most instances) by measuring the duration of a certain number of cycles and averaging. Initially, this was performed on the modulated output signals (section 6.4), and then on the demodulated signal from the signal processor (sections 6.5, 6.6). VCO non-linearities meant that often the VCO output frequencies were not in a linear relationship with the input voltage (section 5.5), and this resulted in beat frequencies which were different along the ramp. Therefore it is important to measure as many cycles as possible in one ramp period, and then average them to obtain the correct frequency.

To obtain an optimum measurement system, several factors were investigated. Firstly, the air path alignment was improved, using a parabolic mirror, to give a nearly constant reflectance over several metres (section 6.3) which offers the potential of long range measurements. Secondly, an anti-reflection (AR) coating has been deposited onto the fibre tip of the target path to minimise the unwanted Fresnel reflection (section 6.6.1).

When the optimised system was used, and the average beat frequency was determined over the whole ramp, a measurement range of 3.8 metres and a resolution of 8 cm were achieved.

## Chapter 7 Final conclusion and future work

### 7.1 Final conclusion

An optical fibre based ranging sensor using the FMCW principle and incoherent light has been developed, with a resolution of a few cm over an air path of several metres. Low-cost fibre optic components and relatively simple modulation and processing circuits have been used and an initial processing scheme evaluated. Compared to other sophisticated (and therefore expensive ranging devices), this sensor may be suitable for medium range determination where accuracy is less important, but low-cost is desirable.

### 7.2 Future work

To optimise the range sensor described in this thesis, some further work needs to be conducted, and is described as follows:

- \* In order to improve the system resolution, a compensation circuit for the VCO will need to be developed in order to ensure a linear output frequency sweep.
- \* A near perfect anti-reflection coating on the fibre tip of the target path would be preferable and may be investigated by using a multilayer coating technique (Stuart, 1983). By doing this, the unwanted Fresnel reflection would be diminished and the resolution improved.
- \* The air path alignment may also be enhanced by improving further the optical collimator or reflector for potentially longer range measurements.

- \* A digital read-out system needs to be developed by employing an electrical zero-crossing and timing circuit after the Schmitt trigger to directly indicate the ranging information on a liquid crystal display.
- \* Finally, it is envisaged that several sensor heads may be optically multiplexed by a single laser transmitter using a reflective or transmissive network, for multiple range sensing.

**References :**

Abbas G L, Babbitt W R, de la Chapelle M, Fleshner M L, McClure J D and Vertatschitsch E J, 1990. "High-precision fibre-optic position sensing using diode laser radar techniques", Proc. SPIE Vol. 1219, pp. 468-479.

Bowick C, 1991. *RF Circuit Design*, 8th edn (Sams, Indiana USA)

Caranto N R Y, Kaddu S C, Szajman J, Murphy M M, Collins S F and Booth D J, 1993. "An optical fibre thin film thickness monitor", Meas. Sci. Technol. Vol. 4, pp. 865-869.

Champeney D C, 1985. *Fourier Transforms in Physics* (Adam Hilger, Bristol UK).

Collins S F, Palmer A W, Meggitt B T and Grattan K T V, 1991. "Intensity chirped laser diode modulation techniques for fibre optic based ranging applications", Proc. 16th, ACOFT (IREE, Sydney), pp. 210-213.

Connor F R, 1986. *Waves*, 2nd edn (Edward Arnold, London).

Dakin J and Culshaw B, 1988. *Optical Fibre Sensors*, Volumes 1 & 2 (Artech House, Boston USA).

de la Chapelle M, McClure J D, Vertatschitsch E J, Beausoleil R G, Bull J G and McGarvey J A, 1989. "Diode laser radar system analysis and design for high precision ranging", Proc. SPIE Vol. 1043, pp. 228-237.

de la Chapelle M, Vertatschitsch E J, Abbas G L and Porter C R, 1991. "Multiplexed ladar fiber-optic sensor system", Proc. SPIE Vol. 1586, pp. 146-154.

Edmund Scientific Co., 1989. *Annual Reference Catalog for Optics, Science and Education*, #19N1 (Edmund Scientific Co., Barrington USA).

Eichen E, Silletti A, Carlsen W J, Melman P and Cook K, 1987. "Fiber based chirped frequency interferometric distance sensor", OSA 1987 Technical Digest Series Vol. 12, pp. 30-33.

Fortney L R, 1987. *Principles of Electronics : Analog and Digital* (Harcourt Brace Jovanovich, Orlando USA).

Fuhr P L, Maynard D N and Kunkel D L, 1988. "Laser diode frequency sweeping techniques for fibre optic sensors and systems", Proc. SPIE Vol. 1169, pp. 114-125.

Giles I P, Uttam D, Culshaw B and Davies D E N, 1983. "Coherent optical-fibre sensors with modulated laser sources", Electron. Lett. Vol. 19, pp. 14-15.

Gnanalingam S, 1954. "An apparatus for the detection of weak ionospheric echoes", Proc. IEE Vol. 101, pp. 243-248.

Grattan K T V, Palmer A W and Meggitt B T, 1990. "Proposed ranging technique with coherent optical radiation from laser diode using phase shift method", Proc. SPIE Vol. 1219, pp. 480-488.

Hewlett Packard, 1988. *Fibre Optic Handbook* (Hewlett Packard, Germany).

Hodges D J and Greenwood J B, 1971. *Optical Distance Measurement* (Butterworths, London).

Horowitz and Hill, 1989. *The Art of Electronics*, 2nd edn (Cambridge University Press, Cambridge).

Hymans A J and Lait J, 1960. "Analysis of a frequency-modulated continuous-wave ranging system", Proc. IEE Vol. 107, pp. 365-372.

- Imai M and Kawakita K, 1990. "Optical-heterodyne displacement measurement using a frequency-ramped laser diode", *Opt. Commun.* Vol. 78, pp. 113-117.
- Jackson D A, Kersey A D, Corke M and Jones J D C, 1982. "Pseudoheterodyne detection scheme for optical interferometers", *Electron. Lett.* Vol. 18, pp. 1081-1083.
- Jelalian A J, 1992. *Laser Radar Systems* (Artech House, Boston USA).
- Kay L, 1985. "Airborne ultrasonic imaging of a robot work space", *Sensor Review*, January 1985, pp. 8-12.
- Kobayashi T and Jiang S D, 1988. "Optical FM heterodyne interferometry for range and displacement measurements", *CPEM '88 Digest*, pp. 133-134.
- Koskinen M, Ahola R, Kostamovaara J and Myllylä R, 1988. "On the use of an optomechanical sensing head in time-of-flight laser rangefinding", *Proc. SPIE* Vol. 952, pp. 400-405.
- Kubota T, Nara M and Yoshino T, 1987. "Interferometer for measuring displacement and distance", *Optics Lett.* Vol. 12, pp. 310-312.
- Lynn P A, 1987. *Radar Systems* (Macmillan Education, Basingstoke).
- Määttä K, Kostamovaara J and Myllylä R, 1988. "A laser rangefinder for hot surface profiling measurements", *Proc. SPIE* Vol. 952, pp. 356-365.
- Manhart S and Barthel G, 1984. "Laser diode rangefinder - target acquisition and tracking system functional model/demonstration model", *Proc. ESA Workshop on Space Laser Applications and Technology*, March 1984, pp. 261-265.

- MacDonald R I, 1981. "Frequency domain optical reflectometer", *Appl. Optics* Vol. 20, pp. 1840-1844.
- McClure J D, 1990. "Diode laser radar: applications and technology", *Proc. SPIE* Vol. 1219, pp. 446-457.
- Ohba R, Uehira I and Kakuma S I, 1990. "Interferometric determination of a static optical path difference using a frequency swept laser diode", *Meas. Sci. Technol.* Vol. 1, pp. 500-504.
- Oppenheim A V, Willsky A S and Young I T, 1983. *Signals and Systems* (Prentice-Hall, London).
- Palais J C, 1984. *Fibre Optic Communications* (Prentice-Hall, Englewood Cliffs USA).
- Rao M K and Tam S C, 1990. "A microprocessor based laser range finder", *Proc. SPIE* Vol. 1399, pp. 116-121.
- Rogowski R S, Heyman J S and Holben M S, 1986. "An amplitude modulated laser system for distance and displacement measurement", *Proc. SPIE* Vol. 663, pp. 86-89.
- Rueger J M, 1990. *Electronic Distance Measurement* (Springer-Verlag, New York).
- Schwarte R, 1984. "Performance capabilities of laser ranging sensors", *Proc. ESA Workshop on Space Laser Application and Technology*, March 1984, pp. 61-67.
- Shelamoff A, 1992, 1993. Private communication.
- Smith J R, 1970. *Optical Distance Measurement* (Lockwood, London).

Smith D E, 1980. "Electronic distance measurement for industrial and scientific applications", Hewlett-Packard Journal, June 1980, pp. 3-11.

Smith D E and Brown T L, 1980. "Industrial distance meter applications", Hewlett-Packard Journal, June 1980, pp. 11-18.

Sorin W V, Donald D K, Newton S A and Nazarathy M, 1990. "Coherent FMCW reflectometry using a temperature tuned Nd:YAG ring laser", IEEE Photonics Technology Letters Vol. 2, pp. 902-904.

Stuart R V, 1983. *Vacuum Technology, Thin Films, and Sputtering* (Academic Press, New York).

Taylor M and Jackson D A, 1986. "High precision non-contacting optical level gauge", Optica Acta Vol. 33, pp. 1571-1586.

Vertatschitsch E J, Abbas G L, de la Chapelle M and Porter C R, 1991. "High-precision fibre-optic position sensor system using ladar techniques", OSA 1991 Technical Digest Series Vol. 4, p. 209.

*Publication*

The following paper has been accepted for publication

in

Measurement Science and Technology

# **A SIMPLE LASER DIODE RANGING SCHEME USING AN INTENSITY-MODULATED FMCW APPROACH**

S F Collins, W X Huang and M M Murphy,  
Optical Technology Research Laboratory, Department of Applied Physics, Victoria University  
of Technology, Box 14428 Melbourne Mail Centre, Melbourne, Victoria, Australia 3000

K T V Grattan and A W Palmer,  
Department of Electrical, Electronic and Information Engineering, City University,  
Northampton Square, London EC1V 0HB, UK

## **ABSTRACT**

A simple frequency modulated continuous wave (FMCW) optical sensor using intensity-modulated light, for use in non-contact ranging applications, is discussed. Results over a range of several metres were obtained with an accuracy of a few centimetres.

## **THIS WORK WAS CONDUCTED AT:**

Optical Technology Research Laboratory, Department of Applied Physics, Victoria University  
of Technology, Box 14428 MMC, Melbourne, Victoria, Australia 3000

and

Department of Electrical, Electronic and Information Engineering, City University,  
Northampton Square, London EC1V 0HB, UK

## 1. Introduction

There has been considerable interest in recent years in the development of simple ranging methods based upon optical fibre technology. The techniques proposed have been reviewed elsewhere [1, 2], revealing a wide variety of possible approaches to the optical sensing of range. Some are more practically feasible than others, and there remains a need for potentially inexpensive and accurate systems, involving recently developed optoelectronic components, to be developed.

The availability of the laser diode as a simple, lightweight and battery powered optical source, with good directionality and operating in the visible part of the spectrum, has been of considerable benefit in the evolution of new ranging schemes. However, in those which have been reported, limitations are evident. For example, time-of-flight techniques are limited to resolutions of the order of centimetres, and the electronic data processing that is required to measure accurately the temporal displacement of a light pulse is prohibitively expensive in many cases. Another technique involves the phase change in the sinusoidal intensity modulation of the light when the phase of the reflected signal is compared with that originating from the source, in which case the resolution depends upon the modulation frequency and the use of high-speed electronics. Other techniques take advantage of recent progress in optical fibre-based interferometry for a wide variety of sensing methods [3]. Here a frequency modulated continuous wave (FMCW) approach is utilized. This method is relatively simple, employing a small number of optical components, and is potentially available for use over a wide sensing range.

## 2. Review of Previous Work

FMCW techniques were devised originally for ranging methods using radio waves [4]. The method has been demonstrated optically, in which either the carrier or a sub-carrier is modulated with a periodic frequency-sweep (or chirp). In either case the superposition of such signals, from a distant reflector and a reference path, results in a beat signal whose frequency is dependent on the ranging distance. Previously we discussed [5] the operational details and demonstrated the second approach employing intensity modulation. Using an all-fibre

configuration it was shown that distance measurements could be made over a wide displacement range.

The field of FMCW using light intensity modulation was pioneered by MacDonald [6], as a method for the detection of faults in optical fibres. More recently it has been developed by Boeing with a view to the production of high-precision sensor systems [7]. This application envisages high-speed actuator position measurement for the new generation of high technology, "fly-by-light" aircraft for both military and commercial purposes. Fibre optic sensors in this role offer the usual advantages of light weight, EMI immunity and compactness over conventional electronic and mechanical sensors. A typical aerospace requirement [7] is a linear position sensor with a resolution of 50  $\mu\text{m}$  over a 0.5 m range and a fast response ( $\sim 200$  Hz), and so the sophisticated, and consequently expensive, approach is justified. Vertatschitsch *et al* [8] reported a repeatable resolution of 50  $\mu\text{m}$  using a single 1 ms chirp at a pulse repetition rate of 143 Hz, with chirp linearity and repeatability the dominant performance limitations. With digitally generated RF chirps the best resolution achieved was 9  $\mu\text{m}$  but the authors describe the electronics as "too complex for near-term integration into aircraft avionics". The resolution of an FMCW system is inversely proportional to the frequency chirp range, so a reduced chirp range gives poorer resolution. However if the chirp range was reduced from several GHz (as used by Boeing) to hundreds or even tens of MHz this would offer the useful advantage of simpler electronics.

Conversely, sub-micron resolution is possible [9] using a chirp in the optical carrier of tens or hundreds of GHz. However, in this case, the dynamic range is limited by the coherence length of the source. Ranges of the order of metres could only be achieved using an expensive single-frequency, single mode laser diode.

In this work the intensity-modulated FMCW technique is employed, using a small chirp range, with the aim of providing a low-cost ranging device which takes advantage of the effort put into the demanding aerospace research. The device would be configured into a simple ranging system, suitable for longer range, less accurate systems where performance requirements are less stringent and budgets are more limited. Thus applications could include the ullage of inflammable fluids (e.g. petroleum products in storage tanks), vehicle ranging for automatic

braking schemes, robotics and machine vision, structure monitoring, etc. In these applications a less complex and inexpensive device, which is potentially mass-produced, would be useful. Here the experimental arrangement and the results showing the characterization of such a system are presented.

### 3. Experimental Arrangement

The intensity chirped laser diode ranging system was set up as a Michelson interferometer, as shown in figure 1. A 780 nm, 5 mW laser diode was connected into a high-speed laser diode power supply circuit. The laser diode drive current was modulated by the output of a voltage-controlled oscillator (VCO) whose frequency was swept from 230 to 265 MHz. The VCO input was a 100 Hz sawtooth wave. The light was launched into one arm of a 50/125  $\mu\text{m}$  multimode optical fibre 2  $\times$  2 coupler. At the coupler, the light was directed into two unequal paths, one of which was launched into an air path and collimated onto a distant mirror (corner cube), whilst the other path was terminated by a reflective coating on the fibre's end. Light reflected back into the coupler's fourth arm from these two paths was detected by a high-speed PIN photodiode and amplifier, and the output was displayed on a digitizing oscilloscope. At the point where light is launched into the air path the fibre's end was anti-reflection (AR) coated with a  $\text{TiO}_2$  stack, to ensure that there were only two dominant reflections in the system.

### 4. Results and Discussion

Typical beat signals obtained with the oscilloscope are shown in figures 2(a) and 2(b), at ranges of 3.60 m and 0.20 m. The ramps are consecutive cycles of the VCO input. Owing to VCO non-linearities the beat frequency was not constant during the chirp. Therefore these beat signals were analysed as follows: a frequency of the beat signal was determined over the mid-region of the ramp by averaging the time taken for two cycles of the beat envelope. It is clearly evident, from figure 2, that there is a significant difference in the essential beat signal shown over the region marked at the mid-point of the ramp, indicative of the range of the target.

In this study, to characterize the system, the frequency information is extracted from the digitizing oscilloscope signal and plotted in figure 3. This shows the change in beat frequency is linearly related to the distance over the measured region. The beat frequency decreases with range because the optical path length of the reference arm is greater than the ranging distance. The accuracy of the measurement is limited by VCO non-linearities and the signal averaging used, and a more sophisticated digital signal averaging method is being developed using proprietary software on a PC. This will enable the rapid averaging of many more measurement signals, although there will be a potential "trade-off" in response time versus accuracy, which may restrict its use to slow-speed applications. These results show a displacement accuracy of only approximately 0.05 m, for measurements over a single 10 ms chirp period. This will be improved when more sophisticated averaging is developed, with a standard response time of 1 second.

Thus a simple optical ranging system suitable for distances up to several metres has been demonstrated. Measurements over a wider range with adequate accuracy for non-aerospace applications, where low unit cost is a major priority, should be possible by improving the optical alignments to give greater return power at the detector. The scheme should be competitive against other techniques, and is especially suitable for use in hazardous environments.

### Acknowledgments

This work was conducted by the authors initially at the Department of Electrical, Electronic and Information Engineering, City University, UK, and then at the Optical Technology Research Laboratory, Victoria University of Technology, Australia.

S F Collins would like to thank colleagues at City University for their kind hospitality. A Shelamoff is thanked for his technical assistance.

### References

- [1] Dakin J and Culshaw B 1988 *Optical Fiber Sensors* Volumes 1 & 2 (Norwood MA: Artech House)

- [2] Grattan K T V, Palmer A W and Meggitt B T 1990 Proposed ranging technique with coherent optical radiation from laser diode using phase shift method *Proc. SPIE* **1219** 480-9
- [3] Jackson D A 1986 Monomode optical fibre interferometers for precision measurement *J. Phys. E: Sci. Instrum.* **18** 981-1001
- [4] Hymans A J and Lait J 1960 Analysis of a frequency-modulated continuous-wave ranging system *Proc. IEE B* **107** 365-72
- [5] Collins S F, Palmer A W, Meggitt B T and Grattan K T V 1991 Intensity chirped laser diode modulation techniques for fibre optic based ranging applications *Proc. 16th ACOFT* (Sydney: IREE) 210-3
- [6] MacDonald R I 1981 Frequency domain optical reflectometer *Appl. Opt.* **20** 1840-4
- [7] Abbas G L, Babitt W R, de La Chapelle M, Fleshner M L, McClure J D and Vertatschitsch E J 1990 High-precision fiber-optic position sensing using diode laser radar techniques *Proc. SPIE* **1219** 468-79
- [8] Vertatschitsch E J, Abbas G L, de La Chapelle M and Porter C R 1991 High-precision fiber-optic position sensor system using ladar techniques *Digest of Conference on Optical Fibre Communication, 1991 OSA Technical Digest Series Vol. 4* (Washington DC: OSA) 209
- [9] Giles I P, Uttam D, Culshaw B and Davies D E N 1983 Coherent optical-fibre sensors with modulated laser sources *Electron. Lett.* **19** 14-5

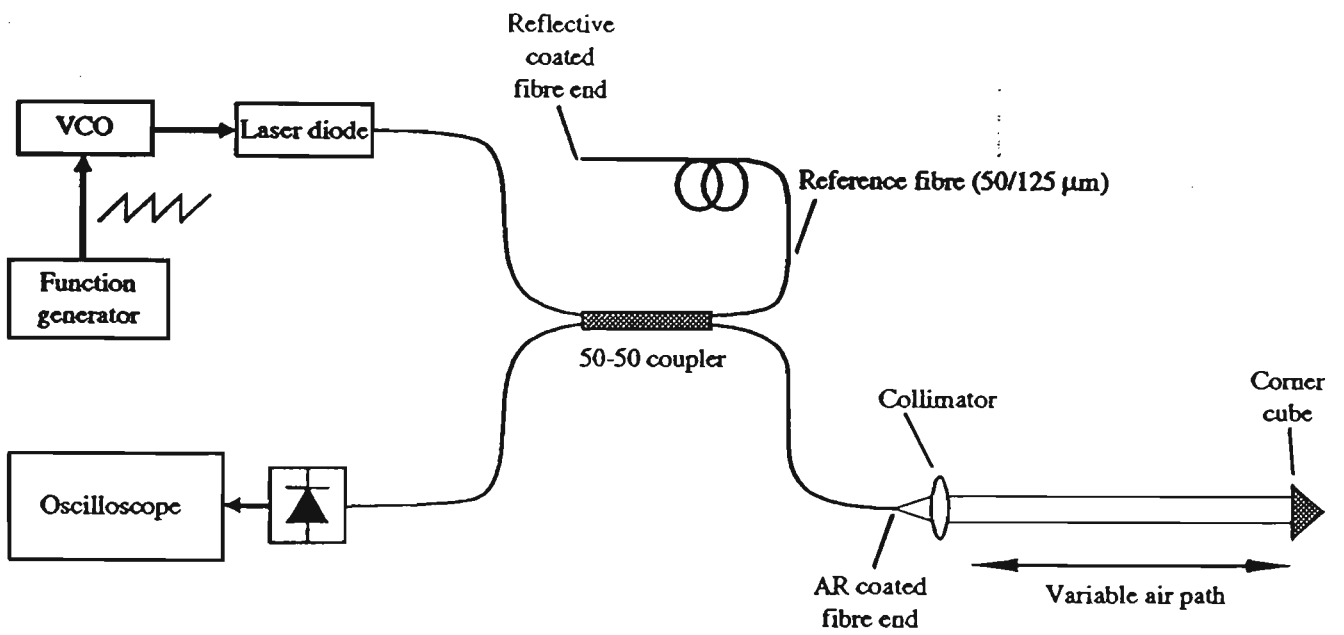


Figure 1 - Experimental arrangement

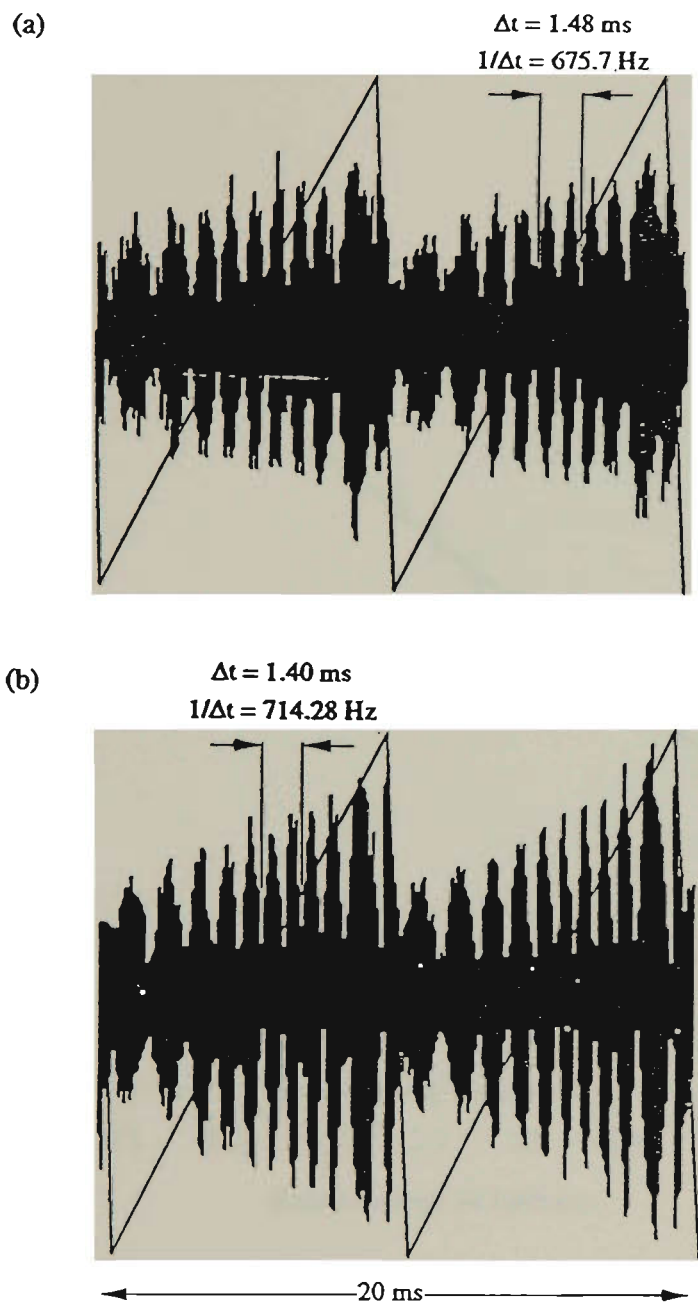


Figure 2 - Sawtooth and beat waveform for an air path of (a) 3.6 m and (b) 0.2 m

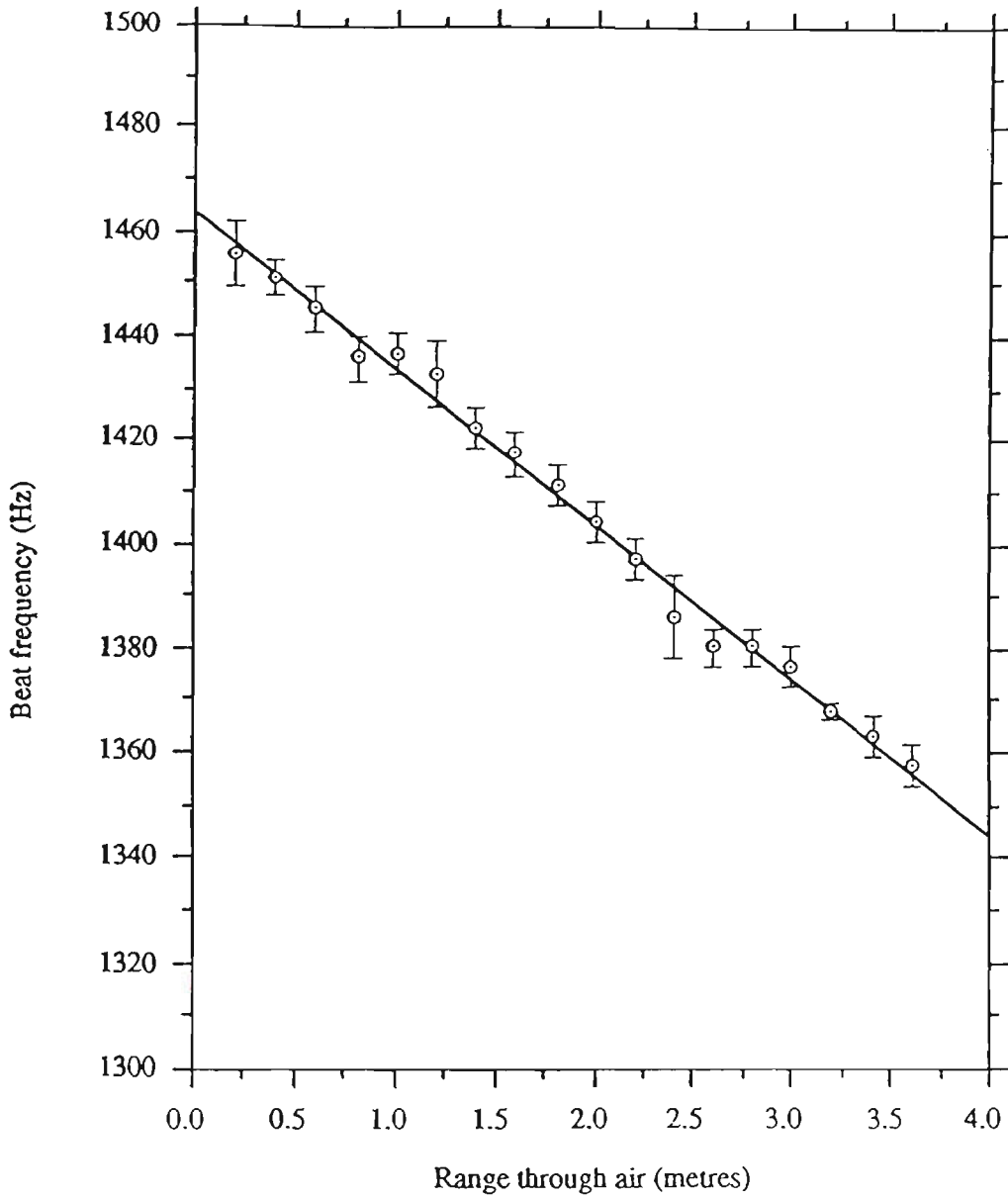


Figure 3 - Experimental results: variation of beat frequency with range